Christine Bandl, BSc

Investigation of olefin metathesis degradation as an alternative method for the exposure of rubber metal interfaces in tires

Master thesis

zur Erlangung des akademischen Grades

Diplom-Ingenieurin

In Technischer Chemie

eingereicht an der

Technischen Universität Graz

Betreuer

Assoc. Prof. Dr. Gregor Trimmel

Institut für chemische Technologie von Materialien

Graz, September 2014

Statutory declaration

I declare that I have authored this thesis independently, that I have not used other than the declared sources/resources, and that I have explicitly indicated all Material which has been quoted either literally or by content from the sources used. The text document uploaded to TUGRAZonline is identical to the present master thesis.

Graz, _____ _____

Date Signature

Eidesstattliche Erklärung

Ich erkläre an des Eides statt, dass ich die vorliegende Arbeit selbstständig verfasst, andere als die angegebenen Quellen/Hilfsmittel nicht benutzt, und die den benutzten Quellen wörtlich und inhaltlich entnommenen Stellen als solche kenntlich gemacht habe.

Graz, _____ _____

Datum Unterschrift

Abstract

Tires represent a very important part of vehicles because they provide the only contact to the street. The performance is influenced by the construction and composition of the tires. Besides fillers and other additives tires consist of about forty percent rubber. Brass coated steel cords are applied as reinforcing elements within the vulcanized rubber network. The adhesion mechanism of the resulting rubber metal interface is a present topic in industry and research. The selective removal of the rubber without damaging the adhesion interface is advantageous for the investigation of the adhesion mechanism. In this master thesis olefin metathesis degradation is examined for this purpose.

In the first part of this work metathesis degradation is compared to the filter paper method, which is a popular technique for the investigation of rubber metal interfaces. Optical light microscopy, 3D-microscopy and scanning electron microscopy are used to investigate the exposed adhesion interfaces. Additionally conclusions about the rubber network and the interface can be drawn from physical data like pullout forces, coverage and tensile strength etc. The influence of some rubber compound ingredients on the adhesion strength is investigated by altering the rubber compositions of the samples. There are samples without cobalt stearate, samples which are vulcanized by different accelerator systems and samples which contain lower amounts of sulfur. Furthermore the effect of different aging conditions is examined. The samples are aged for two days under oxygen at 70 °C, for five days under steam at 105 °C and for fourteen days under humidity at 70 °C.

Usually the samples are vulcanized isothermally. In the second part of this work one series of samples is treated athermally in order to investigate the influence of modified heating conditions. For this purpose different maximum temperatures and heating rates are applied.

Additionally two different sample geometries are compared. While the T-test block samples of part one consist of brass coated steel cords which are vulcanized into rubber, brass coated monofilaments are used in the second part.

The results of this work show that olefin metathesis degradation is a suitable technique for the exposure of rubber metal interfaces in tires. One big advantage of this method is that intact real adhesion interfaces can be exposed by the selective degradation of the rubber compound.

Zusammenfassung

Da Reifen den einzigen Kontakt zur Straße herstellen, zählen sie zu den wichtigsten Bestandteilen von Fahrzeugen. Der Reifenaufbau und die Zusammensetzung der Reifen beeinflusst das Fahrverhalten wesentlich. Neben Füllstoffen und Additiven bestehen Reifen aus etwa vierzig Prozent Gummi. Außerdem werden messingbeschichtete Stahlkorde als Verstärkungselemente im vulkanisierten Gumminetzwerk verbaut. Die Untersuchung des Haftungsmechanismus zwischen Gummi und Metall ist noch immer ein aktuelles Forschungsthema in der Industrie. Um diesen Mechanismus untersuchen zu können, ist es vorteilhaft den Gummi selektiv abzubauen, ohne dabei die Haftschicht zu verletzen. In dieser Masterarbeit wird untersucht, ob sich die Olefin-Metathese für diesen Zweck eignet.

Im ersten Teil dieser Arbeit wird der Abbau mittels Olefin-Metathese mit der Filterpapier-Methode verglichen, welche eine verbreitete Technik zur Untersuchung von Gummi-Metall-Haftschichten darstellt. Die freigelegten Grenzflächen werden anschließend mittels optischer Lichtmikroskopie, 3D-Mikroskopie und Rasterelektronenmikroskopie untersucht. Physikalische Daten wie Ausziehkräfte, Bedeckungsgrad und Zugfestigkeit lassen ebenfalls Schlüsse über das Gumminetzwerk und die Haftschicht zu. Durch das Verändern der Gummizusammensetzung wird untersucht, wie sich einige Mischungsbestandteile auf die Haftkraft auswirken. Es werden Proben hergestellt, die kein Cobalt-Stearat enthalten, denen ein anderes Beschleunigersystem beigemengt wird, und die verringerte Mengen Schwefel enthalten. Außerdem werden die Proben unter verschiedenen Bedingungen gealtert. Der Effekt verschiedener Alterungsbedingungen auf die Gummi-Metall-Grenzschicht wird ebenfalls untersucht. Dazu werden die Proben für zwei Tage unter Sauerstoff und 70 °C, für fünf Tage unter Dampf und 105 °C und für vierzehn Tage unter Feuchtigkeit und 70 °C gealtert.

Großteils werden die Proben unter isothermen Bedingungen vulkanisiert. Im zweiten Teil dieser Arbeit wird eine Probenserie anisotherm behandelt, um den Einfluss verschiedener Heizbedingungen zu untersuchen. Dazu werden sowohl die Maximaltemperaturen, als auch die Heizraten verändert.

Im Zuge dieser Masterarbeit werden zwei verschiedene Probengeometrien verglichen. Während die T-Test Probenblöcke im ersten Teil aus vermessingten Stahlkorden bestehen, die in einen Gummiblock einvulkanisiert werden, werden im zweiten Teil messingbeschichtete Monofilamente verwendet.

Die Ergebnisse dieser Arbeit zeigen, dass der Gummiabbau mittels Olefin-Metathese geeignet ist, die Gummi-Metall-Haftschicht in Reifen freizulegen. Ein großer Vorteil dieser Methode ist, dass durch den selektiven Abbau des Gummis intakte reale Haftschichten freigelegt werden können.

“Each day’s a gift and not a given right.”

Chad Kroeger, 2008

Acknowledgments

First of all I want to thank my supervisor Assoc. Prof. Dr. Gregor Trimmel who gave me the opportunity to write my master thesis about this interesting topic. Furthermore I would like to thank Dr. Thomas Kramer from Continental Reifen Deutschland GmbH who set up the research project and answered any of my questions during my stay in Hannover.

I owe many thanks to Prof. Dr. Jorge Lacayo-Pineda for the opportunity to do some research in his working group at Continental Reifen Deutschland GmbH. Moreover I want to thank Vladimir Cernyj who spent a lot of his time with me doing the SEM investigations. I also thank Sabine Fuge and Jose-Manuel Cumbre-Fernandez who introduced me to 3D-microscopy and always supported me with their experience.

I thank my dear colleagues for a great atmosphere at the working place and for their readiness to help me whenever I needed support. Especially I want to thank my colleagues from the office for the constructive discussions and the fun during the breaks. Additionally I would like to thank Renate for her hospitality and her support during my stay in Hannover.

My special thanks I dedicate to my family and my friends. My deepest gratitude I direct to my mother who has been there for me my entire life, and my father who always supported me proactively.

Furthermore I want to thank my dear friends Lisa and Vera for the amazing lunch and coffee breaks as well as their readiness to listen to me.

Last but not least I want to thank my boyfriend, Tobias, for encouraging me during rough times.

Content

1. Introduction

1.1 Tires - a general introduction

According to statistics from 2013 the annual car tire production amounts to 32.1 billion dollars whereof passenger vehicle tires make up 21.8 billion dollars.[1] In 2008 the global rubber production amounted to 23.4 million tons. 75% of the rubber are used in the automotive sector; 60% are even used for tire production.[2]

Tires are one of the most important parts of vehicles because they represent the only contact to the street. Several properties of the vehicle are influenced by tires; the three most important properties are the resistance to rolling, the braking at wet conditions and the stability of the tire. It is not possible to produce tires with all three properties at optimum. Thus priorities according to the individual vehicle type have to be set.[3]

The properties of tires are determined by their composition - especially by the rubber which accounts for about 40% of the tire[2]. Furthermore the environmental conditions and the temperature at which they are used have an impact on the tires' characteristics. For example summer tires are not suitable for winter conditions because they become stiff at low temperatures and hence have little braking power on wet streets. On the other hand winter tires used in summer would cause high costs and high consumption of fuel due to their soft rubber compound which rises the resistance to rolling at elevated temperatures.[3]

There are five basic groups of materials which build up tires: rubbers, fillers, plasticizers, aging-resisters and vulcanizing agents. Synthetic rubbers like polybutadiene, styrol-butadiene-copolymers or polyisoprene are often used as main components, but still natural rubber (cis-1,4-polyisoprene) remains the most important polymer in tire production. This is due to its special property - the elongation crystallization - which is not or barely found in synthetic rubbers. The force one needs to elongate natural rubber rises with higher elongations because crystallites develop which align in the direction of elongation. They act like further entanglements of the polymer causing a self-reinforcing effect.[3]

Carbon black and silica represent the most important reinforcing fillers. The former reduces abrasion, the latter the resistance to rolling.[3]

Natural or mineral oils as well as resins serve as plasticizers. They influence the viscosity and hardness of the unvulcanized mixture and therefore control the processability. After vulcanization they increase the resilience and have a positive effect on the resistance to rolling. Resin systems additionally improve the road grip.[3]

Aging-resisters like phenyl amine or phenylen diamine protect the rubber from oxygen and ozone. Light stabilizing resins prevent the degradation of the polymer caused by radicals which develop during UV-irradiation.[3]

The most important part of the vulcanizing system is sulfur. It crosslinks the polymer chains to a three dimensional network and the rubber gets elastic. Promoters like the combination of zinc oxide, stearic acid and organic mediators (thiazoles or sulfonamides) accelerate the slow vulcanization reaction by building an active intermediate. This complex reacts with sulfur and further attacks the double bonds of the polymer initiating the formation of the network.[3]

The construction of tires is another important factor which influences their properties and the desired performance. Brass coated steel cords are used as strengthening elements which optimize the physical characteristics of tires such as strength, stiffness, modulus, stability and uniformity. The stiffness of tires leads to good tread wear, handling and low rolling resistance.[4]

Tires can be divided into nine construction parts (see Figure 1): The tread (1) supplies the contact to the street. Beneath the tread there is a layer of rubberized textile fibers called the jointless bandage (2) followed by the breaker belt (3) which consists of steel cords. The angle in which the breaker belt is arranged determines the driving comfort. The consecutive layer consists of textile cords (4) and reinforces the construction. The inside of tires is sealed by the inner liner (5) - a special butyl rubber mixture that prevents decrease in pressure. The walls on the side (6) are very tough to resist against road holes and curbs. The bead (7) is stabilized by a steel core (8) and fits the tires to the rims. The bead reinforcement (9) supplies stiffness and influences the driving behavior as well.[3]

Figure 1: construction of tires[3]

1.2 Scope of this thesis

As can be concluded from the construction (see Figure 1) the rubber metal adhesion is very important for the stability and properties of tires.[4] It is influenced by the additives and fillers of the rubber compound. The improvement of the rubber metal adhesion is still a present topic in industry.

In order to investigate the adhesion interface the rubber has to be removed from the metal surface. Different approaches for the exposure of the rubber metal interface are stated in literature. The most popular technique is the filter paper method which uses a filter paper to separate the rubber from the metallic substrste.[5,6,7,8] Another approach for the investigation of the adhesion interface is the application of squalene as a model compound for rubber.[6,9] However both do not provide real adhesion interfaces. Thus a method which selectively degrades the rubber without damaging the adhesion interface is required. Olefin metathesis is considered to fulfill these requirements since it selectively degrades the double bonds of the rubber.[10]

The aim of this master thesis is to examine olefin metathesis degradation as a method for the exposure of the rubber metal interfaces in tires.

Olefin metathesis degradation is going to be compared to the filter paper method which is a popular technique for the investigation of rubber metal adhesion interfaces. Furthermore different sample geometries are going to be examined with regards to handling during sample preparation, during the exposure of the adhesion interface and during microscopic investigation. For that purpose brass coated steel cords will be vulcanized into rubber in the first part of this work, while in the second part brass coated monofilaments will be used.

Metathesis degradation is going to be used for the exposure of the samples' adhesion interfaces. In order to investigate the influence of some rubber compound ingredients the recipe of the rubber compounds will be altered with respect to the cobalt stearate content, the accelerator system and the level of sulfur. Additionally the effect of different aging conditions on the rubber metal interfaces is going to be examined. For this purpose the different recipes will be aged for two days under oxygen at 70 °C, for five days under steam at 105 °C and for fourteen days under humidity at 70 °C. Afterwards the adhesion interfaces are going to be exposed by olefin metathesis degradation and they are going to be investigated by means of optical light microscopy, 3D-microscopy and scanning electron microscopy. Moreover physical data like pullout forces, the coverage and tensile strength etc. are going to be recorded in order to gain informations about the adhesion strength and the rubber properties of the different samples.

Most of the samples will be vulcanized isothermally. In contrast one sample series will be treated athermally using different maximum temperatures and heating rates in order to investigate the influence of the heating conditions.

2. Theoretical background

2.1 Theory of vulcanization

Vulcanization is the process which crosslinks linear polymer molecules to a 3D-network.[11,12] The rubber is mixed with a combination of additives called the vulcanization system and heated in a mold under pressure. Vulcanization causes significant changes of the rubber at molecular level. The vulcanisate is of higher elasticity and strength than the uncured polymer chains. During vulcanization the solubility and the hysteresis of the rubber decrease whereas the viscosity and the static modulus increase.[12]

The basic recipe consists of organic accelerator (0.5-2phr), elemental sulfur (0.5-4phr), zinc oxide (2-10phr) and stearic acid (1-4phr). Typical accelerators are benzothiazoles like MBT and MBTS (see Figure 2) or benzothiazolsulfenamides like CBS, TBBS, MBS and DCBS (see Figure 3).[12] Zinc oxide and stearic acid form soluble zinc stearate which has an activating effect on the reaction between the organic accelerator and elemental sulfur.[11] The resulting polysulfidic species Ac-S_x-Ac interacts with the double bonds[12] of the rubber molecules forming rubber-S_x-Ac and finally different rubber-sulfur-crosslinks.[11,12]

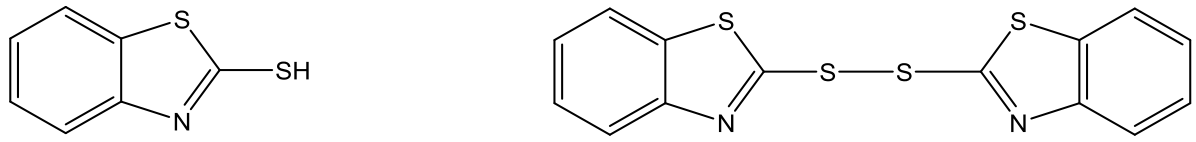

MBT (2-mercaptobenzothiazole)

MBTS (2,2'-dithiobisbenzothiazole)

Figure 2: benzothiazole accelerators[12]

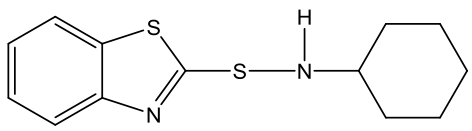

CBS (N-cyclohexylbenzothiazole-2-sulfenamide)

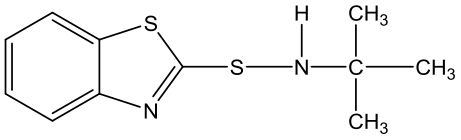

TBBS (N-t-butylobenzothiazole-2-sulfenamide)

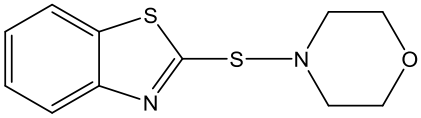

MBS (2-morpholinothiobenzothiazole)

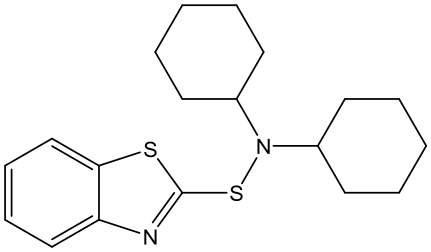

DCBS (N-dicyclohexylbenzothiazole-2-sulfenamide)

Figure 3: benzothiazolsulfenamide accelerators[12]

The type and distribution of the resulting linkage is influenced by the type and amount of organic accelerator as well as the level of sulfur. Figure 4 shows that, besides mono- and disulfide crosslinks (a and b), there are polysulfide bridges (h) with x in the range of 3-6. Moreover there are intramolecular cyclic mono- and disulfides (c and g) and parallel vicinal crosslinks (d) with n in the range of 1-6. Position e shows an intermolecular crosslink. Furthermore pendant sulfidic groups terminated by accelerator fragments (f) can be found. Figure 4 shows the variety of sulfur linkages which are possibly found in vulcanized rubber networks.[11] Furthermore the polymer chains can be linked by carbon-carbon bonds.[11,12]

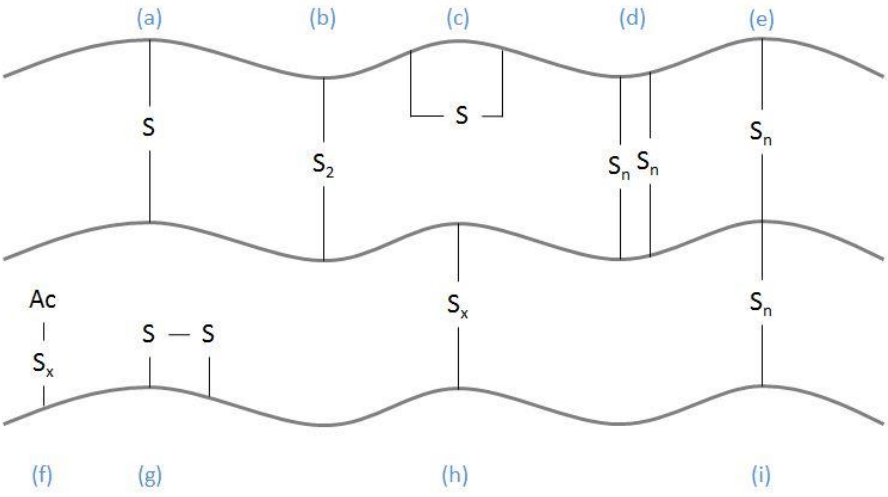

Figure 4: variety of sulfur linkages in rubbers[11]

Mono-, di- and polysulfide crosslinks, as well as the parallel vicinal and intermolecular crosslinks strengthen the vulcanisate and influence its performance. The sulfur in intramolecular cyclic mono- and disulfides and the accelerator terminated fragments is wasted and contributes to poor aging resistance. This is also true for double bonds along the chains in the vulcanized rubber.[11] A high level of mono- and disulfide crosslinks can be achieved by a high accelerator : sulfur ratio.[12] In this case there is little free sulfur resulting in good aging resistance.[11] At an excess of sulfur polysulfidic crosslinks develop.[12] They rearrange at high temperatures and result in short sulfide linkages.[11] This so called reversion is a consequence of too long lasting vulcanization processes and high temperatures (<155 °C).[12]

The onset of the crosslinking process has to be sufficiently delayed to permit an adequate mixing as well as the forming and modeling of the elastomer. Once started, the crosslinking process should proceed rapidly and the extent of vulcanization has to be controlled. The onset of the network formation can be detected by the associated increase of the viscosity.[11,12] Typical cure times for efficient vulcanization systems are 2-5 minutes.[11]

Sulfur free systems are also possible but less common. They use urethanes, peroxides[11,12], metal oxides or resins to cross link the polymer.[11]

2.2 Rubber metal adhesion

Usually steel cords incorporated in car tires are brass coated to provide a proper adhesion between rubber and metal since steel itself is not able to bind to rubber.[13,14] The resulting rubber-brass bond is durable and resistant to high temperatures as well as dynamic loading.[4] Typical brass layers consist of 60-70%[4,15] copper. The optimum thickness for binding to natural rubber amounts to 0.2-0.3 µm[15,16].

Zinc ions originating from the brass coating diffuse to the surface where they are oxidized.[17] The resulting ZnO layer passivates the brass surface. It contains metallic copper and is covered by a very thin Cu_2O film (Figure 5).[13,18]

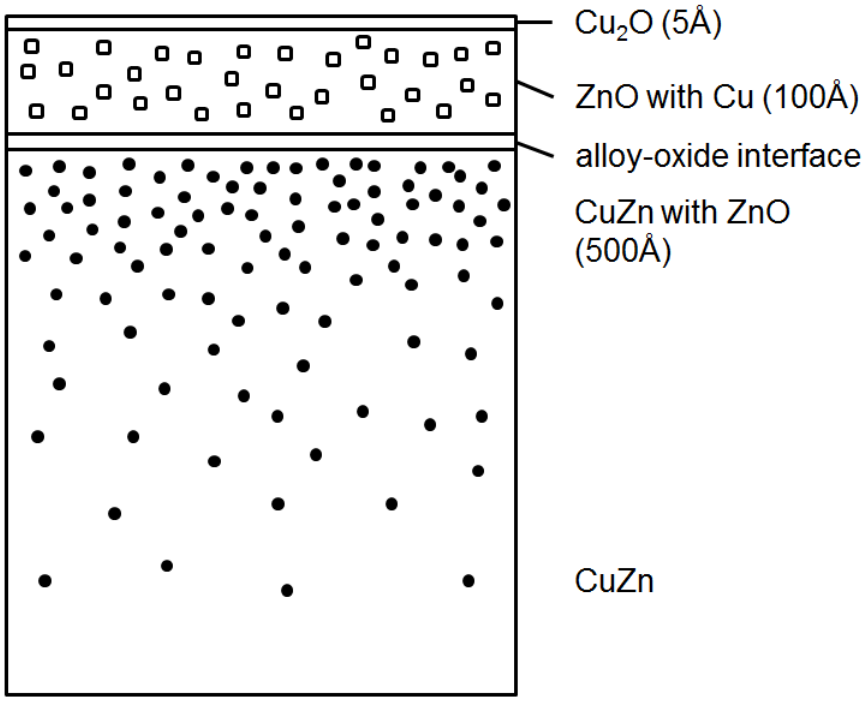

Figure 5: model of brass coated steel cord surfaces[18]

At the beginning of the vulcanization process the so called sulfidation reaction takes place: Before the rubber is crosslinked, copper ions, zinc ions and electrons migrate to the brass surface.[19] They react with the sulfur which originates from the vulcanizing agents.[5,13,15,20] The initial formed ZnS is quickly overgrown by a rough nonstoichiometric Cu_xS layer which contains some ZnS.[7,13,15,19,20,21]

As metal oxides and sulfides are imperfect structures point defects permit diffusion processes.[15] In the early stages interstitial atoms of the zinc oxide lattice diffuse to the surface and contribute to the growth of the ZnS layer.[13,15,20] The ZnO fillers in the rubber formulation are an additional zinc ion source here.[17,22,23] Later copper ions incorporated in the ZnO layer migrate to the top of the ZnS surface and build dendritic Cu_xS there.[7,13,15,19,20,24] The latter process is based on cation vacancy diffusion and is slowed down due to the fact that copper ions have a larger radius than zinc ions. Hence their migration through the zinc lattice is sterically hindered.[13,15,17,19,20] In contrast copper ion diffusion is accelerated as the ions reach the non-stoichiometric Cu_xS layer.[19]

During the following aging process the copper sulfide layer remains growing and more Cu_xS dendrites develop.[15,20,25] As this layer excesses its optimum thickness of about 30-50 nm[13,16,22] adhesion is reduced because the copper sulfide dendrites turn from an amorphous into a more crystalline and brittle form.[15,22] The resulting Cu_2S crystals are described as needlelike and more stoichiometric.[26,27]

Figure 6 shows a typical rubber brass interface after vulcanization.

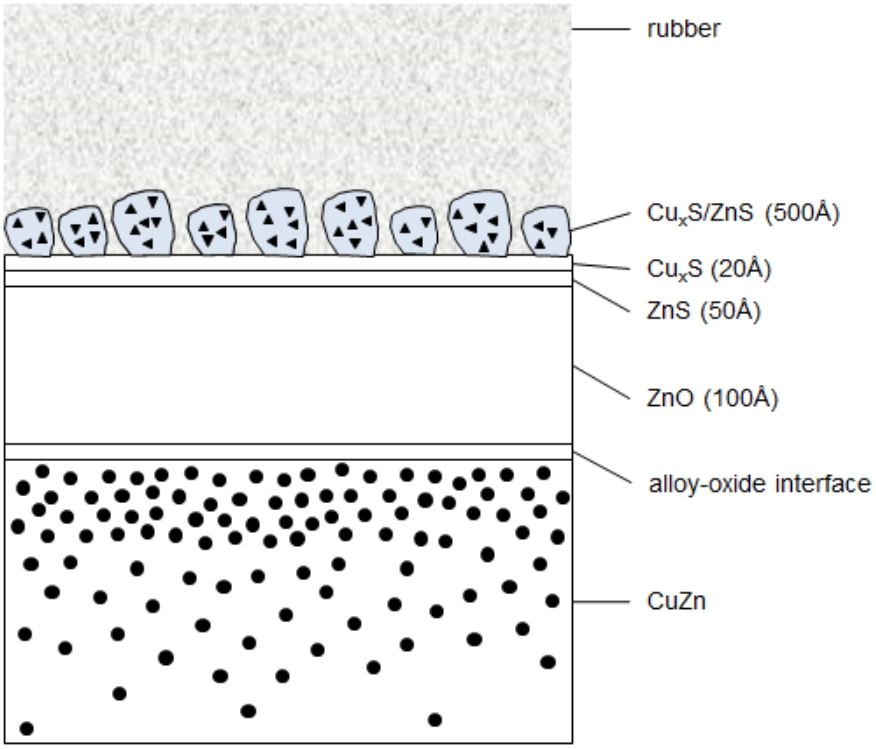

Figure 6: model of rubber brass interfaces after vulcanization[18]

When the Cu_xS layer stops growing zinc ions diffuse through the entire interfacial layer to create more ZnO at the brass surface.[7,15] As the ZnO layer thickens the Cu_xS detaches and debonding occurs.[15] This consumption of zinc ions is called dezincification and thought to be the most important factor causing adhesion failure.[15,19,28] The zinc ions originate from brass where they leave a porous brittle lattice of copper behind. Atmospheric oxygen is adsorbed to the surface and reduced to O^{2-} by electrons descending from the conduction band of the ZnO (see Figure 7). O^{2-} ions coordinate with Zn^{2+} ions forming ZnO which additionally weakens the adhesion to the rubber. The ions are transferred via the overlapping conduction bands of the already existing ZnO.[15,20]

Humid conditions accelerate dezincification and decrease the adhesion strength.[7,15,19 ,28] Hydroxide anions are built at the presence of water and oxygen: $O_2 + 2H_2O + 4e^- \rightarrow 4OH^-$.[18] The Cu_xS layer is possibly overgrown by ZnS, ZnO and $Zn(OH)_2$[6,18] depending on the moisture and oxygen present at the interface. At dry conditions this process is much slower.[18]

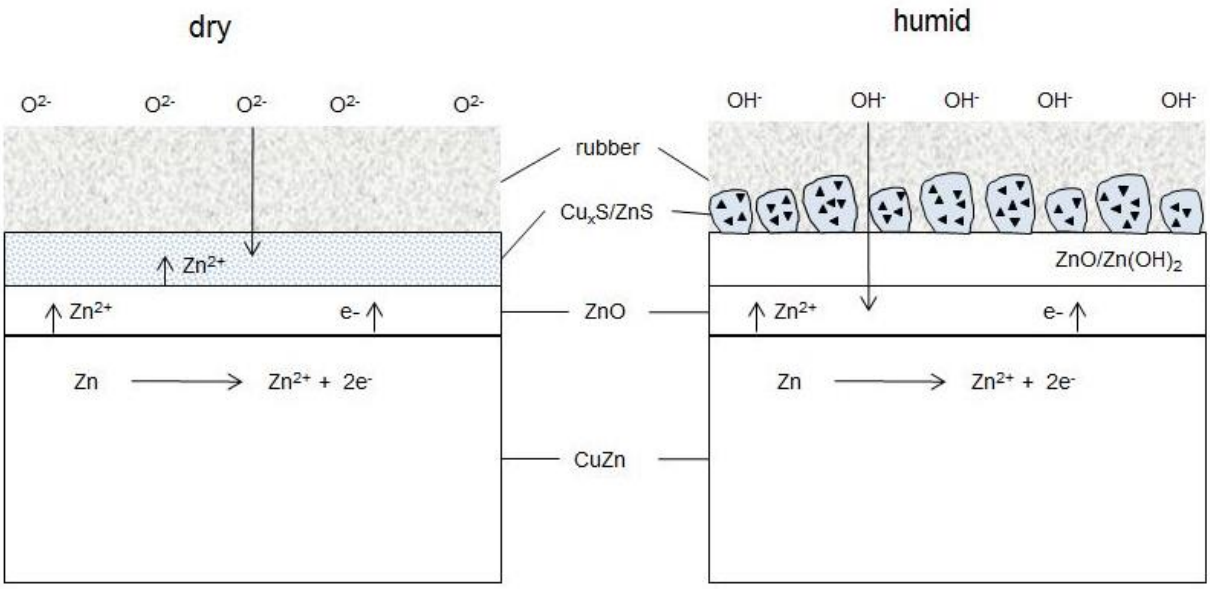

Figure 7: mechanism of the dezincification process[15,18,29]

Cu_xS and ZnS are responsible for the rubber metal adhesion whereas ZnS is less important.[13,15] On the one hand the vulcanized rubber develops a physical interlocking with Cu_xS dendrites[30]. They provide a large specific area for the interaction with rubber. The size of the dendrites ranges in the nanometer scale.[31] On the other hand there is a chemical crosslinking via Cu_xS-S_y-rubber bonds which is thought to be a minor factor of the total adhesion strength. The amount of Cu_xS depends primarily on the copper inclusions in the ZnO layer[18] and is directly related to the degree of sulfidation.[19] Therefore it is essential to delay the crosslinking process of vulcanization long enough to achieve a Cu_xS layer of critical thickness.[5,13,15] Adhesion fails if there is too little Cu_xS and thus not enough sulfur bridges to connect the rubber to the metal. On the other hand an excessively grown Cu_xS layer often detaches from the metal surface due to its brittleness.[13,21] This rupture is thought to occur between Cu_xS and ZnO.[28]

In general there are different forms of copper sulfide depending on the temperature and formulations. Besides the two stable sulfides CuS and Cu_2S there are a number of non-stoichiometric phases of Cu_xS. At higher curing temperatures the amorphous structures turn into a more crystalline form.[18,22,30] The index x varies between 1 and 2 in general, but typically ranges from 1.8-1.97.[15,22,28,9] Copper has mainly Cu^+ character with small contributions of Cu^{2+}.[15] Furthermore the phenomenon of desulfurization during vulcanization is discussed in literature. The flexible CuS is suggested to turn into the more crystalline Cu_2S generating a bond between rubber and brass:

rubber + 2CuS→ rubber-S-Cu_2S[9]

To get an idea of the rubber-brass-adhesion mechanism the interactions between the sulfen amide group of the accelerator, the double bonds of the rubber, the promoters and sulfur have to be considered[13]:

The reaction of zinc oxide and stearic acid generate soluble zinc ions. They build complexes with the organic accelerator molecules. The introduction of sulfur completes the formation of the sulfurizing intermediates.

Since the accelerator acts as sulfur donor it plays a very important role in the formation of the adhesion interface. Copper ions migrate to the surface and bind to the sulfen amide group of the accelerator.[15,20,32] The resulting in Cu_xS dendrites have a high specific area and grow into the liquid polymer compound[6,15,18,20,32] until all accelerator molecules are consumed. Simultaneously the rubber is crosslinked to a three dimensional network incorporating the Cu_xS dendrites.[15,20,32]

The adhesion mechanism discovered by Van Ooij is widely accepted and can be divided into five steps. This model of the adhesion layer development is applicable for all sulfonamide accelerators. It is exemplarily illustrated using N-cyclohexylbenzothiazole-2-sulfenamide (CBS) as accelerator in the following figures.

1. **Building of active intermediates**
   a. Interaction between accelerator and rubber

The S-N bond of the accelerator is polarized. The induced scission of the molecule results in a negatively charged sulfur- and a positively charged nitrogen-part. The intermediate charge transfer π-complex is stabilized by the high electron density of the π-orbitals of the rubber's double bonds. Sulfur is able to stabilize the negative charge because of its size and capability of resonance stabilization.[15,20,32] Ion formation is supported by the high electronegativity of sulfur and the tendency of nitrogen to form positive ions.[15,20]

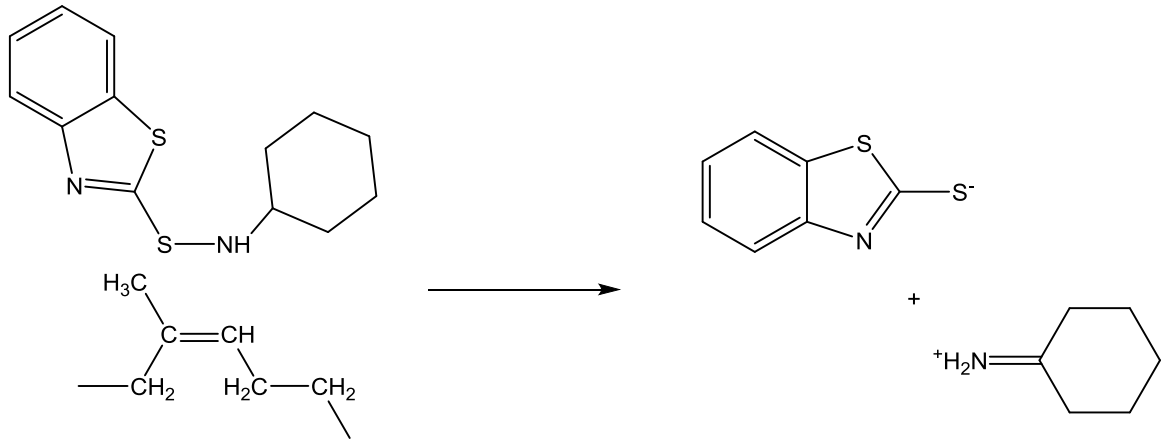

Figure 8: polarization of the S-N bond and scission of the accelerator molecule[33]

Then the negatively charged sulfur receives one of the hydrogen atoms that are originally bound to the positively charged nitrogen and MBT (2-mercaptobenzothiazol) is generated.[20] Once built, MBT catalyzes the accelerator decomposition and the formation of MBTS (2,2'-Dithiobisbenzothiazole).[32]

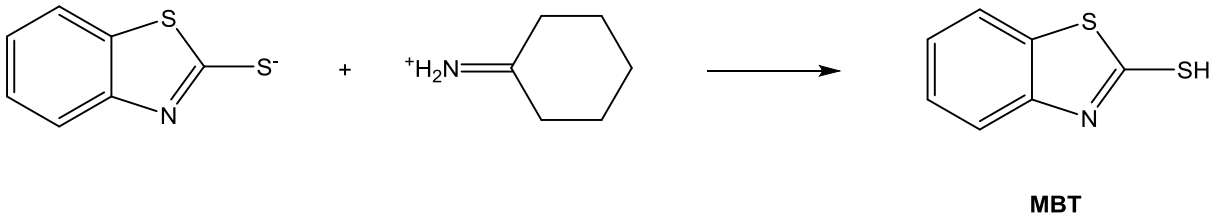

Figure 9: generation of MBT[33]

b. CBS + MBT → MBTS

A further CBS molecule reacts with the MBT built in step 1a. The two molecules are connected via a disulfide bridge.[20]

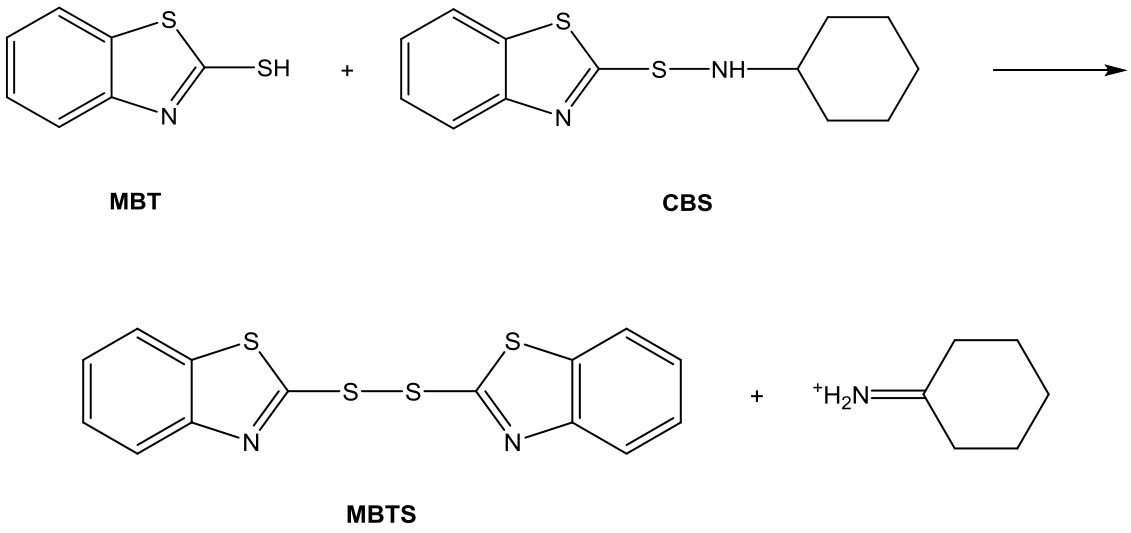

Figure 10: generation of MBTS[33]

c. Persulfidation reaction through complexation with zinc ions

Zn^{2+} forms a complex with nitrogen and one of the sulfur atoms of the disulfide bridge. After that ZnO/S_8 is able to introduce further sulfur atoms between the two ring systems. This results in sulfidizing complexes which are the active intermediates of the overall reaction.[13,20]

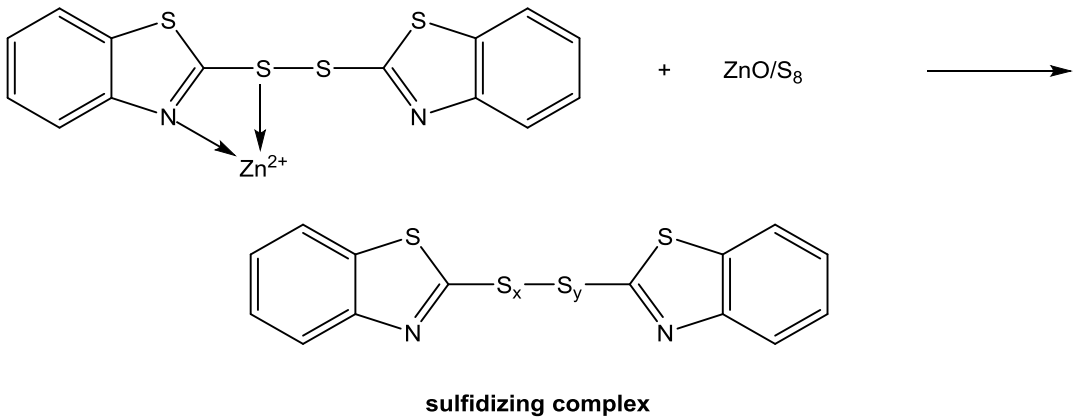

Figure 11: generation of the sulfidizing complex[33]

2. Adsorption of accelerator fragments on the metal surface

During the activation of the brass surface by stearic acid, the superficial oxides are partially dissoluted and MBT or MBTS are adsorbed to the pretreated surface via a metal-sulfur bond.[15,20]

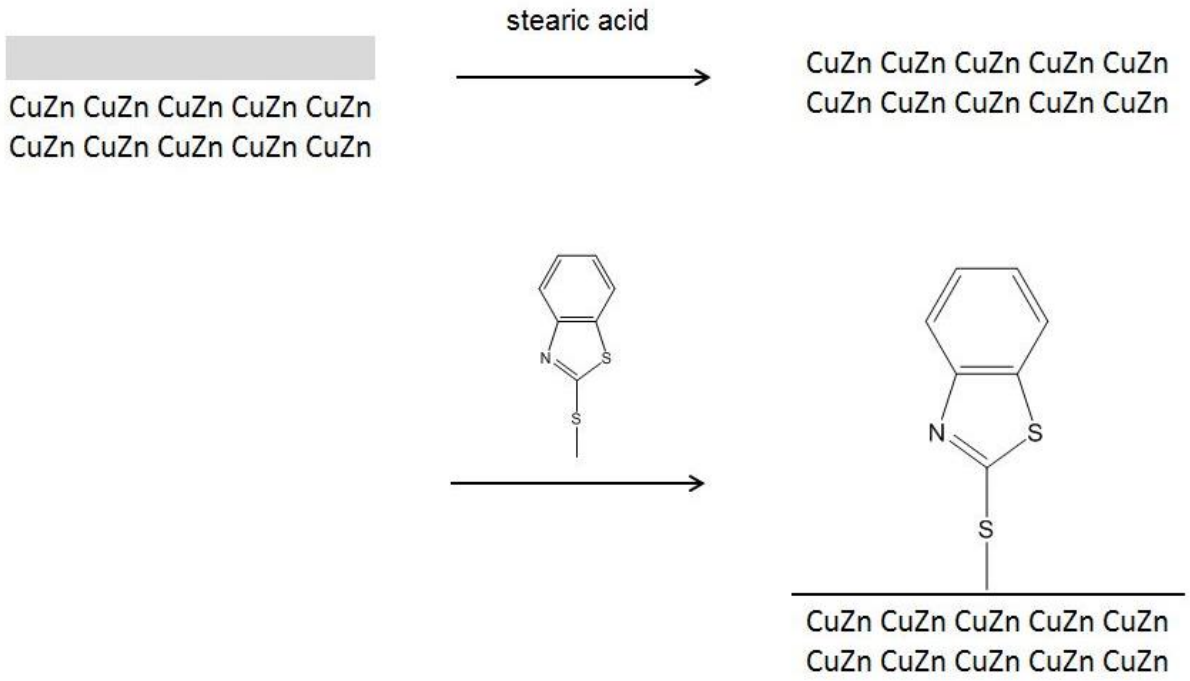

Figure 12: adsorption of the accelerator on the metal surface[33]

3. Insertion of sulfur

The metal-sulfur bond promotes the opening of the S_8-ring and the further insertion of sulfur between the accelerator and the metal surface. The addition of rubber soluble zinc further supports this process. The zinc chelates with the sulfur and nitrogen of MBTS forming a polysulfonic link between thiazole and copper as described above (step 1c).[15,20]

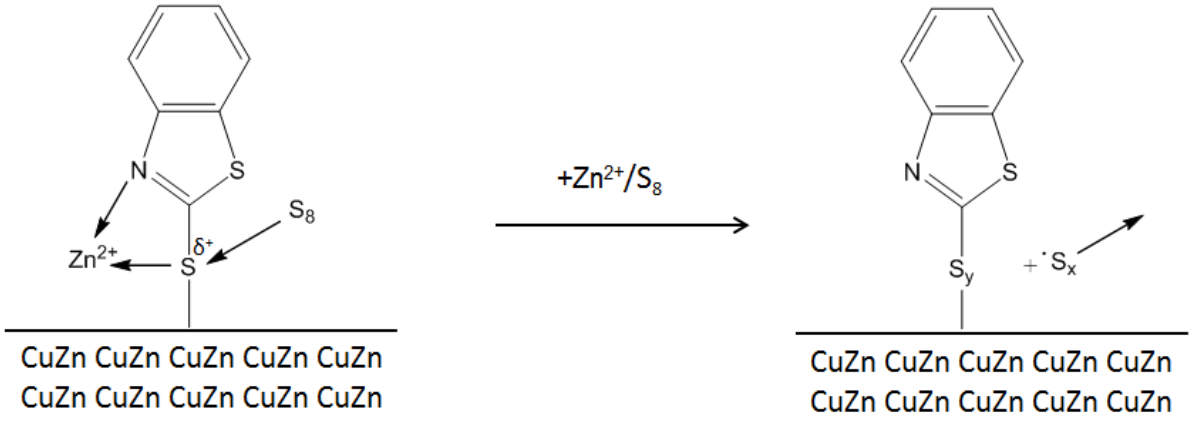

Figure 13: insertion of sulfur[33]

4. Complex breakdown and growth of sulfide layer

As vulcanization proceeds the temperatures rise and the complexes decompose to metal sulfides located at the brass surface and sulfurized accelerator fragments S_{y-1}-X. On the one hand these fragments can initiate the crosslinking of rubber near the metal surface, on the other hand they can be adsorbed again and react with copper atoms that have diffused to the surface before.[15,20]

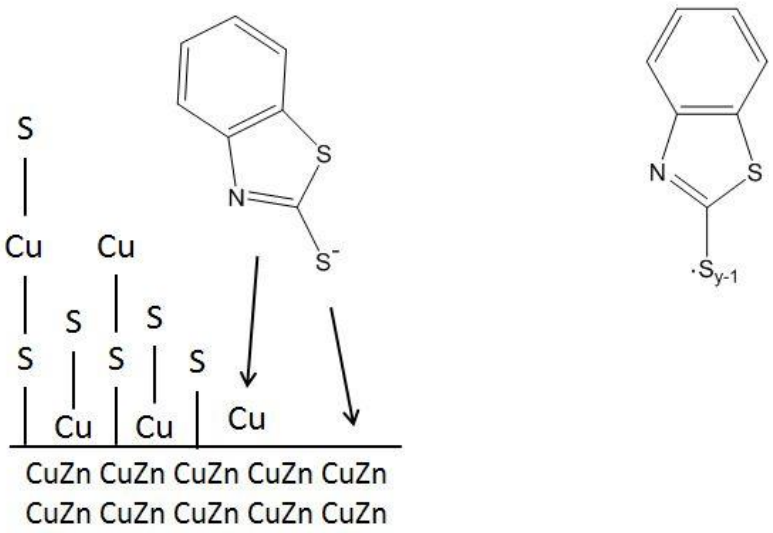

Figure 14: complex degradation and growth of the sulfide layer[33]

5. Crosslinking of rubber

The crosslinking of the rubber and the formation of the adhesion interlayer proceed simultaneously. The applied accelerator system influences the delay of vulcanization and hence the time available for sulfidation.

The crosslinking of the rubber is initiated by the elemental sulfur in the compound or the sulfurized intermediate from step 1c (see Figure 15).[13,20] A very important aspect of the mechanism is that the concentration of the active crosslinking species decreases from the surface to the bulk rubber. The density of the Cu_xS-S_y-rubber network decreases from the rubber metal interface towards bulk rubber and a called “modulus gradient” is generated.[15,20]

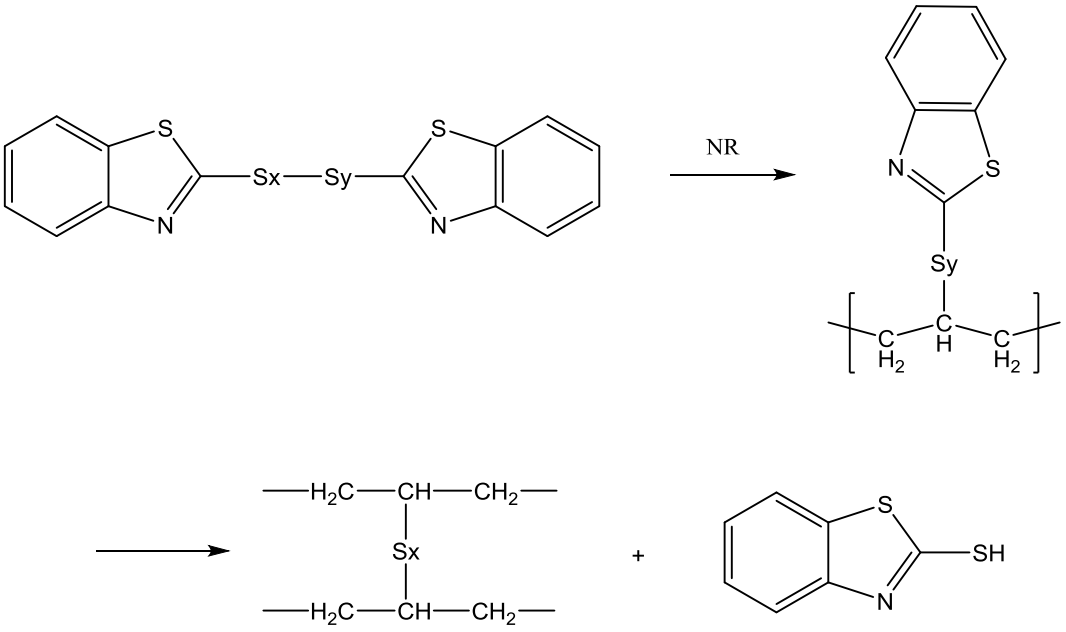

Figure 15: crosslinking reaction[33]

2.3 Influence of rubber composite ingredients

The formation and aging of the rubber metal interface is profoundly influenced by the different compounds of the rubber composite. The three most influential ingredients are silica, adhesive promoters like cobalt salts and resins.[20] The cure system (sulfur and accelerator) and the composition of the brass coating also play an important role.[5]

Crystalline **brass** has little lattice defects and hence allows only slow diffusion of metal ions. This results in more uniform interfacial layers and sulfides.[15,20] Brass of low copper content is covered with a more homogenous ZnO layer and subsequently a thinner Cu_xS layer develops at the surface.[18] The homogeneity of the brass coating is influenced by deformation during the drawing process.[34]

Silica can replace parts of carbon black filler and leads to better structural performance and an improvement of mechanical properties like tear strength, abrasion resistance, heat build-up, hardness, modulus, resilience and adhesion.[20,35,36] It alters the composition and thickness of the interfacial layer by chemical interaction.[15,35] Due to its polar surface silica can adsorb some rubber compound ingredients like sulfen amide accelerator molecules. This slows down the cure rates and results in very homogenous rubber compounds and interfacial layers. The overgrowth of the adhesion layer is inhibited as the Cu_xS development is suppressed by silica. In contrast the formation of ZnS[35,36] is accelerated and the resulting interface is more stable against humidity aging.[36] In combination with cobalt

salts and resin systems it improves adhesion - especially after aging and treatment with humidity or salt solutions.[20,35]

Organic cobalt salts like cobalt stearate, cobalt boroacylate or cobalt naphthenate are typical adhesion promoters.[15,37] They increase the adhesion strength and durability of the rubber metal bond especially after aging.[15,29,38,39] The cobalt cation is the actual promoter as it lowers the activation energy of the sulfurating intermediate.[5,15,32] Moreover it slows down dezincification and thus provides protection during aging under corrosive and humid conditions.[17,19]

The performance of the cobalt promoters is characterized by their participation in rubber curing, their influence on the modification of the interfacial layer and their chemical stability :[37]

Cobalt salts reduce the viscosity of the rubber compound because the corresponding anion acts as a lubricant.[39] In contrast the curing rates of the rubber and the crosslinking density are increased.[8,15,29,38,39] As a result hardness, modulus and tensile strength increase while elongation at break decreases.[8,15,39,38] The corresponding anions only have a secondary effect on the efficiency of the cure.[15]

Cobalt ions promote the formation of Cu_xS and retard the ZnO development. They are incorporated into ZnO, ZnS and Cu_xS layers and alter the migration rates of copper and zinc ions.[15,18,19,24,25,30,32] Large voids in the wurtzite structure of ZnO allow cobalt ions to be integrated as interstitial impurities.[17,19] Before the onset of sulfidation Co^{3+} ions replace some cations in the ZnO lattice. This leads to an excess of positive charge which is compensated with an increase of interstitial electrons. As a consequence the diffusion rate of Zn^{2+} slows down resulting in a thinner ZnO layer.[19] Copper ions migrate along the grain boundaries of ZnO and hence are not affected by the Co^{3+} interstitials. Thus cobalt incorporations improve the resistance to dezincification and promote the Cu_xS formation.[15,18,25,29,30,32] During the sulfidation process cobalt ions are incorporated into the Cu_xS layer as Co_2S on vacancies.[15,17,19] This lowers the defect density in Cu_xS and reduces the diffusion rates of copper and sulfur ions.[15,19] Instead of the excessive amounts of crystalline Cu_xS dendrites thin amorphous layers develop when cobalt ions are present. This is how cobalt salts protect the interfacial layers against aging.[15,19,25,30,32]

Cobalt is not only incorporated as Co_2S, but also present as organic cobalt compounds at the surface (Co-S-rubber species).[24,40]

To sum up incorporated cobalt ions regulate the thickness of the ZnO and Cu_xS layer and hence improve adhesion.

Incorporation of high amounts of cobalt salt drastically increases copper ion diffusion towards the adhesion interface. This causes defects in the brass which in turn activate zinc ion diffusion there. As a result thick ZnO and Cu_xS layers develop which finally lead to adhesion failure. This effect is even worse in humidity aging.[39] However

too high concentrations of cobalt have negative effects on the Cu_xS layer.[18,41] This is especially emphasized for systems with low sulfur contents.[18]

Boroacylate-anions are known as corrosion inhibitors for steel[18] and found to accumulate at the adhesion interface.[15,42] They are especially effective against steam aging[37] and it is reported that boron increases the mobility of cobalt ions.[15,42] The benefits of boroacylate-complexes are the increased cobalt content (see Figure 16 (a)) and the higher chemical stability compared to disoaps like stearates (Figure 16 (b)).[15]

Stearates indeed are corrosive[15,18] and have an activating effect on sulfur.[15] Due to their weak bonds stearate complexes dissociate rapidly and activate more accelerator molecules. This results in poor adhesion because the cure of the rubber is not delayed long enough.[37]

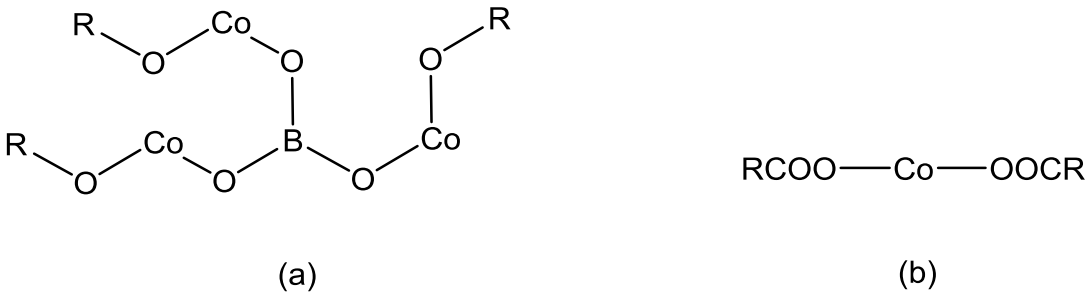

Figure 16: general structures of different cobalt salts[15]

The major role of **stearic acid** is the activation of the accelerator and the improvement of the crosslinking process. In combination of ZnO stearic acid builds zinc stearate which is a rubber soluble activator in the formation of the adhesive interface (see also adhesion mechanism in chapter 2.2).[21] Due to the accelerator activation excessive amounts of sulfur are set free. Moreover stearic acid dissolutes ZnO at the adhesion interface.[18,21,43] The resulting loss of zinc causes dezincification and activates copper. Thick and brittle Cu_xS layers develop and finally lead to poor adhesion.[21,43] As interfacial structures develop the surface gets rougher. This allows a mechanical interlocking with the rubber. The optimum amount of stearic acid results in the maximum surface roughness.[21] Low loads of stearic acid increase hardness, tensile strength, modulus and elongation at break, whereas high loads decrease these rubber properties and cause poor adhesion.[43]

High levels of **ZnO** in the rubber inhibit dezincification by reducing the diffusion of zinc ions originating from the brass to the surface.[19]

Low loads of **zinc borate** enhance adhesion retention for long aging and aging in humidity. Moderate Cu_xS and ZnO formation can be achieved because zinc borate depresses copper migration. High loadings however cause excessive growth of the interfacial layers and lead to poor adhesion.[44]

Chlorotriazine and tetrachlorbenzoquinone reduce the vulcanization rate but have little influence on the physical properties. Chlorotriazine is estimated to accelerate sulfidation by converting ZnO to ZnS whereas tetrachlorobenzoquinone leads to increased copper migration and hence to a growth of Cu_xS at the interface. Both substances release chlorine or chloride ions which activate the brass. However too much promoter causes adhesion failure because of too thick or corroded interfaces.[20]

The **resin system** influences the rubber properties and adhesion strength. It controls the structure of the sulfide layer and promotes the building of amorphous copper sulfide.[30,45] Cure rates decrease whereas hardness increases in the presence of resins.[38] As polar resins are not soluble in rubber they are proposed to migrate to the rubber metal interface where they build a polymerized network.[15,30,38,41,46] This resin layer reinforces the adhesion interface[46,41] and is a barrier to moisture. As a result resin systems retard the absorbance of water.[15,30,38,41] There are two or one component systems:

Two component resins usually consist of methylene acceptors like resorcinol or resorcinol-formaldehyde (RF) and a methylene donor like hexamethoxymelamine (HMMM).[38] The so called HR-system consists of HMMM and RF (see Figure 17)[20] and condenses to an interpenetrating network which acts as adhesion promoter.[5,45] It improves adhesion by suppressing the ion migration of copper, zinc, sulfur and oxygen.[15] The addition of cobalt salts enforces this effect.[20,47] HMMM and RF diffuse to the interface where Cu_xS catalyzes the resin polymerization.[15,41] The share of free resorcinol can be reduced by the addition of styrene or the reaction with epoxy.[15]

One component resins consist of HMMM dimers where the triazine rings are not fully substituted by the methoxymethyl groups (see Figure 18).[30,45] During the self-condensing reaction water or water and formaldehyde are eliminated[45] and a polymeric network is generated. There is no need for a second component.[15,38] The amine type hydrogen atoms of one component resins are labile and can dissociate. Subsequently they may diffuse to the adhesion layer and alter the crystal structure by interacting with the metal defects. As a result the Cu_xS layer stays amorphous during the aging process, even under humid conditions.[45]

Even without RF HMMM prevents the excessive formation of Cu_xS.[46] Moreover it is able to trap free amine residues which develop during the decomposition of the accelerator. These amines easily penetrate the interface between rubber and metal where they promote stress induced corrosion cracks.[41,46] Furthermore they cannot

react with the mercapto radical intermediates. Hence amine entrapment improves adhesion properties and crosslinking density.[46] It is advantageous to apply an excess of HMMM in order to build the resin and trap the free amines.[41]

Melamine resins are another one component alternative which can be applied with less cobalt salt and sulfur contents than two component resins.[20]

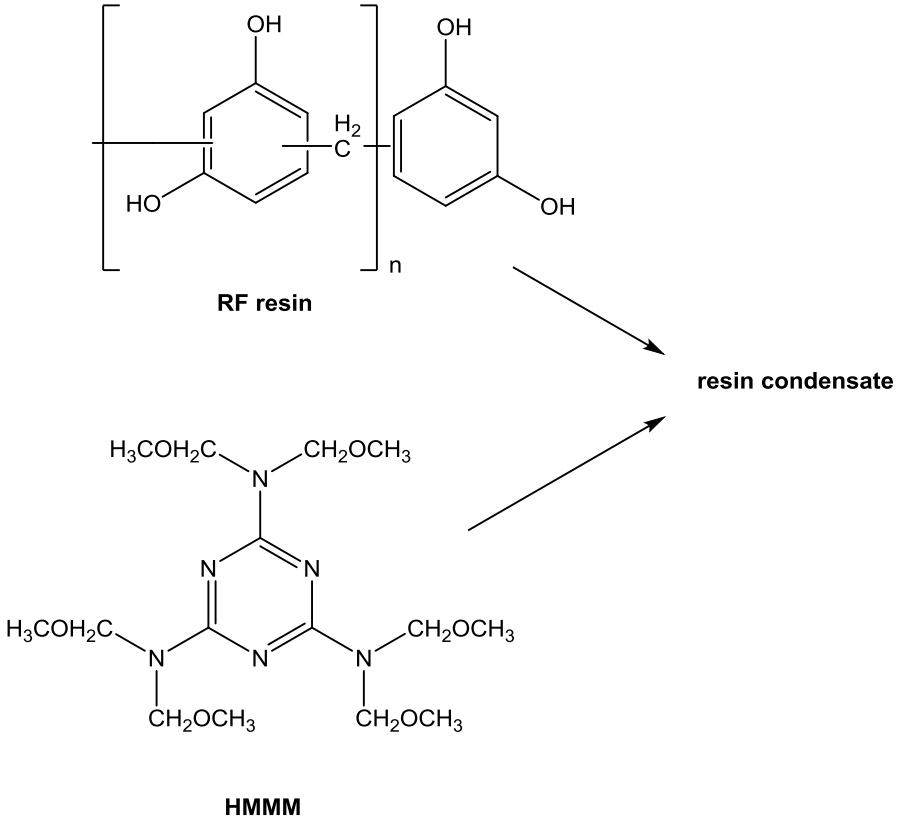

Figure 17: HR resin system[45]

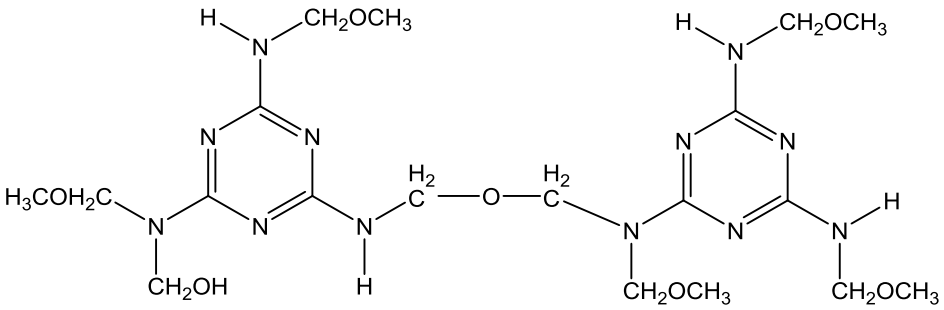

Figure 18: one component resin[45]

Carbon black does not only have a reinforcing effect on rubber compounds, but also influences the adhesion strength of rubber metal interfaces. This filler preferentially entraps amine residues from the vulcanization accelerator and thus enhances the adhesion between rubber and metal. It is suggested that this occurs by physical adsorption in the carbon filled network.[46] Moreover the vulcanization process and the decomposition of the accelerator are delayed in the absence of cobalt salt and carbon black. A lack of carbon black delays the onset of vulcanization and promotes the formation of a thick cobalt layer on the rubber metal interface. The absence of cobalt salt also retards the start of vulcanization and additionally lowers the crosslinking density.[32]

2.4 Different treatment of cords and alternatives to brass

For a long time **silica and silicates** are known as additives in rubber compounds. Recent researches show a synergetic effect for organo-functional silanes on brass coated steel.[20] They are applied as adhesion promoters and anti-corrosion agents. For example bis(trimethoxysilylpropyl)amine and bis(trimethoxysilylpropyl)tetrasulfide are applied in a ratio of 1:3.[15,20,48] The amino silane forms a dry film which adheres to the metal, the sulfur silane builds a network with the rubber.[20,48] Si-O-Si and Si-O-metal bonds develop on the surface. The corrosion of the brass substrate is inhibited as the presence of water preferentially leads to a further crosslinking of the silanes.[48] Due to the high strength of the rubber-to-metal adhesion achieved by the silane coatings little sulfur and cobalt contents are required.[15,20]

Other **non-metallic systems** are based on the use of pyrimidine derivatives, chlorotrazine derivatives, hydroxyl-benzoic acid and tetrachlorobenzoquinone.[15]

Another possibility is to apply **plasma polymerized acetylene or thiophene** to the steel surface. The sulfur originating in the rubber diffuses through the polyacetylene coating towards the metal surface. Parts of the superficial iron oxide are converted to iron sulfide[49] which plays a key role for the adhesion in the thiophene mechanism.[20] Plasma polymerized thiophene provides sulfur which promotes vulcanization and the formation of iron sulfide. Moreover its unsaturation is advantageous for strong adhesion. Thiophene is less flammable than acetylene and hence less hazardous. The optimum film thickness is about 50 Å. To activate the surface the substrate is pretreated with a hydrogen/argon plasma.[49]

Etching as well as polishing roughens the brass surface. The treatment with sodium hydroxide or hydrochloric acid leads to fine grained structures whereas mechanical polishing releases coarse dendritic grains. NaOH dissolves ZnO present at the brass surface and causes zinc depletion.[50]

Moreover thin layers of **zinc or copper** can be used instead of the brass alloy. Single copper coatings show a better behavior at aging conditions due to the absence of zinc which forms ZnO and $Zn(OH)_2$ in brass leading to loss of adhesion.[20]

A **combination of cobalt and copper** can be added to the metal surface to increase the resistance against ZnO and $Zn(OH)_2$ formation.[20]

Ni/Zn and Zn/Co alloys can be electrochemically metallized onto steel surfaces and represent an alternative to brass coatings. In this case ZnS connects rubber and metal. The presence of cobalt suppresses ZnO formation and dezincification. Furthermore it influences the formation of ZnS at the interface which is more stable than Cu_xS.[15,20]

Another possibility is a **double layer** consisting of **Zn/Ni-Zn/Co**. Good results are reported for ductile zinc rich inner layers consisting of Zn/Co and porous nickel rich outer coatings of Zn/Ni.[20,23,51] The Zn/Ni-Zn/Co coating protects the adhesion interlayer excellently against humidity aging. Failures occur exclusively in the rubber compound.[51] The outer Zn/Ni (α-phase) passivates the steel's surface and hence protects it from corrosion.[20,23,51] Moreover it improves the initial and aged adhesion to natural rubber.[51,52] The expanded structure of the inner Zn/Co (η-phase)[51] is less porous than the structure of conventional brass[20,27,52] and determines the anticorrosion properties.[23] It provides good adhesion to the steel substrate.[52] Dezincification is suppressed hence no adhesion failure due to the growth of $ZnO/Zn(OH)_2$ occurs. The initial loss of Zn^{2+} in the ZnO lattice is balanced by the incorporation of Ni^{3+} ions which suppress further Zn^{2+} diffusion.[23] A disadvantage of the double layer is the hardness of nickel which makes it difficult to draw. It is also stated that nickel does not play any role in the adhesion mechanism. A better handling and improved adhesion can be achieved by single Zn-Co coatings.[20]

Sequential layers of brass, cobalt and copper improve adhesion as well especially after humidity aging because cobalt suppresses dezincification.[15]

To sum up the basic advantages of brass are that it can be electrodeposited easily on steel cords, its excellent drawability and the good adhesion properties to natural rubber. The bad corrosion behavior in salty and humid environment is the major disadvantage of brass.[51,52]

2.5 Sample preparation techniques

In order to investigate the adhesion interlayer it is advantageous to separate the rubber from the metal without destroying the interfacial structures. This is very difficult because mechanical operations like pulling and peeling are involved.[36] Several techniques for the exposure of a clean interface are described in literature.

The **filter paper method** represents a very easy way to remove the rubber from the adhesion interface. Brass coated steel cords are covered with filter paper and sandwiched between two un-vulcanized rubber pads.[5,6,7,8] The filter paper is permeable to sulfur, the accelerator and cobalt salt, but is a barrier to the interrupting rubber and carbon black.[6,9] Thus an adhesion layer model develops on the metal surface. After vulcanization the rubber can be peeled or cut off easily[5,6,7,8] because the filter paper neither adheres to rubber nor to brass.[5,39,44]

Liquid nitrogen can be used to break down the rubber phase from the brass substrate.[6,9,28] The polymer is freezed in liquid nitrogen and loosened by striking with a hammer. Rubber residues are soaked in a solvent like diisopropylbenzene and wiped off with a lint-free tissue.[26] Although a real adhesion system can be investigated by this method, the exposed interface might not be representative because of mechanical damages.[9]

Moreover **squalene,** a low molecular-weight trans isomer of natural rubber[32,47], can be used as a liquid model compound.[6,9] The wires are added into a solution of squalene and compound ingredients. The mixture is heated to the reaction temperature and later quenched with iced water. The interfaces are cleaned by ultrasonic baths in toluene, acetone and hexane.[32,53] Afterwards there is no need for further treatment.[9] During the reaction nitrogen prevents squalene from oxidation and inhibits side reactions.[32,53] It is important to keep in mind that squalene is only a model system and hence does not represent the real state.[9,21] The dispersion of the ingredients might be inhomogeneous and there might be differences in curing.[9]

Instead of squalene 1-dodecene can be used as model compound as well. It is of lower molecular weight and only contains one double bond. This facilitates the handling during investigation (separation and detection in GC). However a disadvantage of 1-dodecene is the lower sensibility to cobalt compared to the squalene model.[29]

Furthermore the rubber can be removed by organic **solvents**[9] which do not affect the adhesion interface.[6,38] After soaking and heating in o-dichlorobenzene the rubber can be wiped off with a soft tissue.[45] Subsequently the samples might be cleaned ultrasonically in n-hexane.[25] Instead of o-dichlorobenzene xylene can be used for swelling as well.[19]

It is also possible to apply a brass layer by vapor coating copper and zinc onto a glass substrate. After vulcanization the glass and the brass film can easily be

separated. This method holds the advantages of high reproducibility and the development of homogenous layers. Compared to real systems however there might be a difference with respect to the brass and its thickness and homogeneity.[31,42]

Another access to directly investigate the adhesion interface is to use **cross sections** of the rubber metal composites.[6]

In this master thesis **metathesis degradation** is investigated as a method for the exposure of the rubber metal interface. It is revealed by the selective degradation of the rubber's double bonds via metathesis reaction.

Metathesis degradation is not mentioned frequently in literature in this context. However Elisabeth Ziegler describes the use of olefin metathesis degradation for the exposure of some rubber metal interfaces. As a pretreatment the samples are soaked in toluene. Then they are heated in toluene to 80 °C or 110 °C depending on the carbon black content. The degradation of the rubber is started by the addition of 2nd generation Grubbs catalyst (see chapter 2.6.1). After one hour the samples are removed and washed in toluene. The degradation is repeated if the rubber has not been completely removed. Moreover the addition of 1-octene is described in a second series of experiments.[10]

2.6 Theory of metathesis reaction

2.6.1 Metathesis reaction in general

Olefin metathesis is a very popular reaction in modern organic and polymer chemistry. There are many different types like cross metathesis (CM), ring closing metathesis (RCM), ring opening cross metathesis (ROCM), ring opening metathesis polymerization (ROMP), acyclic diene metathesis polymerization (ADMET) and ring rearrangement metathesis (RRM). Metathesis reactions are used in industry and organic chemistry as well as for the production of hydrocarbon polymers.[54,55] Current researches concentrate on the synthesis of very complex functional materials.[54]

The general reaction mechanism according to Chauvin proposes a pairwise exchange of alkylidenes via a metallocyclobutane transition state[56] (see Figure 19).

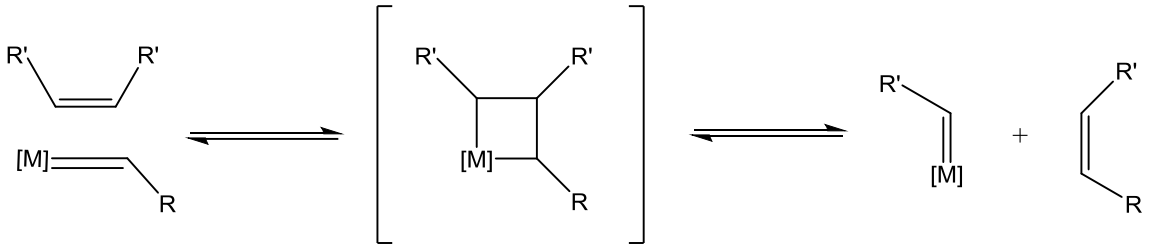

Figure 19: pairwise Chauvin mechanism[57]

The initiator, the monomer, the solvent and the reaction conditions have big influence on the metathesis reaction system.[54]

Metathesis initiators are complexes of transition metals[58,59] coordinated with anionic ligands, neutral electron donors and organic ligands.[59] Typically ruthenium, molybdenum or tungsten are used as central atoms. Halogens are common anionic ligands, whereas phosphines are examples for neutral electron donors. The general structure of metathesis catalysts is shown in Figure 20.[59]

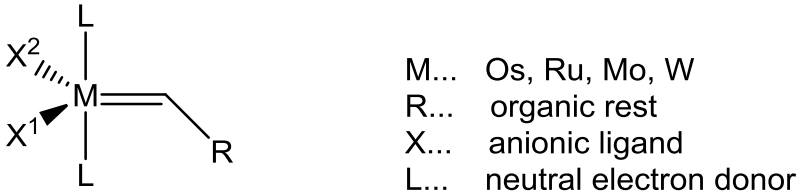

Figure 20: general structure of metathesis catalysts[59]

In the early stages Schrock type catalysts (see Figure 21) were applied to start metathesis reactions. These molybdenum alkylidenes provide rapid initiation[54,55] but are little tolerant towards functional groups[60]. Moreover they are sensitive to protic media and air.[54,61] Nowadays Grubbs catalysts and Hoveyda-type initiators[62] (see Figure 22 and Figure 23) are preferred. Even though the activity of 1st generation Grubbs catalysts is lower compared to Schrock catalysts[54], their compatibility with protic solvents and oxygen is advantageous.[54,55,60] 2nd generation Grubbs catalysts represent a further improvement as they tolerate functional groups[54,55,63] and have an increased activity.[64] A disadvantage however is the rather slow initiation. 3rd generation Grubbs catalysts are ultra-fast initiators which provide high polymerization rates, a high resistance towards functional groups and complete initiation.[54]

Hoveyda catalysts are stable towards oxygen and moisture.[54] Moreover degradation can be controlled efficiently.[62] Nevertheless they are rarely applied.[54]

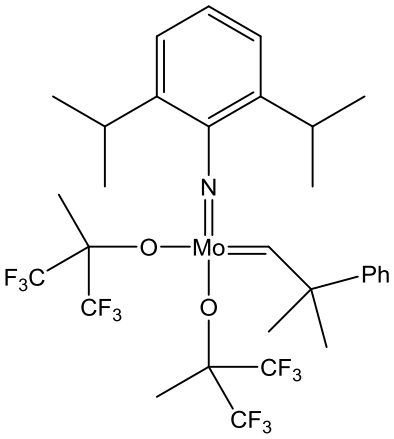

Figure 21: Schrock type catalyst[64]

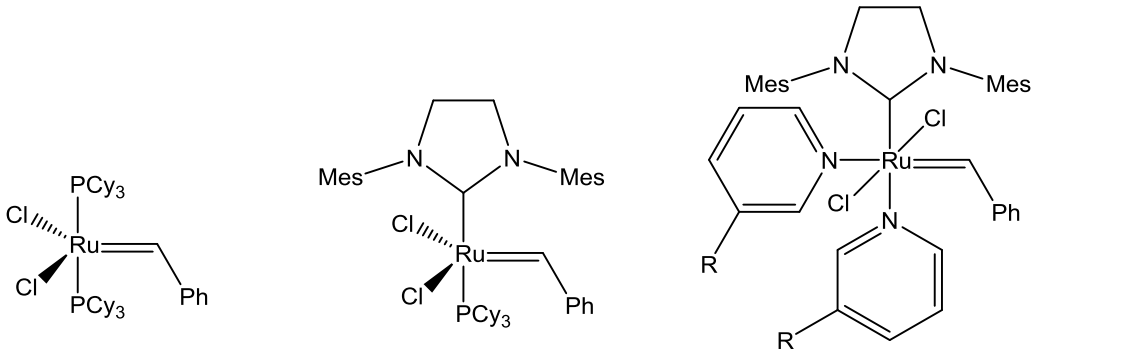

1st generation Grubbs **2nd generation Grubbs** **3rd generation Grubbs**

Figure 22: different Grubbs initiators[54]

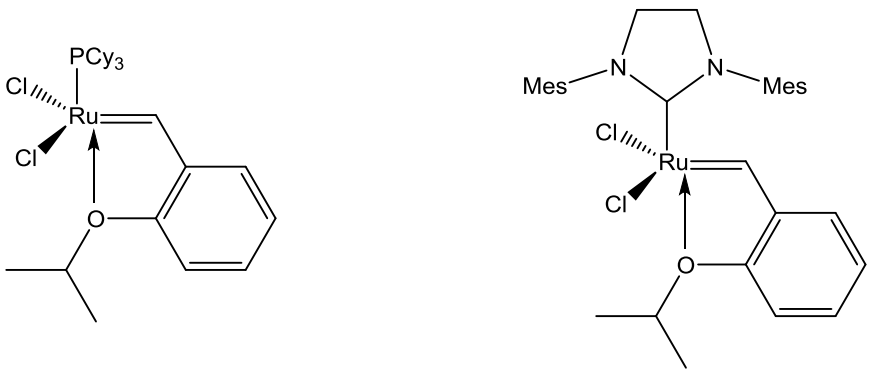

Figure 23: Hoveyda type initiators[54,59]

The olefin replaces one of the neutral ligands of the catalysts via an associative or a dissociative pathway. In the associative mechanism the olefin coordinates to the catalyst building an 18 electron complex. Then one of the neutral ligands dissociates from this transition state. In the dissociative pathway one neutral ligand leaves and the active catalytic species is generated. Thereafter the olefin coordinates to the free coordination site of this 14 electron complex.[56,60] Figure 24 shows these reaction mechanisms using a Grubbs 1st generation catalyst.

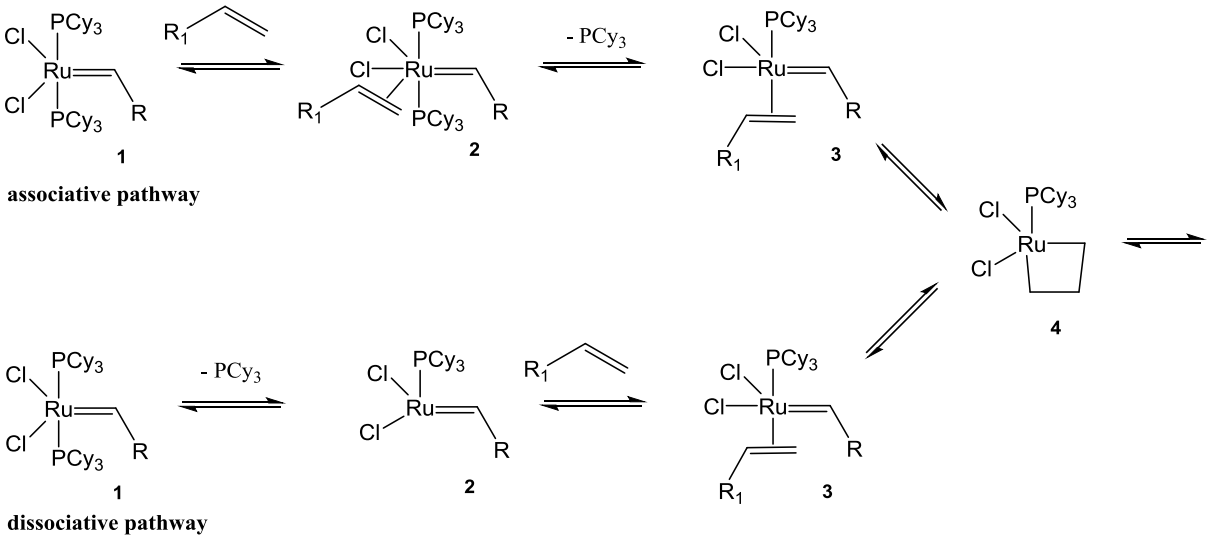

Figure 24: associative and dissociative reaction mechanisms with a Grubbs 1st generation catalyst[56]

Typical monomers for ROMP reactions are norbornene, norbornadiene, azanorbornene and 7-oxanorbornene. Moreover strained cyclic olefins like cyclobutene and cyclooctene can be polymerized with olefin metathesis. For the preparation of functional polymers norbornene derivates are preferred. Functional groups can be linked to the polymerizable moiety by esterification, etherification or amidation of norbornene carboxylic acid or norborneol. In general exo isomers react faster than endo isomers.[54]

Metathesis reactions can be executed in solution, bulk, or heterogeneous systems like emulsions or suspensions. Typical solvents are benzene, toluene, dichloromethane, acetone, alcohols or water. Usually they solute the initiator, the polymer and the monomer[54] providing a good interaction between the reactants. This explains how solvents influence the reaction rate.[65] Additionally donor solvents can be applied to guarantee homogenous reaction conditions. Additives like propan-2-ol, phenol or acetone speed up the reaction whereas diethylamine, pyridine or propan-2-thiol cause a delay or even a failure of the conversion. In bulk higher reaction rates can be observed.[54]

Elevated temperatures increase initiation and propagation and consequently the rate of polymerization. Secondary backbiting reactions become more important at high temperatures and prolonged reaction times.[54]

2.6.2 Metathesis degradation reaction

Inter- and intramolecular metathesis reactions degrade unsaturated crosslinked polymers to linear chains of different length and cyclic products.[66,67] These reactions are carried out in organic solvents like toluene, chlorobenzene[62] or dichloromethane[65] at mild conditions[64]. Due to the fact that natural rubber is very sensitive to side reactions[68,69,70] Grubbs type catalysts, which are selective and stable[70], are rather applied than classical tungsten and molybdenum chloride initiators.[68] Hence Grubbs or Schrock catalysts[63,64,71,72] are state of the art. Low molecular olefins like 1-octene[71,73] or ethylene may further support the reaction since they act as chain transfer agents.[62] Increased amounts of catalyst and a prolonged reaction time increase the degradation.[74]

The formation of linear metathesis products requires two reaction steps while cyclic products develop in a single-step mechanism. Therefore the latter reaction proceeds faster.[67]

Metal carbene catalysts transfer their carbene group to the polymer. Cyclic oligomers are formed in a backbiting mechanism (see Figure 25) or via cross metathesis (see Figure 26). In the latter there is a competition with the formation of linear oligomers.[75]

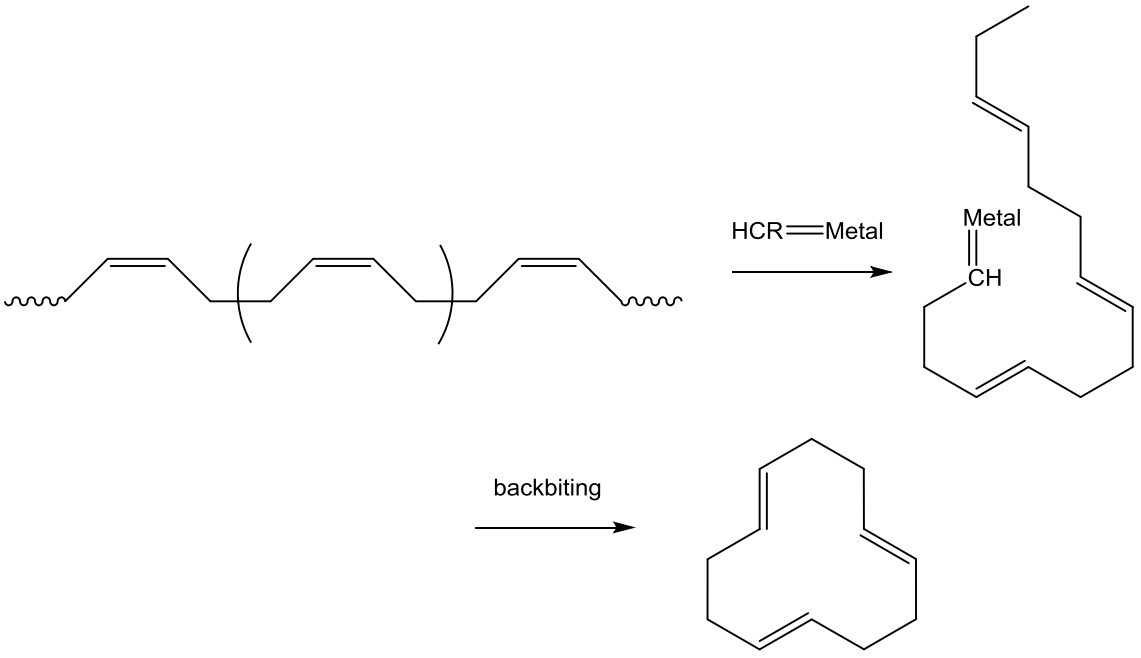

Figure 25: backbiting mechanism in olefin metathesis[75]

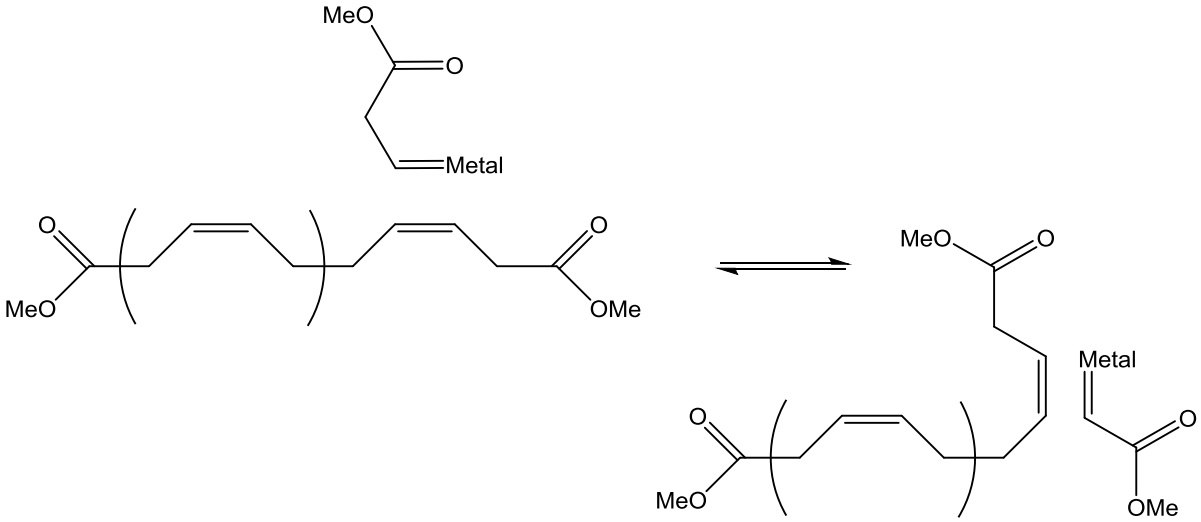

Figure 26: cross metathesis reaction machanism[75]

According to literature olefin metathesis degradation represents an alternative to pyrolysis and chemical dissolution of rubber in order to quantitatively determine the carbon black fillers of the compound.[76] Moreover it can be used to determine the amount of ethylene-propylene rubber in crosslinked blends with 1,4-polybutadiene.[73] Metathesis degradation is also used to study the microstructure and sequences of acrylonitrile/butadiene copolymers[77] and for the production of well-defined cyclic and telechelic oligomers.[75]

2.7 Principles of the applied analytic methods

2.7.1 Optical light microscopy

Optical light microscopes use visible light to produce magnified images of objects that are too small to be seen with the eye.[78] The condenser lens focusses the light onto a small spot of the sample. The objective lens collects the light that is diffracted by the specimen.[78,79] Usually the magnification can be varied by a revolving nosepiece that holds different objective lenses.[80]

The quality of the images depends on the brightness, the focus, the resolution and the contrast. The brightness of an image is related to the illumination system and the numeric aperture (large NA in bright images). Resolution is the ability to distinguish two points apart from each other. Furthermore the wavelength of the irradiated light and the numeric aperture have an influence on the image quality (short wavelengths and high NA for high resolutions).[79] A maximum magnification of 1000 times can be achieved by optical light microscopes.[79,80,81] The resolving power is limited by the number and quality of lenses as well as the applied wavelength.[81,82]

There are various modes of optical light microscopy. The two most important configurations are the bright field and the dark field mode. The bright field mode is the basic configuration.[79] The sample is illuminated with a filled cone of light[83] which allows little contrast. In the dark field mode higher contrasts can be achieved by a specific condenser lens that generates a hollow cone of light.[79,83] Images with a dark background and bright boundary areas can be obtained.[79]

2.7.2 3D-microscopy (infinite focus microscopy)

Infinite focus microscopes are optical 3D-measurment devices which vertically scan the samples' surfaces. A number of 2D-images are taken between the highest and the lowest focal plane. They are combined to one true color 3D-image. This technique provides high vertical and lateral resolutions (vertical: down to 10 nm, lateral: 400 nm) as well as high depths of field.[84] Typically the standard features include profile, area, form, volume and 2D-image analyses.[85] Moreover the roughness and surface texture can be measured.[84]

A variation of 3D-microscopes uses a laser source of short wavelengths for analysis purposes and a white light source for illumination. The sample can be shifted in an x-y-pattern and is scanned in z-axis. For each z-position the laser detects the intensity of the light reflected by the sample.[86]

2.7.3 Scanning electron microscopy (SEM)

In scanning electron microscopes an electron beam is focused onto the sample. Electrons of the sample atoms are excited by interactions between the specimen and the electron beam (2-40 keV[81]).[87,88] As a consequence various signals are produced: Secondary electrons (≤50 eV), backscattered electrons (≥50 eV), Auger electrons and x-rays (see Figure 28) can be detected.[87,89]

Scanning electron microscopy provides information about the topography[87] and the elemental composition of the specimen (contrast images).[89] Since the wavelength of electrons is shorter than that of visible light, electron microscopes offer higher resolutions than optical light microscopes[81,82]. The resolution of modern devices is in the range of 1-20 nm.[82] Magnifications up to 1.000.000 times are possible.[81] The drop shaped interaction volume of the sample ranges within a few micrometers[81,82] depending on the beam energy and the sample composition.[81,89] The spot size of the electron beam and the interaction volume further influence the resolution.[82] Furthermore scanning electron microscopes provide a high depth of field at high magnifications.[81]

The main components of scanning electron microscopes are the electron source, the column, which contains electromagnetic lenses to focus and navigate the electron beam, the sample chamber and the detector(s). A computer converts the signals into images which can be observed on a display. The column and the sample chamber are evacuated during the investigation.[82]

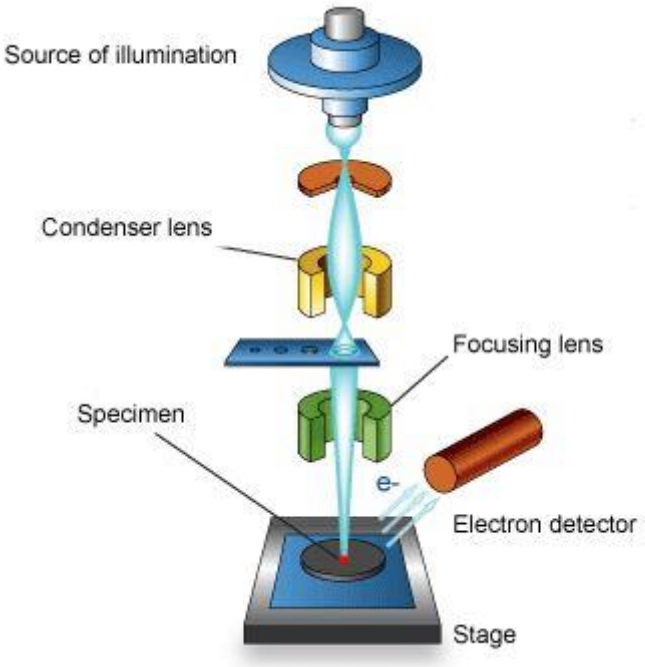

Figure 27: main components of a scanning electron microscope[90]

High energy primary electrons are emitted by thermionic heating or field emission at the top of the column and accelerated downwards by electromagnetic lenses.[82] Typical electron sources are tungsten filaments, solid state crystals of CeB_6 or LaB_6 or field emission electron guns.[81] The emitted electrons are focused to a narrow beam by passing through electromagnetic condenser lenses in the column. Scanning coils deflect the beam in x- and y-axis and allow an investigation of the sample surface in a raster fashion.[82]

Secondary electrons are ejected from sample atoms near the surface by interactions with the primary electrons.[81,89] They originate from depths of 1-10 nm[91] and have energies below 50 eV. Hence they are less energetic than the electrons of the beam.[81] Usually Everhart-Thornley detectors are used to collect secondary electrons. It consists of a Faraday cage which accelerates the secondary electrons towards a scintillator. The produced current is further detected by a photomultiplier.[82] Secondary electron images provide informations about the topography of the sample.[81]

Electrons which are elastically backscattered[89] by the sample's atoms can be detected by a second scintillator or a semiconductor.[82] The interaction volume of backscattered electrons is in the range of 0.1-1 µm.[91] They have higher energies than secondary electrons but still are less energetic than primary electrons.[81,89] These signals provide lower resolutions than secondary electrons because they originate from deeper regions of the specimen.[81] Elements of higher atomic masses backscatter the primary electrons more efficiently than elements of lower atomic masses. Hence information about the chemical composition of the sample can be obtained. The higher atomic mass the brighter the contrast.[81,91] A semiconductor detector additionally provides topographical information and the possibility to control the contrast.[82]

As the beam ejects inner-shell electrons from surface near atoms electron holes develop. They are filled up by electrons from outer orbitals. Due to the different energy levels of these two orbitals energy quants are released during this process.[87] The resulting x-rays develop within an interaction volume of about 0.2-2 µm[91] and have element specific wavelengths. As a consequence they provide information about the chemical composition of the sample.[87,88] Wavelength or energy dispersive x-ray spectrometers (WDX, EDX) are possible detectors whereas the latter is more common.[92] Energy dispersive spectrometers consist of a detector, a pulse processor and a multi-channel analyzer. The main part of the detector usually is a semiconducting silicon crystal which absorbs the x-rays emitted by the sample. Due to the corresponding energy uptake the generation of electron-hole pairs is initiated. A high bias voltage is applied across the crystal and separates the generated charges there. A field effect transistor converts the resulting charge signal to a voltage pulse which is subsequently passed to the pulse processor where it is amplified. The multi-channel analyzer generates a plot of intensity versus voltage.

Since the voltage is directly proportional to the energy of the characteristic x-rays this plot is used for qualitative evaluation.[92,93] Moreover the intensity of the signals allow conclusions about the abundance of the corresponding elements.[81,87]

The above mentioned vacancies can be filled up by a radiationless transition of outer electrons as well. The excess energy is released in form of electron emission. These so called Auger electrons originate from topmost atoms (10-20 Å) and provide information about the elemental composition of the surface and the chemical state of the atoms.[81,87] Compared to secondary and backscattered electrons only small amounts of Auger electrons develop.[81]

The electron-hole pairs generated by the beam-specimen interaction may recombine under emission of light.[81] The wavelength of the so called cathodoluminescence depends on the specimen specific bandgap. Thus it provides information about the composition of the sample.[81]

Figure 28 summarizes the different signals that can be observed in scanning electron microscopy.

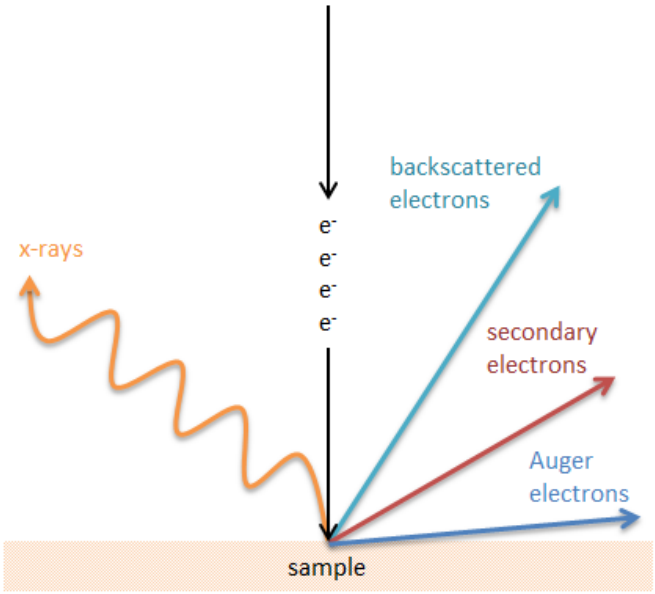

Figure 28: variety of SEM signals

3. Experimental Part

In this master thesis two sets of samples prepared by Continental Reifen Deutschland GmbH are investigated. The T-test block samples consist of brass coated steel cords or monofilaments vulcanized into rubber. The influences of different aging and heating conditions on the rubber metal interface are investigated.

In general the rubber composites contain natural rubber, carbon black, zinc oxide, cobalt stearate, sulfur, aging-resisters, an accelerator system and a resin system. The effects of cobalt stearate, accelerator system and sulfur level are monitored by altering the rubber composition (see Table 1 and Table 3).

3.1 Set 1

The samples of set 1 consist of brass coated steel cords which are vulcanized into rubber. T-test blocks of five different rubber compound compositions (recipes) are produced and aged using four different conditions (series 1-4). Besides the reference recipe there are samples without cobalt stearate, samples which are vulcanized using different vulcanization accelerators and samples which contain reduced amounts of sulfur. Moreover samples without aging-resisters and resin systems are produced. The samples of the unaged series (series 1) are vulcanized at 160 °C for 20 minutes. Additionally all recipes are aged for two days under oxygen at 70 °C, for five days under steam at 105 °C and for fourteen days under humidity at 70 °C (series 2-4). Table 1 and Table 2 list these recipes and aging conditions.

Table 1: different rubber compound recipes, set 1

Sample denotation	Description of the different recipes
Ref	Model recipe for a steel cord adhesion compound
Co	Rubber compound does not contain cobalt stearate
TBBS	TBBS replaces DCBS as accelerator
S	Rubber compound contains less sulfur (1/5)
strip	Recipe does not contain aging-resister and resin system

Table 2: different aging conditions (series 1-4), set 1

Series	Time	Temperature	Medium
1	unaged	160 °C	-
2	2 days	70 °C	O_2
3	5 days	105 °C	steam
4	14 days	70 °C	humidity

3.1.1 Exposure of the rubber metal interfaces by metathesis degradation

The rubber surrounding the cords is cut off as far as possible without damaging the rubber metal interface. Then the samples are put into toluene in order to swell the remaining rubber (see Figure 29). After some hours it is cut again and the prepared cords are stored in toluene. Schlenk-flasks are evacuated and flushed with inert gas (N_2) and further treated with a heat gun to remove possible contaminations. The rubber residuals on the cords are degraded in the following metathesis reaction which can be started after heating the oil bath to 110 °C. The flasks are filled with about 4 ml toluene and 3 mg of catalyst 1 or 2 (see Figure 30) against a counter flow of inert gas. The samples are put into the solutions and arranged in a way they do not get in touch with the flasks' wall or the magnetic stir bars in order to prevent a damage of the rubber metal interfaces (see Figure 31). After adding 100 µl of 1-octene the solutions turn to black and get turbid. This change indicates the reaction's onset and can be derived from the release of carbon black which is used as filler in rubber compounds. After one hour the cords are slewed in toluene to remove loose residues on the surfaces. This process is repeated until no rubber is left on the surfaces and they appear metallic. Finally the exposed interfaces are washed in toluene and carefully treated with a brush.

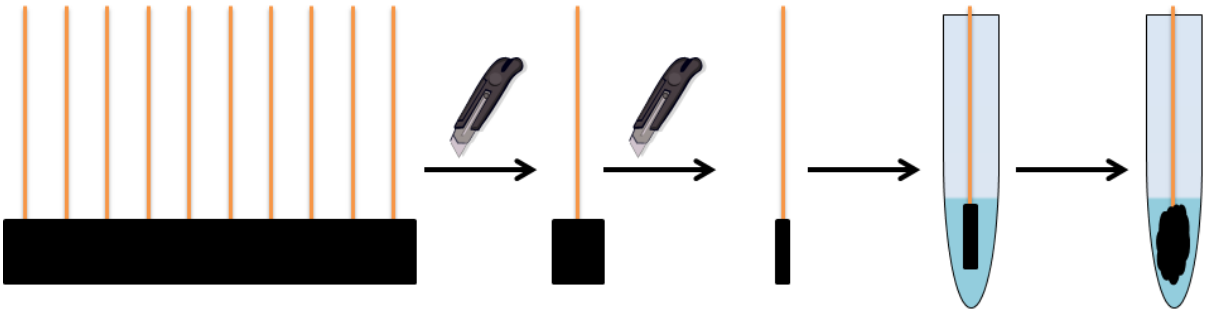

Figure 29: sample preparation, cutting and swelling

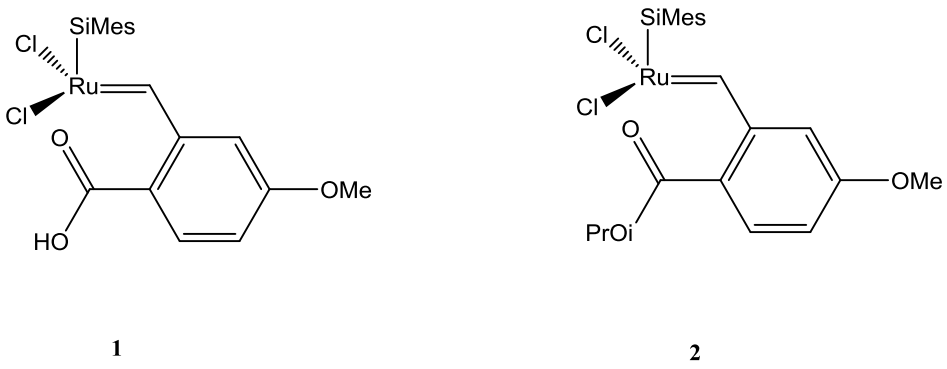

1 2

Figure 30: catalysts 1 and 2

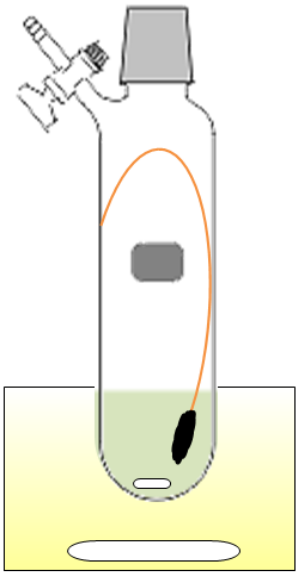

Figure 31: experimental set-up for olefin metathesis degradation

3.1.2 Exposure of the rubber metal interface using the filter paper method

Moreover T-test blocks of the same compositions are prepared by filter paper method. They are aged under the same conditions than the samples which are degraded by olefin metathesis. The rubber can be removed more easily because the filter paper yet separates it from the metal. All aged filter paper samples are exposed using a tension testing machine.

Three cords of each recipe and aging condition are investigated to provide a suitable confidence level by triple determination. This applies not only for the samples exposed by metathesis degradation but also for the filter paper samples.

3.1.3 Optical Microscopy

At first the cords are separated into their filaments. At least two regions of each filament are investigated at various magnifications using an optical microscope. It is essential to pick regions that have been turned to the outside of the cord and hence contacted the rubber. The resulting pictures are analyzed with respect to color and structure.

3.1.4 3D-Microscopy

At least two filaments of each sample are investigated by means of 3D-microscopy. An additional light source provides better illumination at the samples' edges in order to prevent a loss of information due to their bending. The corresponding atomic force microscopy (AFM) software draws a height profile using microscope pictures of fifty

different plains. Moreover it calculates several roughness parameters of which only the roughness average is considered in detail. The roughness profile is illustrated visually as well, although this illustration has to be corrected with respect to the samples' bend: the resulting arch is recalculated to a plane.

Due to the 3D-microscope images and the roughness average one filament of each recipe and aging condition is chosen and further investigated with SEM. A scalpel cut assigns the region investigated in 3D-microscopy in order to be able to relocate it in SEM. Unfortunately this does not work for all samples.

3.1.5 Scanning Electron Microscopy

A total of three areas per filament are investigated by means of scanning electron microscopy at a magnification of 1000 times. For each area the elemental composition is analyzed by the EDX detector. Within the assigned area mappings for sulfur, copper, zinc and iron are recorded. The resulting images monitor the relative distribution of the elements. Additionally the color intensity allows conclusions about their abundance. Moreover point analyses at a magnification of 10,000 times are done. Topographic and material contrast pictures of various areas and selected spots are taken.

Based on the assumption that the copper content changes the least, the EDX results are normalized to 100% copper during data processing. This offers an easy way to compare the elemental content of all elements.

3.1.6 Physical data

In addition to the already mentioned investigations, measurements providing physical data are executed by Continental Reifen Deutschland GmbH. Pullout forces and coverage values are determined according to ASTM D2229 and D1871. Moreover the shore hardness (DIN 53505), the resilience (DIN 53512), the tensile strength, the break energy density and the tear elongation are recorded. The last three parameters are determined according to DIN 51220.

3.2 Set 2

The samples of set 2 consist of brass coated steel monofilaments replacing the cords used in set 1. This holds several advantages concerning sample preparation, degradation and analysis which are discussed below.

In set 2 T-test block specimen using four different rubber compound compositions are produced. Besides the reference recipe there are samples without cobalt stearate, samples which are vulcanized using different vulcanization accelerators and samples which contain reduced amounts of sulfur (see Table 3). All recipes are aged for five days under steam at 105 °C and for fourteen days under humidity at 70 °C (see Table 4). All samples are heated isothermally with the exception of one series. Series 8 contains athermally treated reference samples which serve for the investigation of the influence of different energy inputs (see Table 5).

The unaged specimens of set 1 are vulcanized at 160 °C for 20 minutes while those of set 2 are heated to 170 °C for 10 minutes. Although these samples are prepared differently, concerning temperature and curing time, they receive the same energy input.

Table 3: different rubber compound recipes, set 2

Sample denotation	Description of the different recipes
Ref (5/170)	Model recipe for a steel cord adhesion compound, 5 min energy input
Ref	Model recipe for a steel cord adhesion compound, 10 min energy input
Co	Rubber compound does not contain cobalt stearate
TBBS+MBT	TBBS and MBT replace DCBS as accelerator
S	Rubber compound contains less sulfur

Table 4: different aging conditions (series 5-7), set 2

Series	Time	Temperature	Medium
5	10 min (unaged 2)	170 °C	-
6	5 days	105 °C	steam
7	14 days	70 °C	humidity

Table 5: different energy inputs (series 8), set 2

Sample	Recipe	T_{max}[°C]	Heating rate[°C/min]
1	Ref	170	60
2	Ref	170	6
3	Ref	140	6
4	Ref	140	60

Again three cords of each recipe and aging/heating condition are prepared to provide a suitable confidence level by triple determination.

Additionally three filaments originating from a real car tire are exposed and investigated in set 2.

Moreover three cords of the reference and the low sulfur recipe of set 1 are degraded after a four months period of storage. Only one filament of each recipe is further investigated in SEM to get an idea if the stored samples have changed significantly.

The exposure of the rubber metal interface is conducted as described for set 1 (see chapter 3.1.1). Three samples of the same recipe can be degraded simultaneously in one Schlenk's flask due to the small diameter of the monofilaments.

Also the investigations using optical light microscopy, 3D-microscopy and SEM are conducted as described for set 1. Again the physical data is provided by Continental Reifen Deutschland GmbH. In set 2 all monofilaments are investigated by means of 3D-microscopy. Two samples of the same recipe and aging/heating condition are investigated with SEM. In set 2 the point analyses at a magnification of 10,000 times are more emphasized whereas only one area per monofilament is analyzed at a magnification of 1000 times. The elemental composition and mappings are obtained from the latter. Moreover pictures are taken at a magnification of 100 times to provide an overview of the investigated monofilament.

4. Results and discussion

Concerning the different recipes the following expectations are reasonable:

The rubber composition of the reference samples is a model recipe for typical steel cord adhesion compounds. An impairment of adhesion is estimated for the samples without cobalt stearate, the samples accelerated by TBBS and the low sulfur samples.

The absence of cobalt stearate is expected to cause separation between rubber and brass. For the samples aged under humid conditions or in steam drastic effects are estimated.[15,25,30]

If TBBS is used instead of DCBS, which is the conventional promoter, sulfur diffusion is accelerated during vulcanization. Thus the crosslinking of the rubber proceeds more rapidly and there is not enough time to achieve an adequate degree of sulfidation. It is assumed that no proper adhesion interface of Cu_xS can be developed.[5,13,15]

Sulfur does not only participate in the sulfidation process but is responsible for the crosslinking of the rubber as well. Thus appropriate adhesion of rubber to brass needs sufficient amounts of sulfur. The low sulfur samples lack these conditions and hence are estimated to build an interface of little adhesion strength.[30]

The strip recipe is reduced to the essential ingredients and expected to show similar behavior than the reference. Due to the absence of aging-resisters in the rubber compound the different aging conditions are estimated to affect the rubber properties significantly.

Unless otherwise mentioned the following statements and conclusions are based on data from isothermally heated samples.

4.1 Evaluation of the physical data

The vulcanization behavior is influenced by the rubber composition of the samples. Figure 32 shows the progress of vulcanization for all recipes of set 2. The evolution of the shear forces during vulcanization is illustrated in Figure 33. The corresponding curves of set 1 are illustrated in the appendix and provide the same results (see Figure 61 and Figure 62).

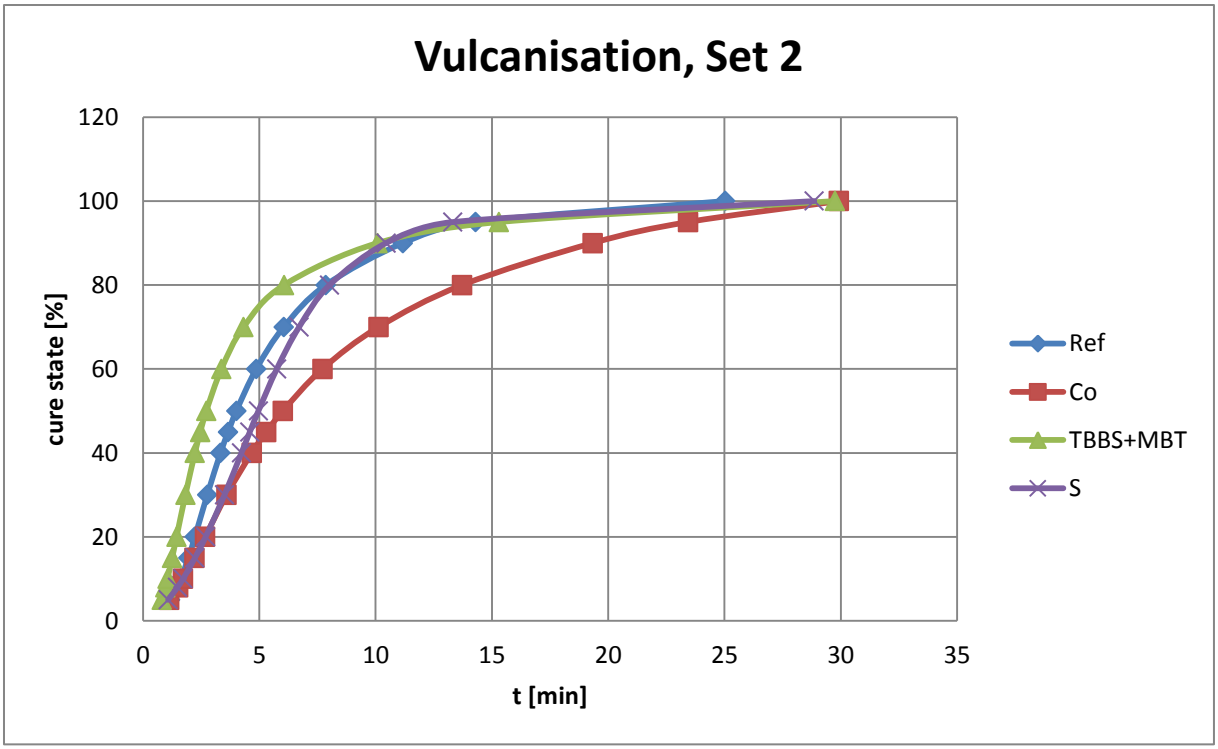

Figure 32: vulcanization progress of all isothermally heated recipes, set 2

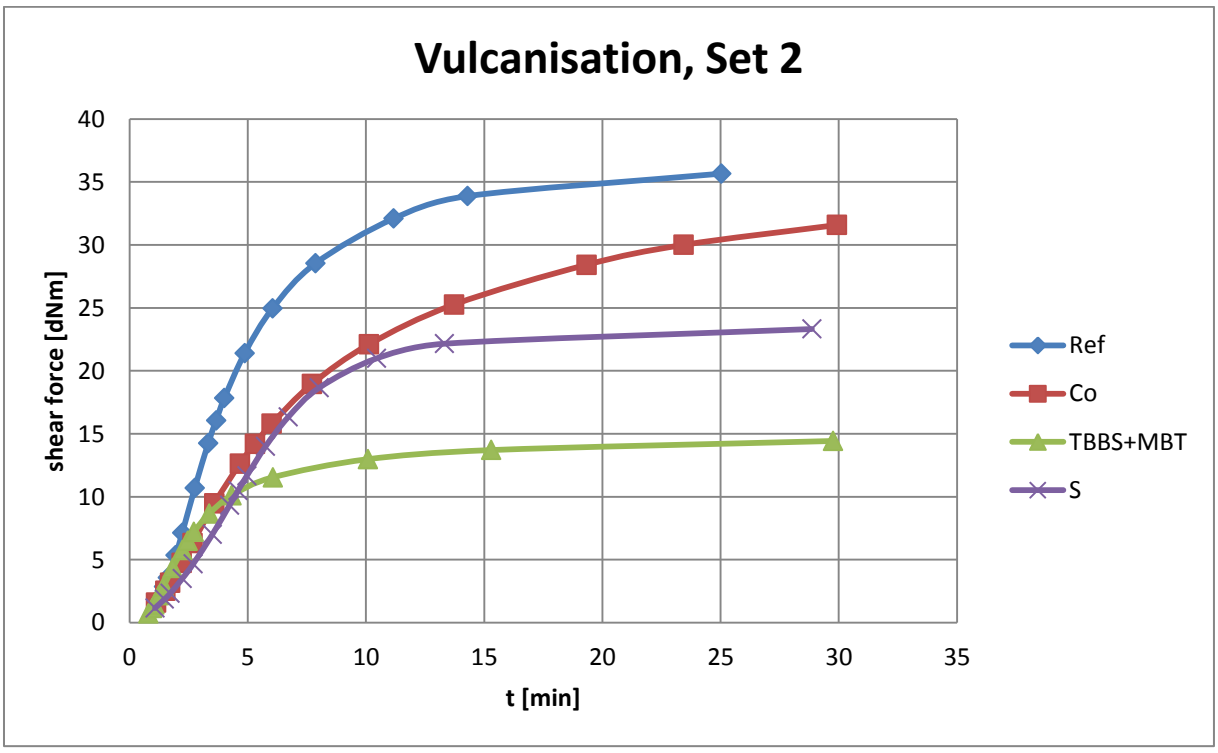

Figure 33: evolution of the shear forces of all isothermally heated recipes during vulcanization, set 2

4.1.1 Unaged samples

As shown in Figure 32 the acceleration with a mixture of **TBBS and MBT** leads to steeper curves for the vulcanization progress than DCBS in the reference samples does. Hence sulfur is consumed more quickly by the crosslinking reaction. One can reasonably expect that not enough sulfur may be able to reach the metal surface in order to contribute to the development of a proper adhesion interface. Nevertheless the corresponding values for the pullout force, the tensile strength, the tear elongation and the break energy density do not deviate significantly from the results of the reference samples (see Figure 34, Figure 36 and Figure 37). In combination with the high coverage values (98%) good adhesion properties can be suggested (Figure 35). The shear forces of about 15 dNm amount to only the half of the reference values (see Figure 33). This, in contrast, indicates that comparatively soft rubber networks develop when a combination of TBBS and MBT is used as vulcanization accelerator.

In set 1 DCBS is replaced by TBBS only. The corresponding shear forces are twice as high as the results of set 2 (see Figure 33 and Figure 62 (in the appendix)). Hence it can be concluded that MBT influences the acceleration of the vulcanization process and therefore the rapid consumption of sulfur more significantly than TBBS does.

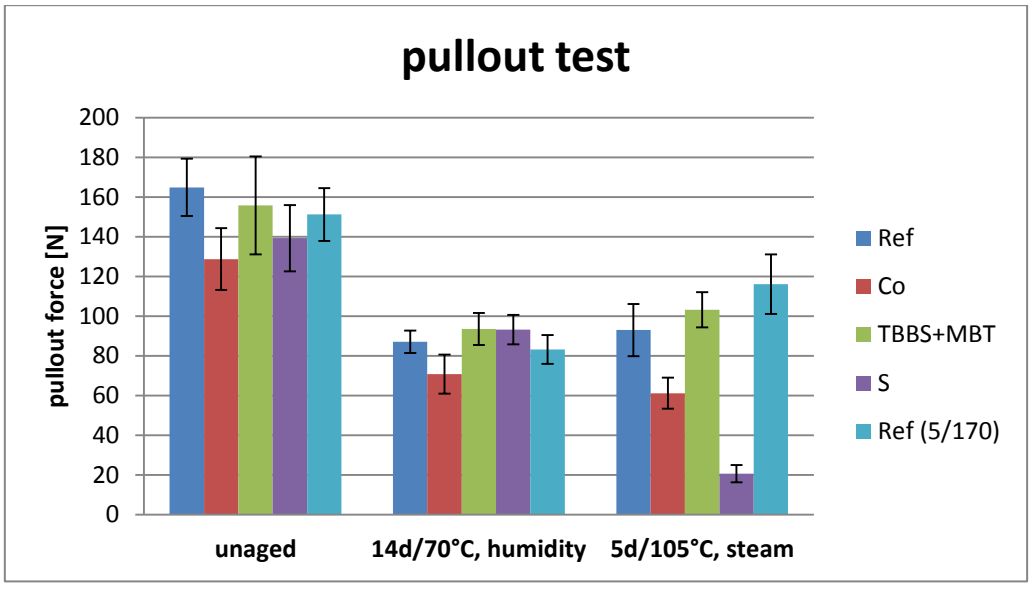

Figure 34: results for the pullout forces of the isothermally heated samples, set 2

The **absence of cobalt stearate** slows down the vulcanization process resulting in a flat curve which is not saturated at the end of the experiment. This implies that vulcanization might not be finished yet and the rubber network has not reached its full strength. However the tensile strength, the tear elongation and the break energy density of the samples without cobalt stearate equal or exceed the values of the

reference samples (see Figure 36 and Figure 37). This indicates that the rubber network is of satisfying strength and elasticity. The shear forces which are only slightly lower than those of the reference samples support this conclusion as well (see Figure 33). Since the coverage values are still over 90% (see Figure 35) a failure in the rubber network and not at the adhesion interface is implied. The reason for the comparatively low pullout forces of 129 N is not completely clarified (see Figure 34).

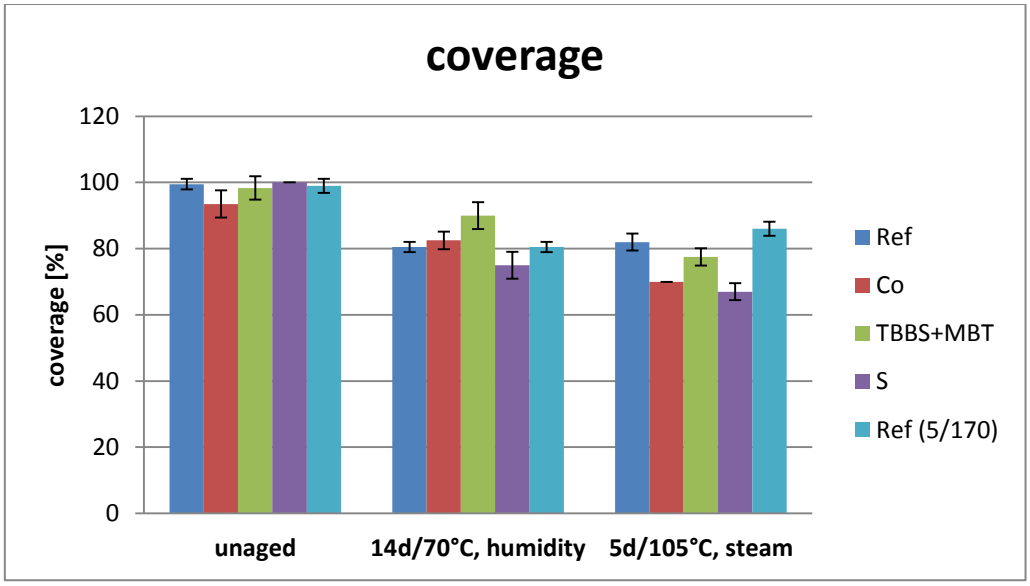

Figure 35: coverage values of the isothermally heated samples, set 2

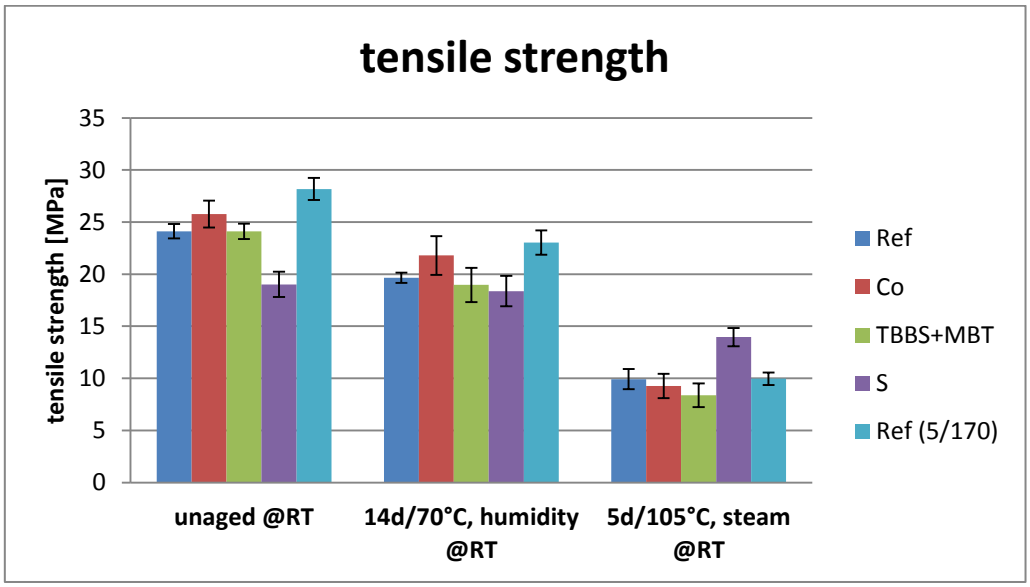

Figure 36: results for the tensile strength of the isothermally heated samples, set 2

Since sulfur is the crosslinking agent in vulcanization relatively loose networks are expected for the samples with **reduced sulfur contents**. Although the course of the vulcanization progress (see Figure 32) is comparable to that of the reference samples the shear forces of about 23 dNm account for only two thirds of the reference values (see Figure 33). Hence a reduced crosslinking density which results in a rather soft rubber compound is indicated. This is further supported by the low values for the shore hardness (65 shore), the tensile strength (19 MPa) and the break energy density (34 J/cm^3) which are illustrated in Figure 36 and Figure 37. The pullout forces of the low sulfur samples amount to 139 N and are therefore lower than the values for the reference samples (165 N). Together with the satisfying coverage values of 100% it can be concluded that the failure does not originate at the adhesion interface but in the rubber again (see Figure 34 and Figure 35).

The reference samples treated with half the energy input (**Ref (5/170)**) show slightly increased values for the tensile strength (28 MPa) and the pullout forces (151 N) compared to the reference (24 MPa; 165 N). This is illustrated in Figure 36 and Figure 34. The shore hardness and resilience are comparable to the results of the reference samples whereas the tear elongation and the break energy density exceed the reference values (see Figure 37). The coverage of the Ref (5/170) amounts to 99% (see Figure 35). The good rubber properties and high coverage values indicate that the failure occurs in the rubber network.

The curve for the vulcanization progress of the **strip recipe** (set 1) declines at the end of the experiment (see Figure 61 in the appendix) indicating the onset of reversion. According to the corresponding shear forces (21 dNm), which are comparable to that of the low sulfur samples, the rubber network is not very dense (see Figure 62 in the appendix). The pullout forces only deviate slightly from the corresponding values of the reference samples (see Figure 63 in the appendix). The coverage is about 92% (see Figure 64 in the appendix). This implies that the failure is located in the rubber network. Nevertheless neither the moderate shore hardness and tear elongation nor the slightly increased values for the tensile strength and break energy density indicate that the rubber component is notably soft (see Figure 65 in the appendix).

In general the shore hardness is little depending on the rubber composition. A slight decrease can be observed when the samples are heated to 70 °C (see Figure 37).

The resilience is also barely influenced by the rubber composition, but increases from about 40% to 52% with rising temperatures (see in Figure 37). The samples without cobalt stearate show the highest resilience (42%) while reduced sulfur levels lead to the lowest values (36%).

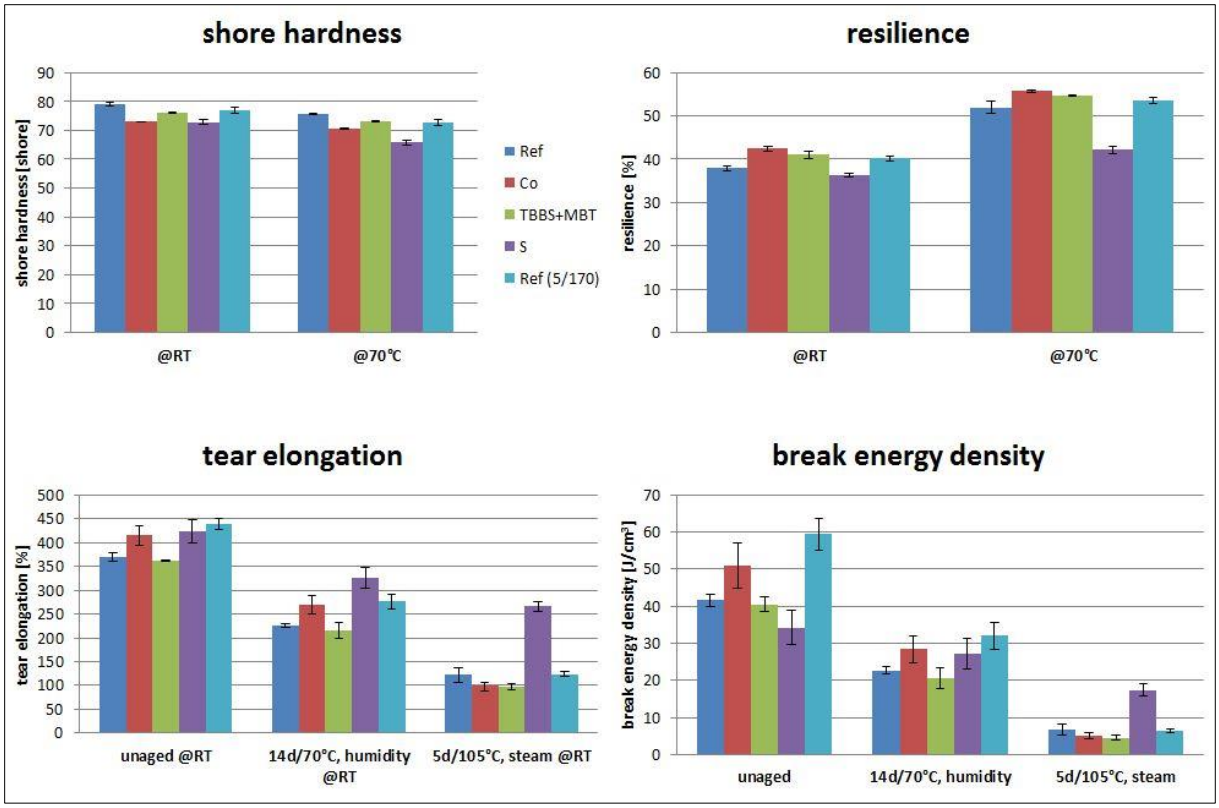

Figure 37: results for the shore hardness, resilience, tear elongation and break energy density of the isothermally heated samples, set 2

Concerning the **athermally heated samples** (series 8, set 2) most of these parameters provide similar results. The pullout forces and the shore hardness values of the samples heated to 140 °C (pullout force: 156 N; shore hardness: 76 shore) slightly exceed those heated to 170 °C (pullout force: 167 N; shore hardness: 80 shore). The samples heated to 170 °C may be compared to the isothermally heated Ref (5/170) samples while the first behave more like the isothermally heated reference sample.

To sum up the expectations concerning adhesion failure are not fulfilled throughout the unaged series. All samples show good coverage values which indicate that the failures provoked in the pullout tests originate in the rubber network.

4.1.2 Aged samples

Generally the pullout forces and the coverage values decrease during the different aging processes (see Figure 34 and Figure 35). While the pullout forces of the unaged series vary between 165 N and 123 N, the corresponding pullout forces of the fourteen days humidity aged series vary between 94 N and 71 N and those of the five days steam aged series between 116 N and 21 N. Aging the samples for fourteen days under humidity at 70 °C reduces the average coverage value of 98% (unaged) to 82% while the five days steam aging at 105 °C lowers it to 77%. The average pullout forces are reduced from 148 N to 86 N after humidity aging and to 79 N after steam aging.

The results of set 1 show that the shore hardness slightly increases during aging. After aging for fourteen days under humidity at 70 °C the average of 75 shore rises to 81 shore (see Figure 65 appendix).

According to the results of set 1 the resilience is not influenced by humidity aging for fourteen days at 70 °C (see Figure 66 in the appendix).

In general, the tensile strength, the tear elongation and the break energy density decrease during aging (see Figure 36 and Figure 37). Especially the five days steam aging at 105 °C has big impact on these three parameters. The only exception is the low sulfur recipe which is influenced in a comparatively small extent during aging.

A striking effect on the pullout forces and coverage values is observed for the **low sulfur** samples after aging for five days under steam at 105 °C. The comparatively low pullout force of 21 N and the decreased coverage value which accounts for 67% indicate that the adhesion failure originates at the rubber metal interface which is severely attacked under these conditions (see Figure 34 and Figure 35). This can also be observed if the low sulfur samples are aged for two days under oxygen at 70 °C and for fourteen days under humidity at 70 °C (see Figure 63 and Figure 64 in the appendix). The effect of the latter is less obvious. The tensile strength, the tear elongation and break energy density of the low sulfur samples only change in a small extent during aging (see Figure 36 and Figure 37). Hence the rubber compound is not attacked heavily. This further supports the above drawn conclusion that the failure occurs at the weakened adhesion interface.

The **absence of cobalt** stearate weakens the rubber which can be concluded from the decreased pullout forces at all aging stages (Figure 34). After aging for fourteen days under humidity at 70 °C the initial value of 129 N is reduced to 71 N, after aging for five days under steam at 105 °C it even drops to 61 N. The coverage values are lowered from 93% to 83% by humidity aging for fourteen days and to 70% by steam aging for five days (Figure 35). As mentioned in chapter 2.3 cobalt ions slow down dezincification[17,19] and increase the durability of the rubber metal bond especially after aging.[15,29,38,39] The corresponding values for the pullout force and the coverage suggest that the adhesion interface is severely attacked by five days steam aging at

105 °C under the absence of cobalt ions. For this reason partial adhesion failure at the rubber metal interface is suggested. Moreover the corresponding values for the tensile strength, the tear elongation and the break energy density decrease considerably during aging (see Figure 36 and Figure 37). This indicates that these rough conditions additionally attack the rubber network.

The coverage of the samples accelerated with a mixture of **TBBS and MBT** decreases from 98% to 90% after fourteen days humidity aging at 70 °C and to 78% after five days steam aging at 105 °C (see Figure 35). Thus it is concluded that only steam aging might cause adhesion failure at the rubber metal interface. The corresponding pullout forces decrease from 156 N to 94 N for the humidity aged samples and to 103 N for the steam aged samples. Moreover the rubber is heavily affected by both aging conditions as the tensile strength, the tear elongation and the break energy density decrease significantly (see Figure 36 and Figure 37).

The samples which are vulcanized with half the energy input (**Ref (5/170)**) show similar pullout forces and coverage values to the reference samples throughout all aging states (see Figure 34 and Figure 35). After steam aging for five days at 105 °C the pullout force is even slightly higher than the reference value. Compared to the reference the Ref (5/170) samples show increased values for the tensile strength, the tear elongation and the break energy density in the unaged and fourteen days humidity aged state (see Figure 36 and Figure 37). In contrast steam aging for five days causes an extreme decrease of these three parameters. The corresponding absolute values for the Ref (5/170) samples nearly equal those of the reference samples. Table 6 lists the corresponding values for the discussed data.

Table 6: results for the tensile strength, tear elongation and break energy density of the reference and Ref (5/170), set 2

		tensile strength [MPa]	tear elongation [%]	break energy density [J/cm^3]
Ref	unaged	24	370	42
	14d, humidity, 70 °C	20	226	23
	5d, steam, 105 °C	10	122	7
Ref (5/170)	unaged	28	439	59
	14d, humidity, 70 °C	23	276	32
	5d, steam, 105 °C	10	124	6

The pullout forces of the **strip recipe** (set 1) decrease during aging (see Figure 63 in the appendix). After humidity aging for fourteen days at 70 °C the pullout force only accounts for 55% of the initial value (unaged). Steam aging for five days at 105 °C has less impact on the strip recipe as the value is only reduced from 92% (unaged) to 80%. The same pattern is observed for the coverage values which are reduced to a higher extent during aging for fourteen days under humidity (see Figure 64 in the appendix). As mentioned in chapter 4.1.1 the corresponding high pullout forces and coverage values suggest a failure in the rubber network for the unaged samples. In contrast the results for the aged strip samples indicate that the rubber metal interface is weakened during aging and adhesion partially fails at the rubber metal interface. This effect is even worse after two days aging under oxygen at 70 °C. Due to the absence of aging-resisters one can reasonably expect that the rubber compound weakens during aging. This is confirmed by the results for the tensile strength, the tear elongation and the break energy density at all aging states (see Figure 65 in the appendix). Extreme effects are observed after oxygen aging for two days at 70 °C and steam aging for five days at 105 °C. The tensile strength, the tear elongation and the break energy density decrease during all aging conditions. Table 7 illustrates the corresponding values for the discussed data.

Table 7: results for the tensile strength, tear elongation and break energy density of the strip recipe, set 1

		tensile strength [MPa]	tear elongation [%]	break energy density [J/cm^3]
strip	unaged	25	426	50
	14d, humidity, 70 °C	19	227	21
	2d, oxygen, 70 °C	8	63	4
	5d, steam, 105 °C	6	147	5

To sum up steam aging for five days at 105 °C heavily attacks the rubber compounds and adhesion interfaces of all recipes. The low sulfur samples and the samples without cobalt stearate show adhesion failure at the rubber metal interface after steam aging. Additional failures located in the adhesion interface are observed for the humidity aged low sulfur samples and the oxygen aged strip recipe.

4.2 Comparison cord - monofilament

Unless otherwise mentioned the following statements and conclusions are based on data from samples degraded by metathesis reaction.

The application of monofilaments holds several advantages over the use of cords with regard to sample preparation, degradation and the analysis procedure. The following findings result from a comparison between set 1 and set 2. The cords of set 1 consist of eleven filaments which are twisted together while the monofilaments of set 2 are straight wires (see Figure 38).

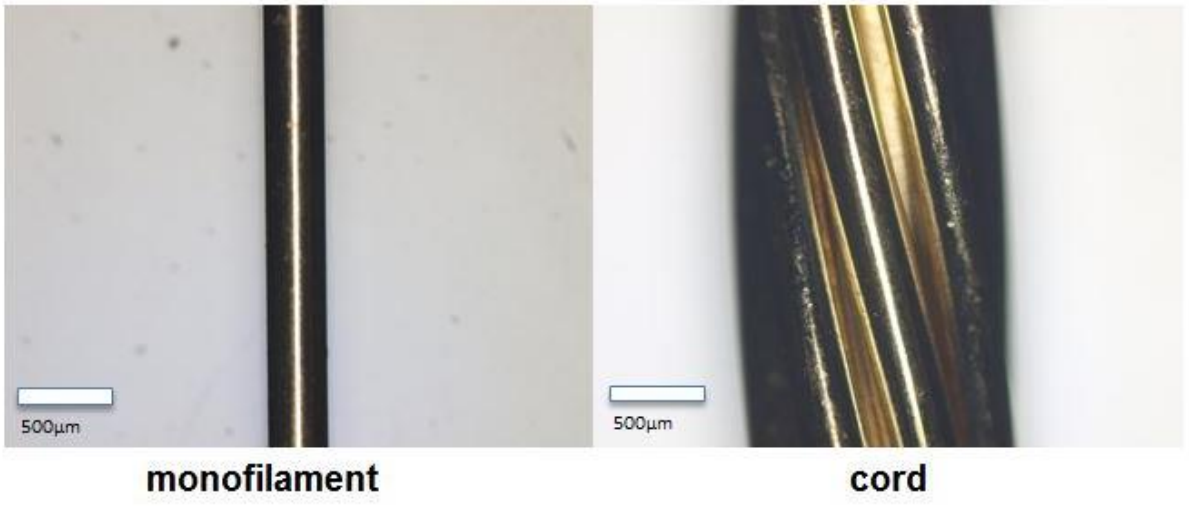

Figure 38: comparison of cord and monofilament (optical light microscopy, 500x)

During sample preparation more rubber can be cut off after swelling in toluene if the thinner monofilaments are used instead of the cords. As a consequence less repetitions of the metathesis degradation reaction are required for a complete exposure of the rubber metal interface. While only one cord can be applied in a Schlenk's flask further time can be saved by the simultaneous treatment of three monofilaments. Another disadvantage of the cords is that little amounts of rubber remain in the gaps between the different filaments. It is assumed that these gaps do not provide sufficient access to the reaction solution. Thus the residuals cannot be removed from the cords. In contrast less rubber residuals remain on the monofilaments. This can be observed in optical light microscopy as well as in SEM (see Figure 39).

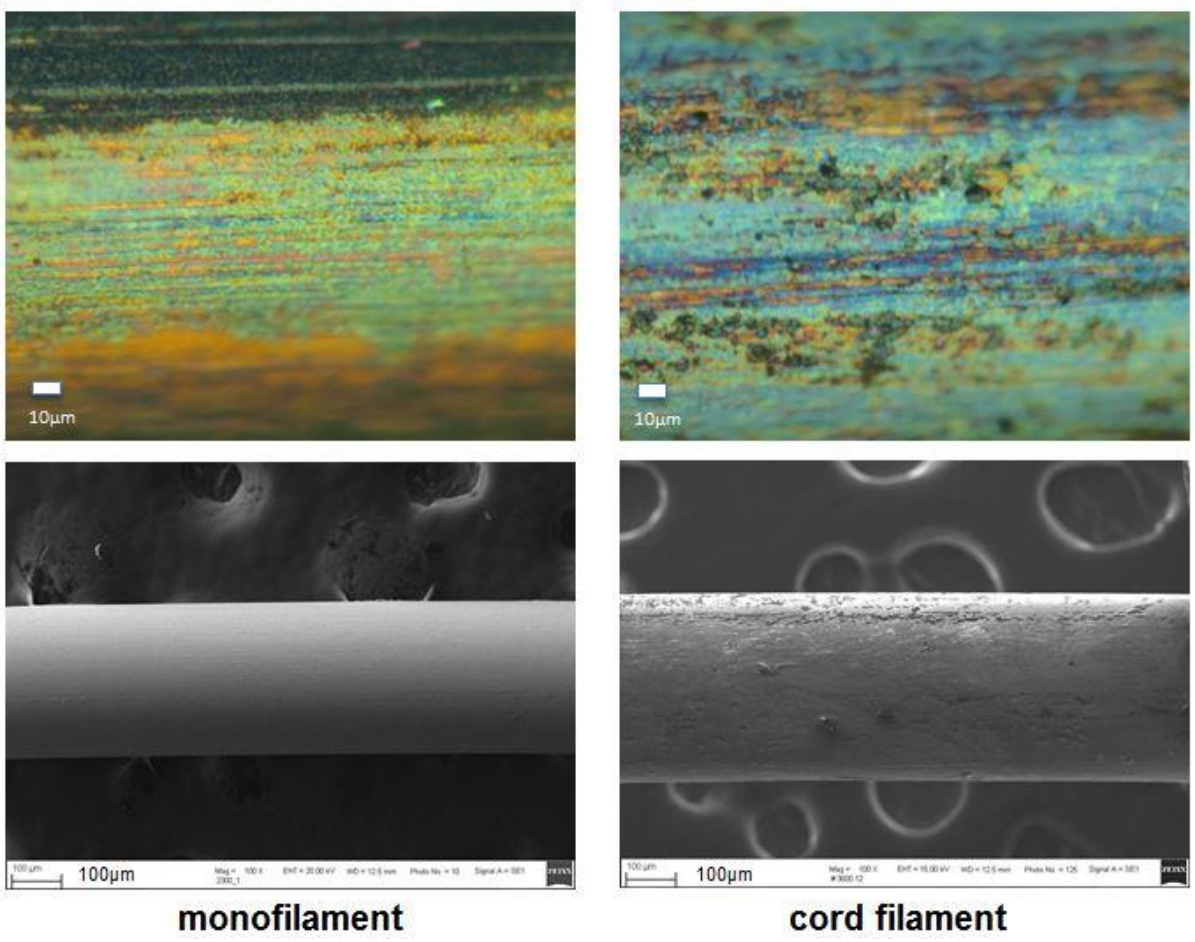

Figure 39: optical light microscopy (1000x) and SEM images (100x) of unaged reference samples, set 2 (left, monofilament) and set 1 (right, cord filament)

Furthermore the straight monofilaments can easily be attached onto the different specimen holding devices while the attachment of the twisted cord filaments is more problematic. For the investigation with optical light microscopy or 3D-microscopy modelling clay is used to fix the samples onto glass or plastic substrates. In general the round shape of wires makes focusing difficult. Additionally some twisted cord filaments cannot be arranged in-plane but protrude from the sample holders' surfaces (see Figure 40). This further complicates focusing and leads to more blurred images. Figure 41 illustrates the different quality of optical light microscopy images of mono- and cord filaments using unaged reference samples of set 1 and 2.

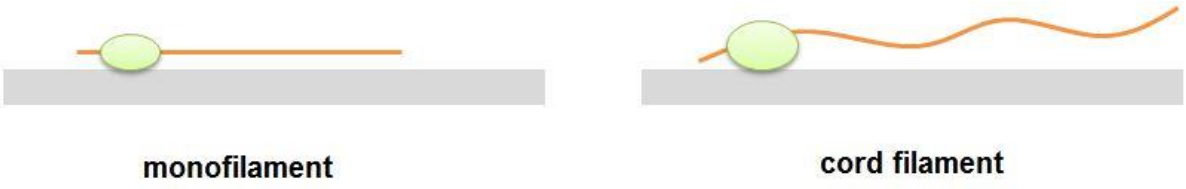

Figure 40: fixation of monofilaments and cord filaments onto the sample holder in optical and 3D-microscopy

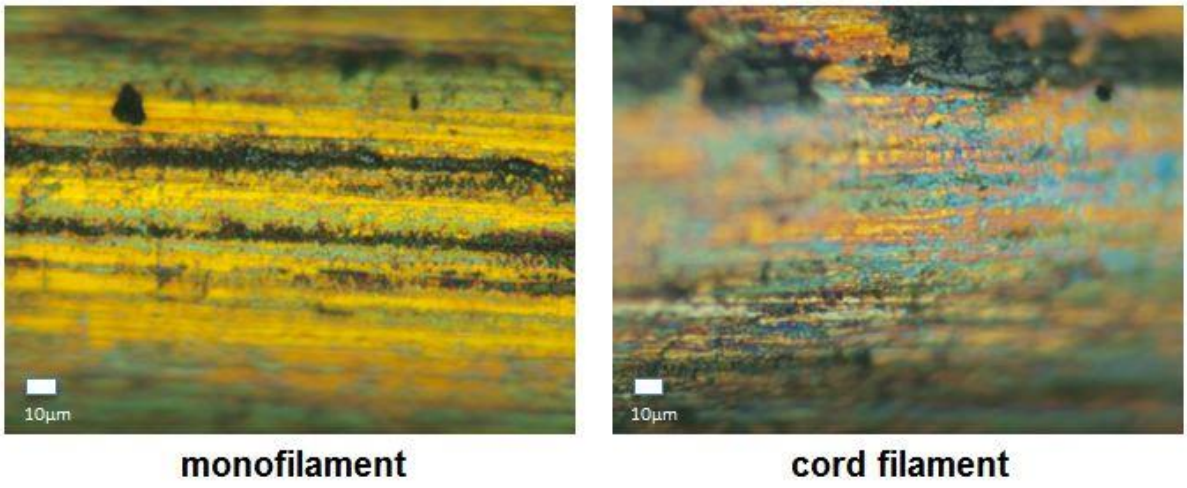

Figure 41: optical light microscopy images of unaged reference samples (1000x), set 2 (left, monofilament) and set 1 (right, cord filament)

Due to the twist of the cord filaments data is lost on the edges in 3D- microscopy resulting in white areas on the edges of the images (see Figure 42).

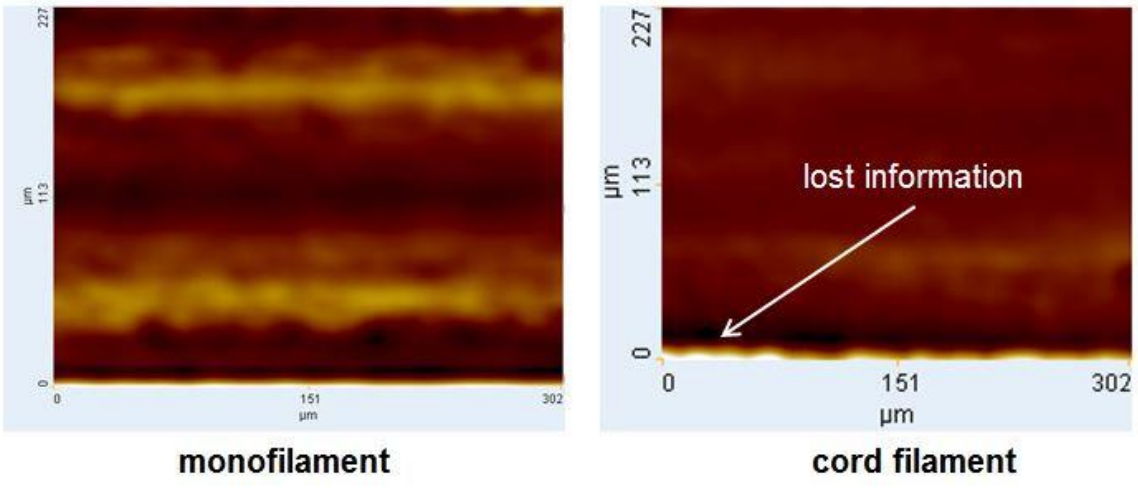

Figure 42: 3D-mocroscopy images of unaged reference samples, set 2 (left, monofilament) and set 1 (right, cord filament)

The holding device for SEM investigation consists of a sticky conductive plate. The straight monofilaments are contacted throughout their entire length while the twisted filaments contact the plate only by a few points (see Figure 43). Some of the latter do not stay in the desired position and the assigned region from 3D-microscopy cannot be relocated during the SEM investigation. A good conducting level prevents the charging of the sample. Thus the degree of contacting influences the image quality. Additionally conducting sticky strips can be used to further enforce the contacting level.

Figure 43: comparison of the sample contacting of monofilaments and cord filaments in SEM

On the one hand cord filaments contain regions which are exposed to the rubber; on the other hand there are regions which face the inside of the cord. The latter do not represent adhesion interfaces because they are never directly in contact with the rubber or with sulfur. In contrast the whole monofilament directly contacts the rubber so there is no risk to select an area which does not represent the adhesion interface.

4.3 Comparison metathesis degradation - filter paper method

A comparison of the metathesis degradation and the filter paper method can be obtained from the results of set 1. The filter paper samples show higher oxygen contents at all aging stages than the samples degraded by metathesis reaction (see Table 13 and Table 14 in the appendix). While corrosion nodules develop on samples prepared by the filter paper method during aging (2 days, oxygen, 70 °C and 14 days, humidity, 70 °C), these structures are not present at samples prepared by metathesis degradation. Thus it can be concluded that the interfaces of the filter paper samples are more easily accessible for the aging media than interfaces which are directly covered by rubber. For this reason the filter paper method is found not to be representative for realistic adhesion interfaces. As a consequence no samples are prepared by this technique in set 2. Figure 44 shows the reference samples which are aged for two days under oxygen at 70 °C and which are exposed by metathesis degradation and filter paper method. The black dots on the filter paper samples can be identified as iron oxide by EDX analyses.

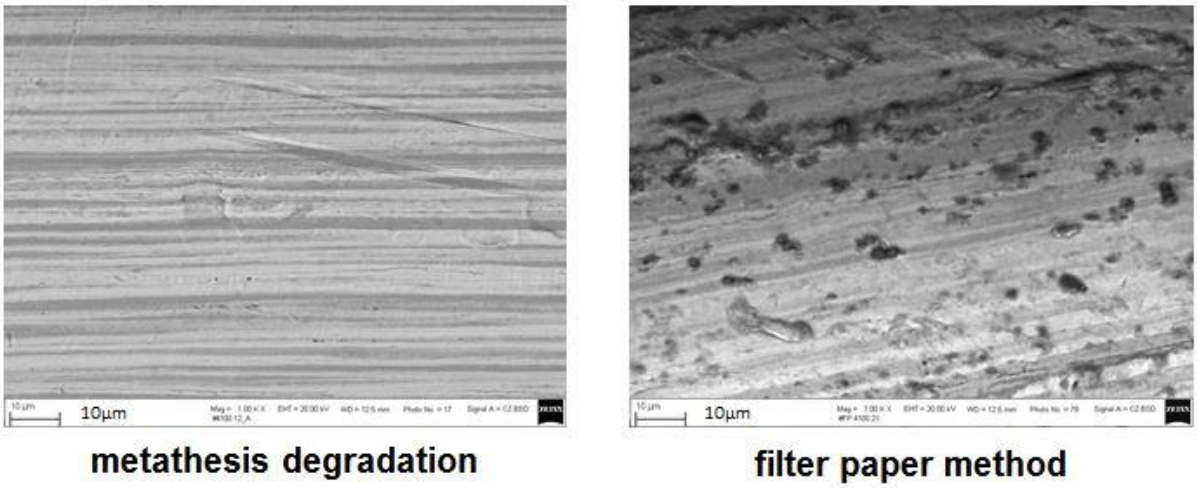

Figure 44: comparison of the metathesis degradation and the filter paper method, reference samples aged for two days under oxygen at 70°C, SEM (1000x), set 1

Since the filter paper is a barrier to substances which may interrupt the formation of the adhesion interface, the crystallization of the sulfide layer is thought to be facilitated.[10] Thus more superficial structures can be expected whereas aging enforces this effect. However the unaged filter paper samples do not clearly show highly structured surfaces with the exception of the reference sample. In contrast the samples aged for fourteen days under humidity at 70 °C do show more needle-like structures than the corresponding interfaces exposed by metathesis degradation (see Figure 45).

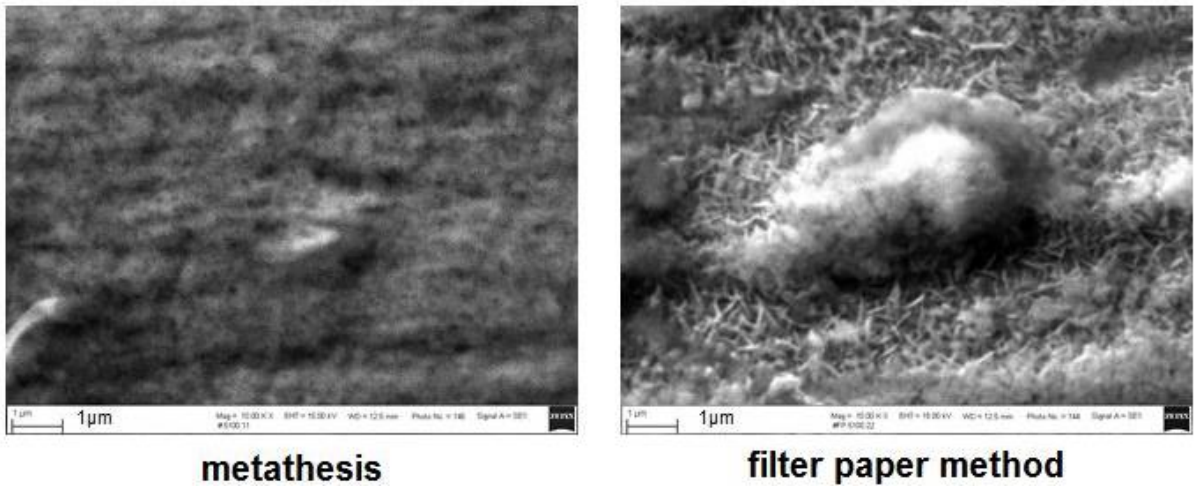

Figure 45: comparison of the metathesis and the filter paper method, reference samples aged for fourteen days under humidity at 70 °C, SEM (1000x), set 1

4.4 The influence of the rubber composition and different aging conditions

In this chapter the individual features of the different recipes and the influence of several aging conditions are discussed. The following discussion is mainly based on data from set 2 because the corresponding samples can be prepared and exposed more easily than those of set 1. Moreover they are investigated in more detail by means of SEM. Thus set 2 provides more reliable results. Of course the conclusions concerning the strip recipe and the two days aging condition under oxygen at 70 °C are drawn from the results of set 1.

4.4.1 Unaged series

Figure 46 illustrates optical light microscopy, 3D-microscopy and SEM images of all unaged recipes. The draw lines, which develop during wire processing, are clearly visible throughout all applied microscopic methods.

The roughness averages are calculated by the AFM software using data from 3D-microscopy. These values range between 3.17 µm and 0.36 µm in set 1 and between 1.21 µm and 0.72 µm in set 2. Significant deviations can not only be observed within the series but even within the triple determination of the same recipes. Therefore it can be concluded that the calculation of the roughness parameters - and the average roughness in particular - is not useful for this investigation.

According to optical light microscopy and 3D-microscopy images the surfaces of the samples without cobalt stearate and the samples which use a mixture of TBBS and MBT as vulcanization accelerator appear more structured compared to those of the reference samples. SEM images show that the TBBS + MBT samples, the samples without cobalt stearate and the Ref (5/170) samples are covered by a moss-like coating. The coverings on the cobalt free samples and Ref (5/170) are more coarsely compared to the TBBS + MBT samples. Moreover a kind of film can be observed on some reference samples as well. In contrast the optical light and 3D-microscopy images of the low sulfur samples show comparatively bare surfaces. SEM investigations further confirm this impression as the backgrounds in the images, which are taken at a magnification of 10,000 times, appear uncovered. This is even visible at a magnification of 1000 times.

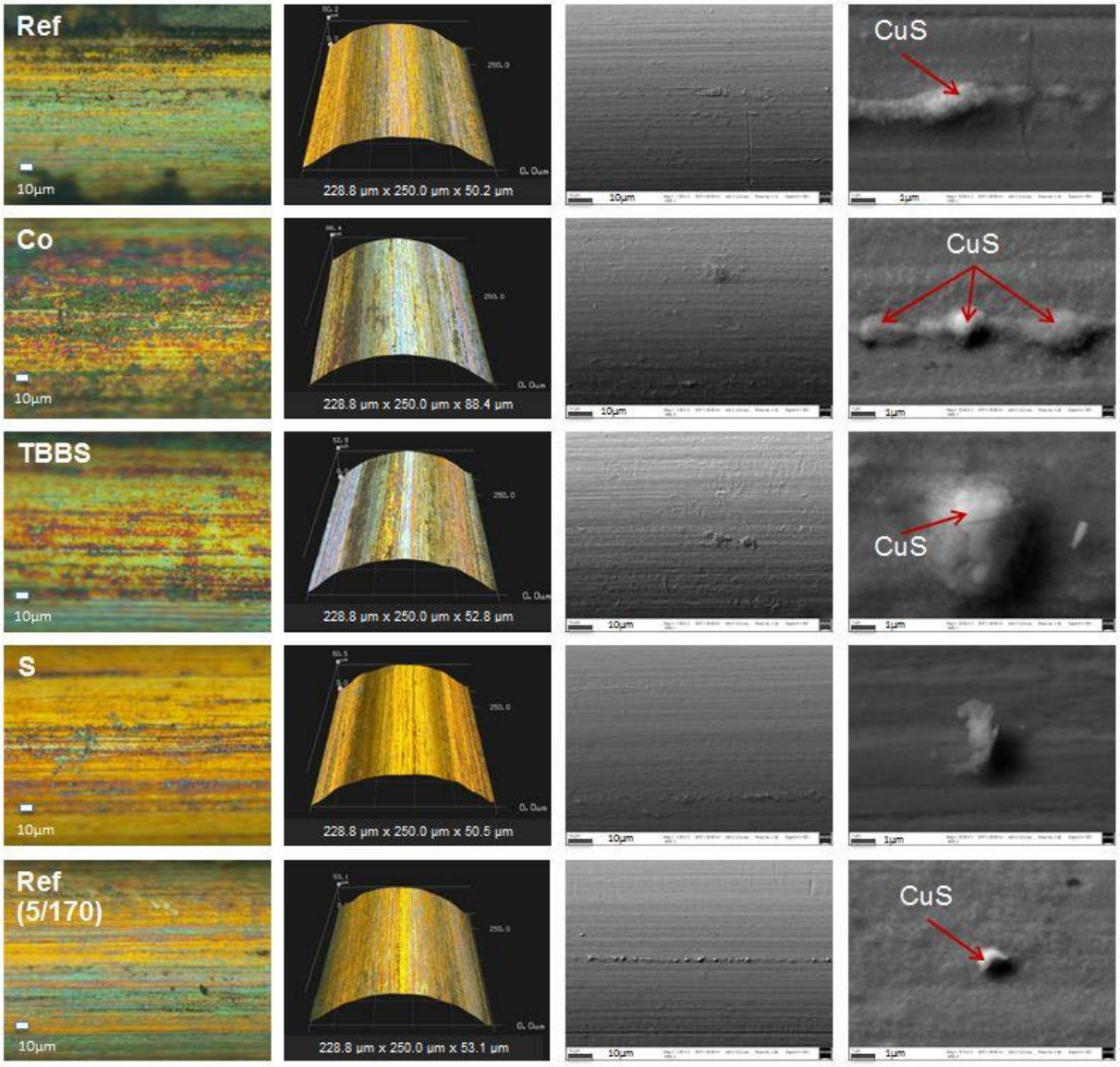

Figure 46: optical light microscopy (1000x), 3D-microscopy (1000x) and SEM images (1000x and 10,000x) of the unaged samples, isothermally heated, set 2

Furthermore it is investigated if there is a relationship between the recipe of the rubber component and the color of the exposed adhesion interface. Unfortunately the results do not show a clear correlation. Even two different positions on one sample may vary a lot (see Figure 47, top row).

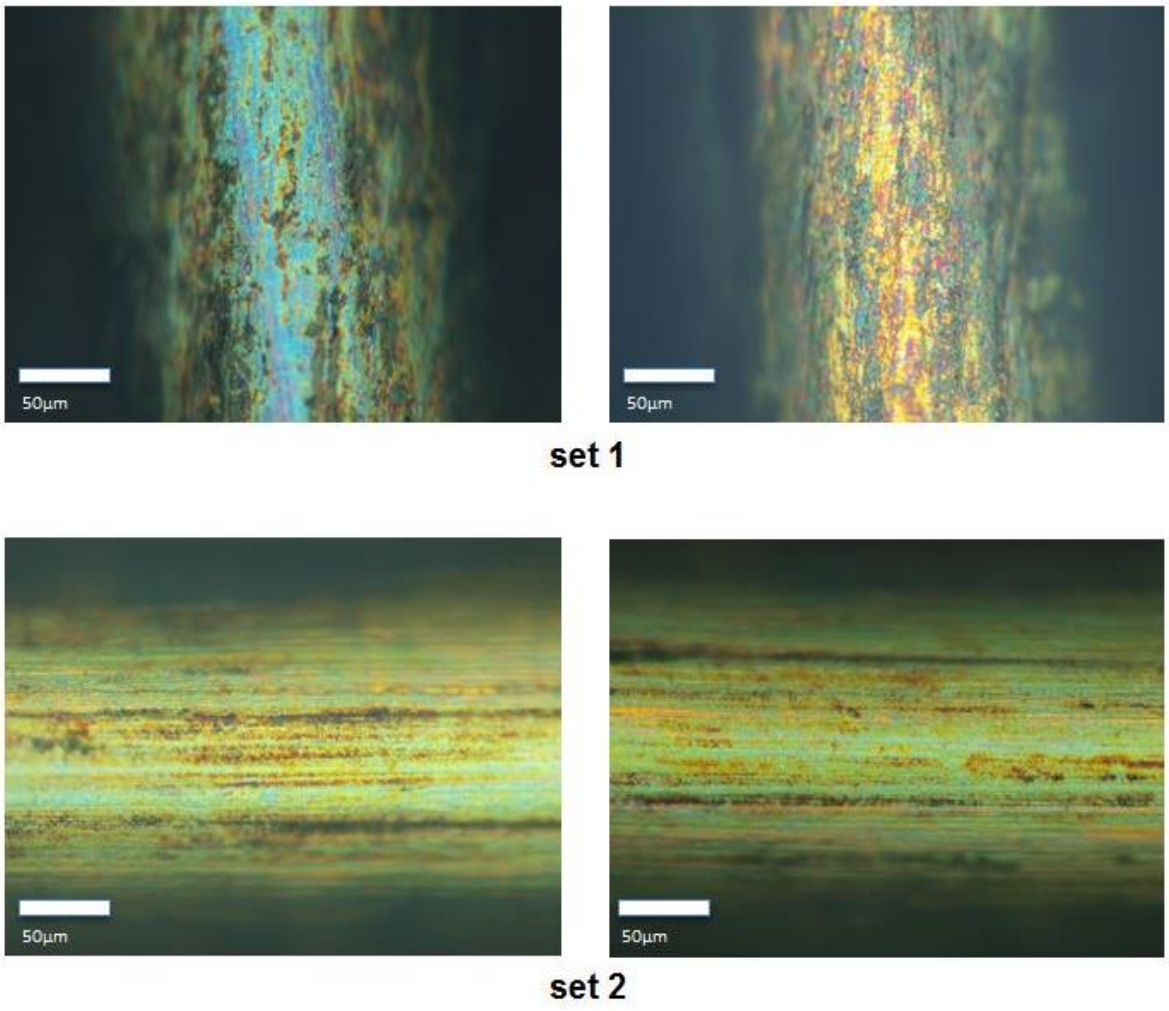

Figure 47: two positions on one cord of the unaged reference recipe from set 1 (top row) and two positions on one monofilament of the unaged Co recipe from set 2 (bottom row), optical light microscopy (500x)

Table 8 lists the normalized results of the EDX analyses of all unaged recipes set 2. Since the sample surfaces are inhomogeneous with respect to their composition and roughness, the penetration volume of the electron beam is inhomogeneous as well. Therefore the concentrations of the elements are only approximated results.[21]

For all recipes of the unaged series similar oxygen and zinc values are detected.

SEM investigations show that the reference samples carry superficial copper sulfide structures (Figure 46 and Figure 48) which are, according to literature, preferentially found along the draw lines of filaments.[94] As demonstrated in the first two images of Figure 48 this is observed within this investigation as well.

EDX analyses result in 3.3% sulfur for the **reference** samples (see Table 8). This moderate sulfur level is another evidence for the good adhesion properties found during the investigation of the physical data (see chapter 4.1.1). The comparatively high carbon values of 100.3% indicate that more rubber residues remain on the

reference samples than on the other recipes. Images from optical light microscopy confirm this statement since more dark areas can be observed (Figure 46).

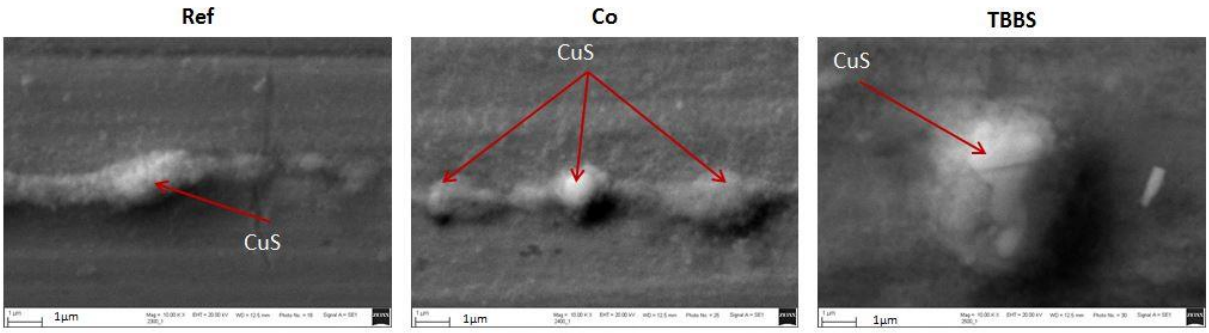

Figure 48: copper sulfide structures along the draw lines on the reference samples and the samples without cobalt stearate, SEM images (10,000x), set 2

Table 8: average elemental contents of all recipes of the unaged series, set 2

		C[%]	Cu[%]	Fe[%]	O[%]	S[%]	Zn[%]
unaged	Ref	100.3	100.0	169.7	5.5	3.3	52.0
	Co	35.5	100.0	187.4	5.3	4.0	54.5
	TBBS + MBT	36.0	100.0	162.3	4.6	3.8	51.2
	S	27.6	100.0	205.8	5.2	1.4	58.0
	Ref (5/170)	44.2	100.0	160.6	4.9	2.1	60.6

The highest amounts of sulfur are detected on the samples **without cobalt stearate** (4.0%). As discussed in chapter 4.1.1 the vulcanization of these samples might not be completed. Thus more sulfur remains unconsumed and might be deposited on the investigated interfaces. The high sulfur content and the copper sulfide structures shown in Figure 46 and Figure 48 indicate the development of a proper adhesion interface. The corresponding coverage value which accounts for more than 90% is another evidence for good adhesion properties.

The samples accelerated by a mixture of **TBBS and MBT** also carry copper sulfide structures (see Figure 46 and Figure 48). Together with the corresponding high sulfur level (3.8%), the pullout force of 156 N and a coverage value of 98% this indicates the development of a proper adhesion interface again. Since the iron signal originates in the steel core[21,94] of the filaments the comparatively low iron content is an evidence for a quite thick covering on the samples' surfaces.

As mentioned above the surfaces of **the low sulfur** samples appear comparatively uncovered. According to EDX analyses these samples show the lowest sulfur and highest iron contents within the unaged series (1.4% S and 205.6% Fe). Hence it can be concluded that the low sulfur samples develop thinner adhesion interlayers than

the other recipes. Nevertheless sufficient adhesion is provided between rubber and metal since the physical data suggest that adhesion failure of the unaged low sulfur samples originates in the rubber compound (see chapter 4.1.1).

The sulfur levels of 2.1% and the iron contents of 160.6% of the **Ref (5/170)** samples are quite low. The latter is an evidence for the above described covering on the samples' surface because less iron of the wire's core can be detected. Although the physical data like the coverage of about 99% suggest good adhesion little copper sulfide can be found on these samples. In contrast many ZnO rods are observed on the samples' surfaces (see Figure 49). They are residuals of the rubber component and do not originate from the dezincification process. Thus this form of ZnO does not contribute to adhesion failure but to the increased zinc content of the Ref (5/170) samples.

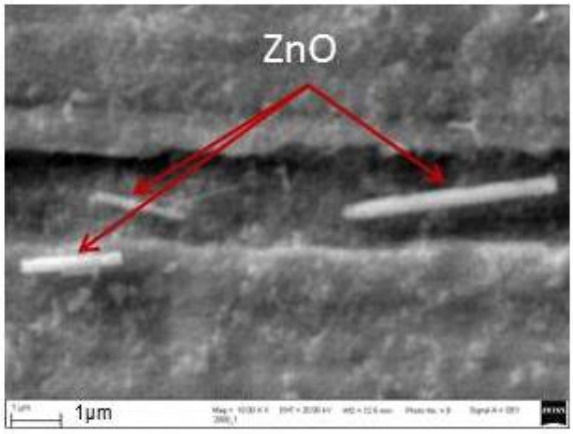

Figure 49: ZnO rods on the surface of the unaged Ref (5/170) samples, set 2

The **strip recipe** is not further investigated in set 2 because the results from set 1 do not show significant differences compared to the reference recipe (see Figure 50). This is exemplarily illustrated by optical light microscopy images although the statement is based on the results of all microscopic investigations (optical light, 3D- and scanning electron microscopy). Concerning EDX analyses the strip recipe shows sulfur levels that double the corresponding values of the reference samples (see Table 14 in the appendix). Besides this exception no deviations to the other recipes are detected.

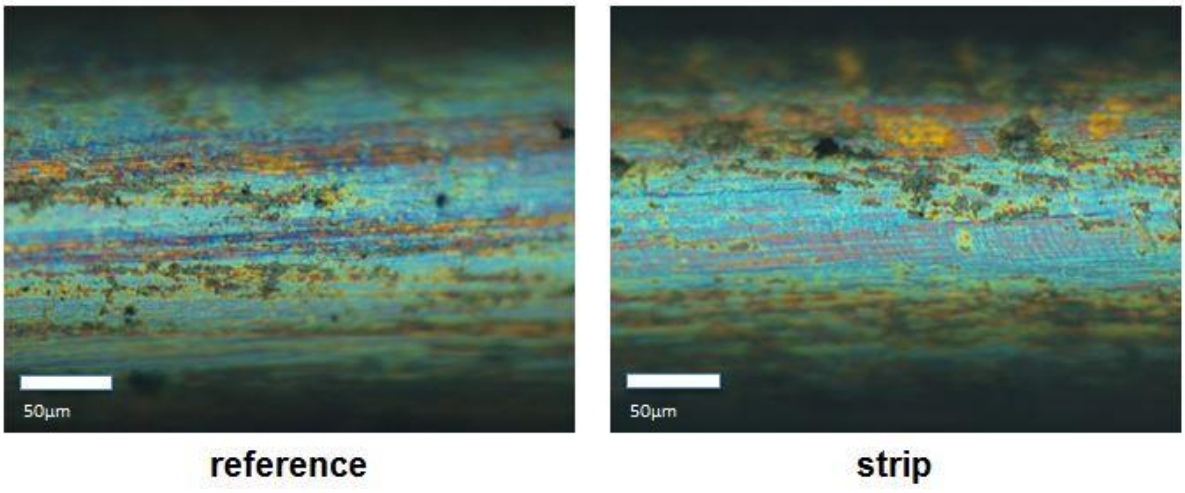

Figure 50: reference and strip samples of the unaged series, set 1 (optical light microscopy, 500x)

4.4.2 The effect of different aging conditions

The microscopic investigations show that samples aged for two days under oxygen at 70 °C do not change as significantly as samples aged for five days in steam at 105 °C or fourteen days under humidity at 70 °C. Thus they are only investigated in set 1. Figure 51 shows the effect of the different aging conditions on the reference samples of set 1.

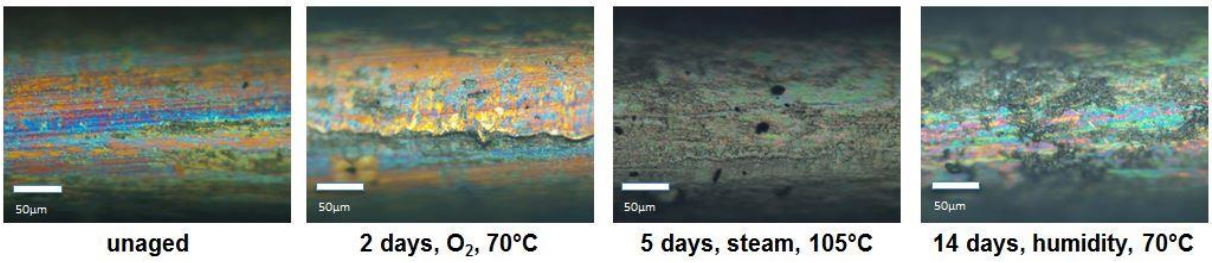

Figure 51: comparison of the reference samples throughout all aging conditions (optical light microscopy, 500x)

These optical light microscopy images are representative for the findings in 3D-microscopy and SEM investigation as well. The samples aged for two days under oxygen at 70 °C have rarely changed whereas grey coatings cover the surfaces after aging for five days in steam at 105 °C. Aging for fourteen days under humidity at 70 °C even initiates corrosion of the samples in set 1. The corresponding series in set 2 however shows copper sulfide structures on the samples' surfaces (see Figure 56). Moreover the EDX analyses of the samples aged for two days under oxygen at

70 °C do not show significant deviations in comparison to the unaged series (see Table 14 in the appendix). The increased carbon, oxygen and sulfur levels of the strip and the TBBS accelerated samples can be derived from rubber residues which are not completely degraded.

However steam aging for five days at 105 °C and humidity aging for fourteen days at 70 °C change the samples significantly. This is even visible in optical light and 3D-microscopy images. The samples aged for five days under steam at 105 °C are covered with grey coatings, while those aged for fourteen days under humidity at 70 °C show nodule-like structures on their surfaces and appear dark (see Figure 52).

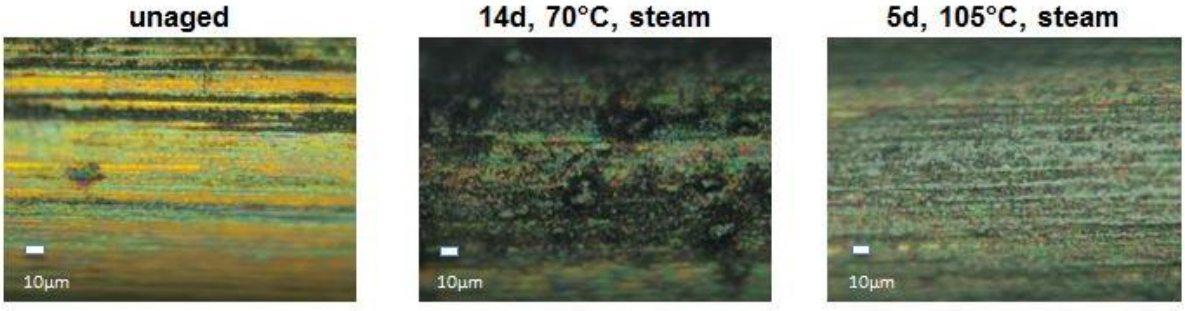

Figure 52: influence of the different aging conditions at the example of the reference samples, optical light microscopy (1000x), set 2

SEM images of all magnifications confirm these findings (see Figure 53). The surfaces of the steam aged samples (105 °C, five days) are covered by a cloudy coating and thus have a more structured appearance compared to the unaged series. The humidity aged samples (70 °C, fourteen days) are dominated by nodules which can be identified as copper sulfide excrescences. This is illustrated by element mapping images in Figure 54. As shown in the SEM images at a magnification of 10,000 times (see Figure 55) the cloudy coating is present on the fourteen days humidity aged samples as well although to a lesser extent.

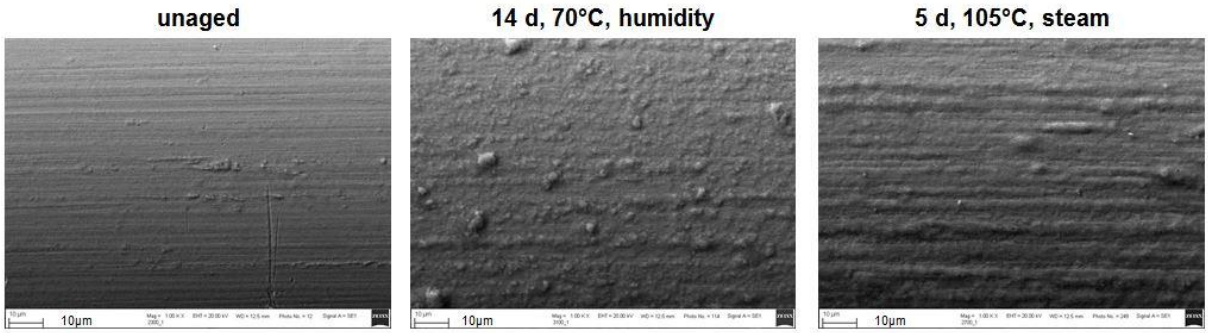

Figure 53: SEM images (1000x) of the unaged reference samples, the humidity aged samples and the steam aged samples, set 2

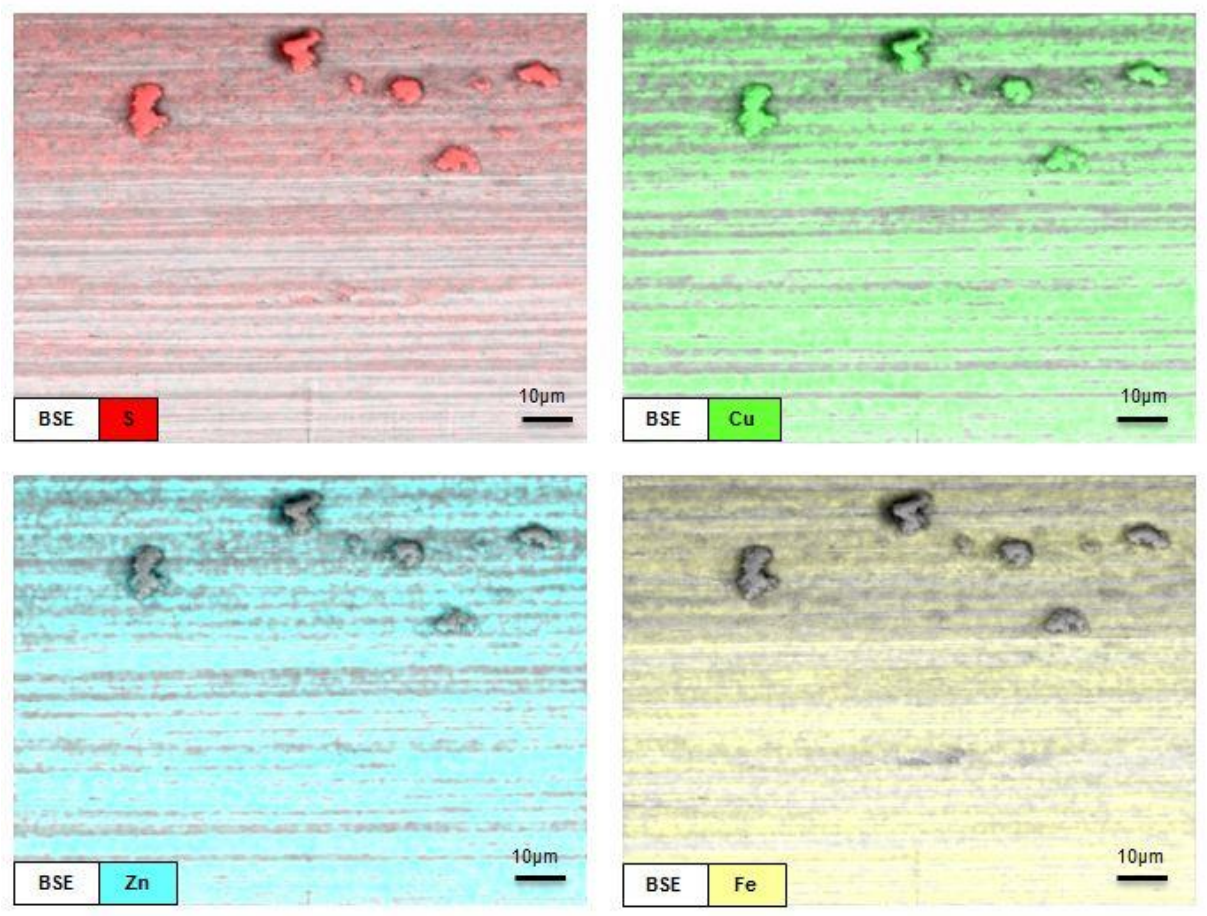

Figure 54: mapping of reference samples aged for 14 days under humidity at 70 °C

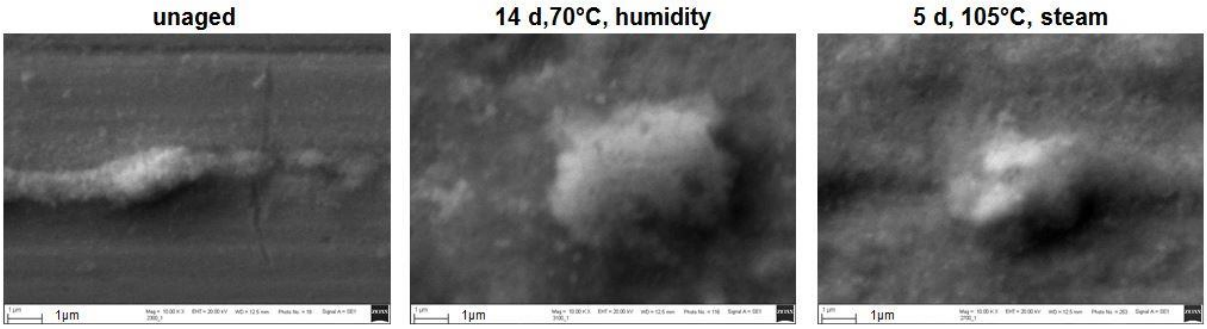

Figure 55: cloudy coverings on the reference samples, SEM (10,000x)

Throughout all recipes both aging conditions (5d, steam, 105 °C and 14d humidity, 70 °C) increase the oxygen, sulfur and zinc contents (see Table 9). This effect is striking, especially for samples aged for five days under steam at 105 °C. Apart from the low sulfur samples all recipes show reduced iron contents under these conditions. This supports the conclusion that a thick covering develops on the steam aged samples.

Table 9: average elemental contents of all recipes of all aging conditions, set 2

		C[%]	Cu[%]	Fe[%]	O[%]	S[%]	Zn[%]
unaged	Ref	100.3	100.0	169.7	5.5	3.3	52.0
	Co	35.5	100.0	187.4	5.3	4.0	54.5
	TBBS + MBT	36.0	100.0	162.3	4.6	3.8	51.2
	S	27.6	100.0	205.8	5.2	1.4	58.0
	Ref (5/170)	44.2	100.0	160.6	4.9	2.1	60.6
14d, humidity, 70°C	Ref	63.8	100.0	197.7	11.3	17.1	62.3
	Co	66.8	100.0	169.8	12.7	27.1	59.6
	TBBS + MBT	43.2	100.0	165.5	6.5	10.3	59.2
	S	39.7	100.0	220.6	13.6	6.4	64.1
	Ref (5/170)	68.3	100.0	194.1	13.9	23.6	67.9
5d, steam, 105°C	Ref	67.6	100.0	134.0	11.5	27.0	86.1
	Co	85.4	100.0	115.8	9.5	42.7	67.2
	TBBS + MBT	61.9	100.0	138.3	10.5	40.9	83.0
	S	85.1	100.0	273.8	18.7	48.4	131.6
	Ref (5/170)	60.3	100.0	147.1	11.2	38.5	80.5

According to literature the copper sulfide layer continues growing during aging.[15,20,25] The initially amorphous Cu_xS thickens and turns into a more crystalline and brittle form which weakens the adhesion strength.[15,22] This is also found during the investigation of this master thesis: As listed in Table 9 the sulfur content increases excessively during aging. After aging for fourteen days under humidity at 70 °C the average sulfur level has increased from 2.9% to 16.9% while aging for five days under steam at 105 °C even raises the average sulfur content to 39.5%.

Furthermore it is stated that dezincification during aging is accelerated by the presence of moisture and oxygen.[7,15,19,28] The copper sulfide layer is possibly overgrown by ZnS, ZnO and $Zn(OH)_2$[6,18] depending on the moisture and oxygen present at the rubber metal interface[18]. As a result the adhesion interface is weakened.[7,15,19,28] This can also be concluded from the results of this work. The average amount of zinc increases from 55.3% (unaged series) to 62.6% after humidity aging and to 79.2% after steam aging. The latter is calculated without considering the very high zinc content of the low sulfur sample. The oxygen content doubles after both aging conditions. These increased amounts of zinc, sulfur and oxygen indicate an accelerated dezincification process and the formation of ZnS, ZnO (and possibly $Zn(OH)_2$) which cause adhesion failure at the rubber metal interface. The according pullout forces and coverage values support this conclusion (see chapter 4.1.2). Additionally ZnO rods which remain on the metal surface after rubber degradation and may contribute to the increased zinc levels.

4.4.3 Humidity aging for fourteen days at 70 °C

As already mentioned the samples aged for fourteen days under humidity at 70 °C appear dark in optical light microscopy in comparison to the unaged series and they develop copper sulfide nodules on their surfaces. These blister-like excrescences are not only observed in SEM but are even visible in optical light microscopy and 3D-microscopy images (see Figure 56). They represent thick and brittle interfacial structures. Thus a reduction of the adhesion strength is expected and confirmed by the corresponding pullout forces, which are reduced from an average of 148 N to 86 N and the coverage values which decrease from 98% to 82% (see also chapter 4.1.2).

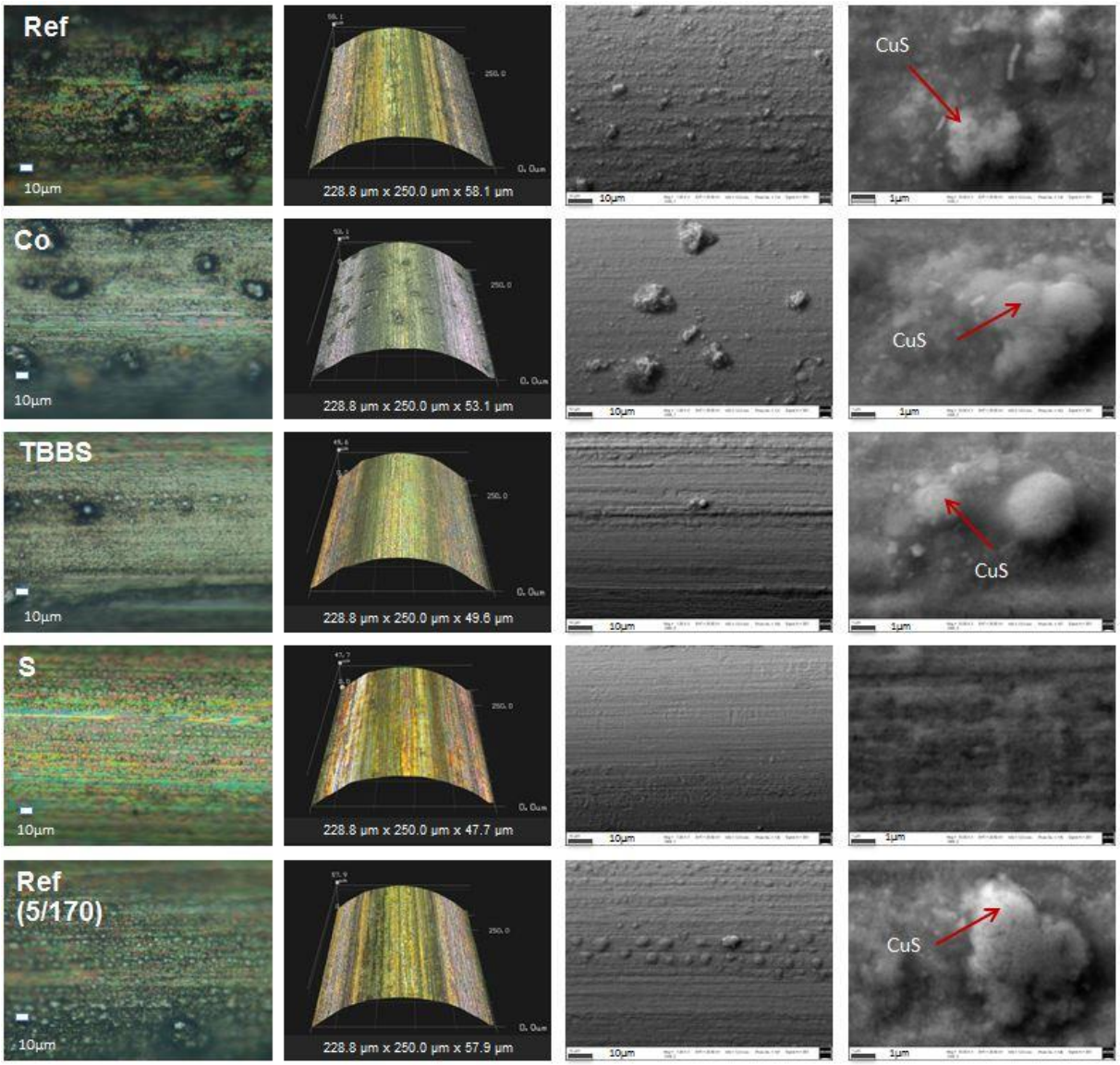

Figure 56: optical light microscopy (1000x), 3D-microscopy (1000x) and SEM images (1000x and 10,000x) of the samples aged for fourteen days under humidity at 70 °C, isothermally heated, set 2

The surfaces of the **reference** samples and the **Ref (5/170)** carry copper sulfide nodules which are visible on images obtained from optical light microscopy and SEM at a magnification of 1000 times. EDX analyses show that the sulfur and zinc levels of the reference samples (17.1% S and 62.3% Zn) are higher than those of the corresponding unaged samples (3.3% S and 52.0% Zn). The Ref (5/170) samples additionally show increased oxygen contents of 13.9%. This indicates the above mentioned development of ZnS as a result of the dezincification process. These findings explain the adhesion failure at the rubber metal interface which is mentioned in chapter 4.1.2.

Similar effects can be observed for all recipes of this series as the oxygen, zinc and sulfur levels increase during humidity aging (see Table 9). In combination with the

decreased coverage values it can be concluded that dezincification takes place and that ZnS and ZnO (and possibly $Zn(OH)_2$) are built on the samples' surfaces which reduce the adhesion strength.

According to optical light microscopy, 3D-microscopy and SEM images the samples **without cobalt stearate** are particularly affected. They develop massive copper sulfide blisters which are suggested to reduce adhesion more excessively compared to the remaining recipes. However this extreme effect on the cobalt free samples is not confirmed by the corresponding coverage values as it is the second highest of this series (83%).

In contrast fewer nodules of smaller grain size develop on the **low sulfur** samples. This is also reflected by the results of the EDX analyses: The average sulfur and carbon contents of the low sulfur samples amount to 6.4% sulfur and 39% carbon while the reference accounts for 17.1% sulfur and 63.8% carbon (see Table 9). Comparatively high levels of oxygen (13.6%) and iron (220.6%) are detected. The latter indicates that the adhesion interface is not very thick since the iron signal originates from the core of the filament again.[21,94] Moreover optical light microscopy and SEM images at the magnification of 1000 times clearly show draw lines on the low sulfur filaments' surfaces. This is an additional evidence of a rather uncovered surface. The coverage value of 75% is comparatively low and further supports this statement. Hence the low sulfur samples show bad adhesion properties after humidity aging.

The high coverage value (90%) of the samples accelerated with a combination of **TBBS and MBT** suggests that the adhesion interface might not be attacked as severely as the interfaces of the other samples of this series. EDX analyses show that the elemental contents do not increase too much with the exception of the sulfur content which rises from 3.8% (unaged) to 10.3% (see Table 9). Hence dezincification occurs to a smaller extent on the TBBS + MBT samples.

4.4.4 Steam aging for five days at 105 °C

The images from optical light microscopy and 3D-microscopy in Figure 57 show the already mentioned grey coating which develops on the samples' surfaces after steam aging for five days at 105 °C. In the SEM images at a magnification of 10,000 times the moos-like appearance of this coating is clearly visible. EDX analyses show increased levels of zinc and oxygen throughout the whole series. These element contents increase from an average of 55.3% zinc and 5.1% oxygen to 79.2%[a] zinc and 12.3% oxygen. Moreover excessive amounts of sulfur (39.5%) are detected (see Table 9). Thus it can be concluded that the covering mainly consists of ZnS and to ZnO (and possibly $Zn(OH)_2$). Furthermore all the samples show reduced iron levels

[a] The average value of the zinc content is calculated without considering the very high zinc level of the low sulfur samples.

after steam aging which is a further evidence for a thick covering on the samples' surfaces. The average iron content of the unaged series amounts to 177% while the average iron content of the steam aged series accounts for 134%[b].

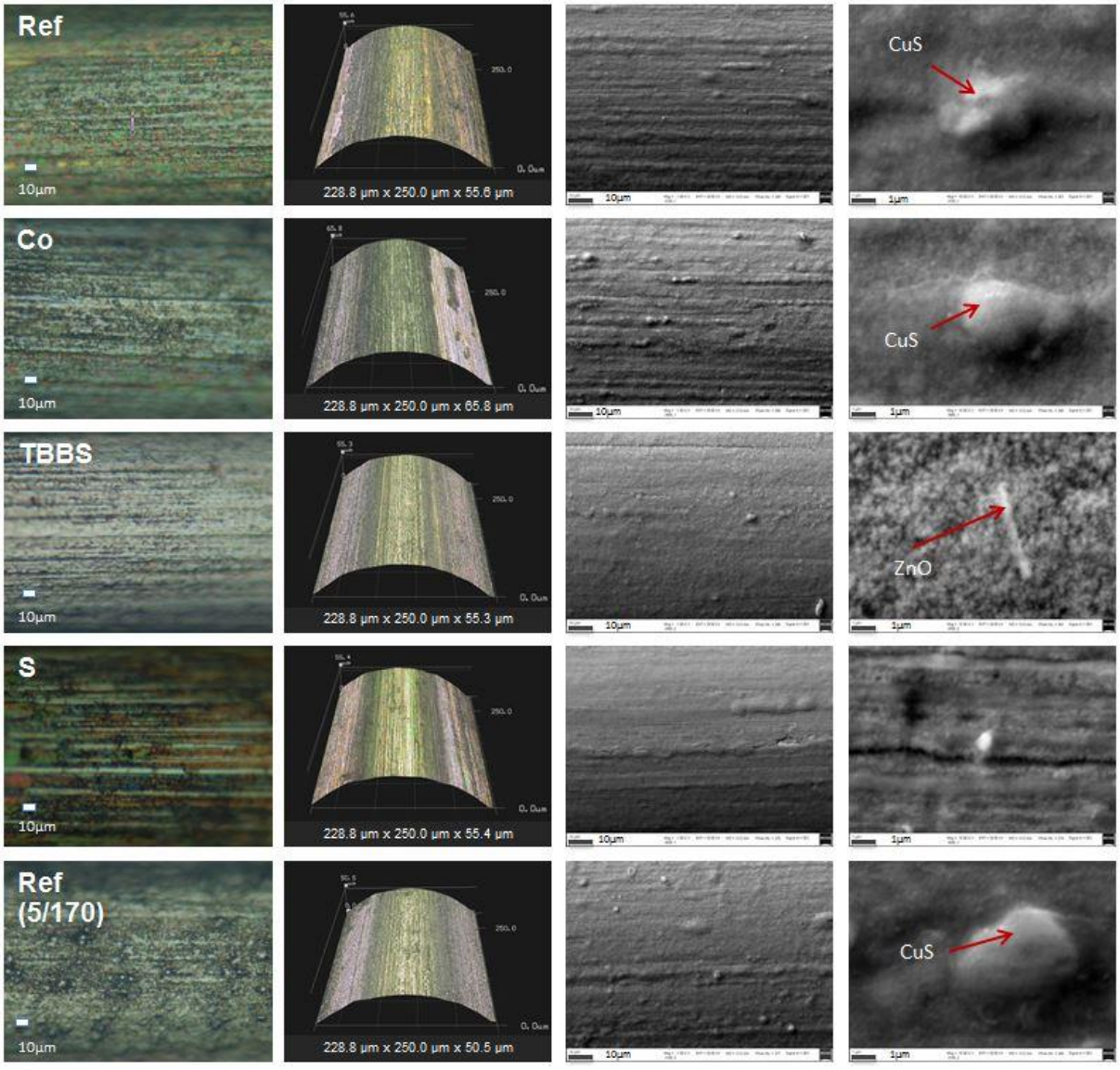

Figure 57: optical light microscopy (1000x), 3D-microscopy (1000x) and SEM images (1000x and 10,000x) of the samples aged for five days under steam at 105 °C, isothermally heated, set 2

[b] The average value of the iron content is calculated without considering the very high iron level of the low sulfur samples.

As can be seen in the SEM images in Figure 57 the reference samples and the **Ref (5/170)** samples carry copper sulfide structures on their surfaces. According to Table 9 the oxygen and zinc contents of the Ref (5/170) samples, which amount to 11.2% O and 80.5% Zn, are similar to those of the reference samples (11.5% O and 86.1% Zn). These similarities are reflected by the coverage values which are 82% for the reference samples and 86% for the Ref (5/170) samples. One deviation from the reference is the sulfur content of the Ref (5/170) which amounts to 38.5% and thus exceeds the reference value of 27.0%.

According to literature organic cobalt salts suppress dezincification.[17,19] This is not clearly confirmed by the results of this work as the zinc level on the samples **without cobalt stearate** is the lowest of the whole series. The results of EDX analyses show little amounts of iron (115.8%) which suggest that these samples are covered by a rather thick coating. Moreover the surfaces of the cobalt free samples appear more structured in the SEM image at a magnification of 1000 times (see Figure 57). The superficial structures can be identified as copper sulfide due to SEM point analyses and the high sulfur content of 42.7% detected by EDX analyses. The reduced coverage of 70% however indicates partial adhesion failure which is often caused by dezincification during aging.[7,15,19,28]

As shown in SEM images at a magnification of 10,000 times the coverings on the samples accelerated by **TBBS and MBT** appear comparatively coarse (see Figure 57). The fact that the ZnO rod is overgrown demonstrates the excessive extent of the coating on these samples. This is further supported by the rather low iron content of 138.3%. The high sulfur and zinc contents (40.9% S and 83.0% Zn) are the result of dezincification and are suggested to cause adhesion failure at the rubber metal interface. The findings in chapter 4.1.2 and the reduced coverage values of 78% confirm this suggestion.

No copper sulfide excrescences can be found on the interfaces of the **low sulfur** samples. This is consistent with the very low pullout force of 21 N and the low coverage values of 67%. Furthermore the draw lines are clearly visible in the images obtained from optical light microscopy. Together with the very high iron contents these facts indicate the development of a thin adhesion interface and bad adhesion properties for the low sulfur samples.

It is important to mention that the absolute copper contents of the low sulfur samples are lower than the contents of all other recipes. As the reason for this deviation is not clarified the results in Table 9 are not reliable. The absolute element contents of the low sulfur samples show less sulfur and more zinc, oxygen and iron than the other recipes do.

4.5 Athermally heated samples

The different curing conditions used in the athermally heated series do not influence the samples significantly. Neither a comparison within the series nor the comparison with the isothermally heated reference samples shows considerable differences. Images obtained from optical light microscopy, 3D-microscopy and SEM analyses show similar results for all athermally heated samples (see Figure 58). The draw lines are clearly visible in all applied microscopic methods. SEM images show homogenous surfaces with some copper sulfide structures. Moreover the physical parameters are rarely affected by the different energy inputs (see chapter 4.1).

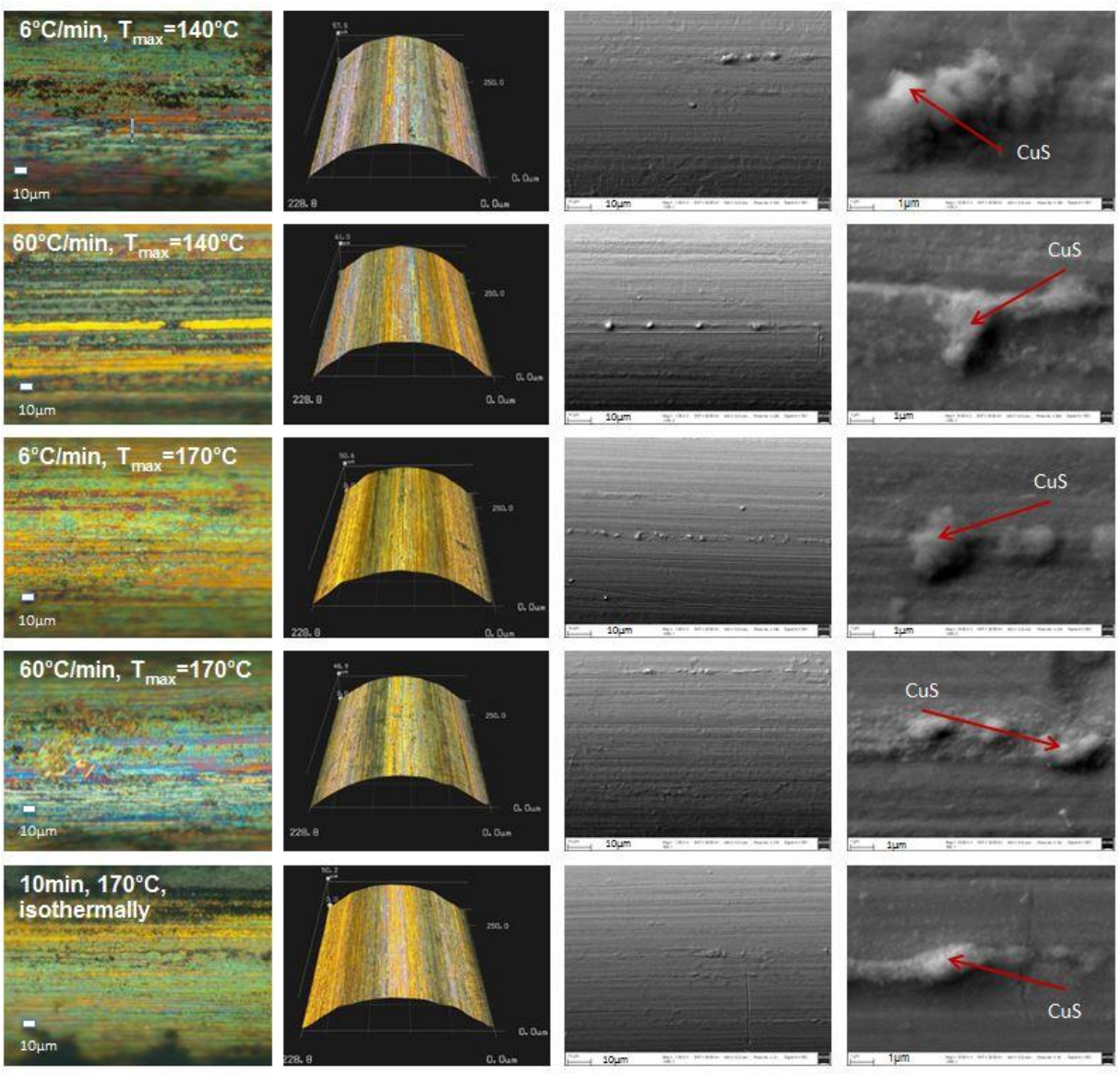

Figure 58: optical light microscopy (1000x), 3D-microscopy (1000x) and SEM images (1000x and 10,000x) of the athermally heated samples and the unaged reference sample, set 2

Concerning EDX analyses only marginal deviations within the whole series are detected (see Table 10). The athermally heated samples contain slightly more iron while the amount of sulfur is equal or lower compared to the isothermally heated reference samples. All athermally heated samples carry some copper sulfide structures (see Figure 58) which is another similarity to the isothermally heated reference sample.

Table 10: comparison of the average elemental content of the athermally and isothermally heated reference samples

		C[%]	Cu[%]	Fe[%]	O[%]	S[%]	Zn[%]
isothermally heated, unaged	Ref	100.3	100.0	169.7	5.5	3.3	52.0
	Ref (5/170)	44.2	100.0	160.6	4.9	2.1	60.6
athermally heated, unaged	Ref (6/140)	28.9	100.0	179.5	4.7	3.4	57.9
	Ref (60/140)	35.5	100.0	197.1	5.5	2.9	60.9
	Ref (6/170)	25.4	100.0	212.7	4.4	2.1	63.0
	Ref (60/170)	45.0	100.0	157.2	4.6	7.6[c]	45.9

[c] average biased by a high single value

4.6 The influence of storage

The reference samples and the low sulfur samples are investigated with regard to the influence of storage on the adhesion interface. Neither the reference nor the low sulfur samples show significant changes in optical light microscopy and 3D-microscopy (see Figure 59).

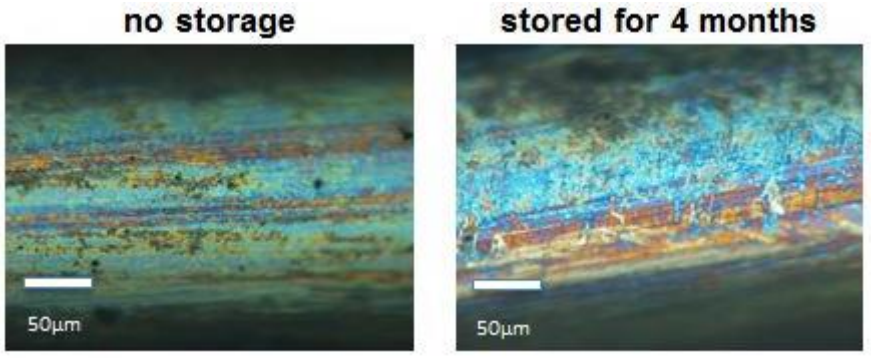

Figure 59: the effect of storage at the example of the reference samples of set 1, optical light microscopy (500x)

SEM investigations show increased amounts of sulfur, oxygen and carbon after a four months period of storage (see Table 11). This effect is more pronounced for the low sulfur. Furthermore the latter show comparatively high zinc levels of 80.6%. The high oxygen, sulfur and zinc contents indicate that dezincification takes place during storage. After four months the detected amount of iron has decreased for both recipes. These facts suggest that a covering develops on the samples surfaces. However this cannot be proved by a comparison of SEM images because set 1 is not investigated to the necessary extent. Moreover no physical data are recorded after the storage.

Table 11: elemental contents of the reference and low sulfur samples before and after a 4 months period of storage

		C[%]	Cu[%]	Fe[%]	O[%]	S[%]	Zn[%]
no storage, set 1	Ref	49.3	100.0	197.9	6.6	3.7	62.7
	S	30.5	100.0	178.5	5.3	3.2	58.1
4 months storage	Ref	102.8	100.0	170.9	9.7	10.3	52.0
	S	139.1	100.0	142.3	20.2	13.2	80.6

4.7 Filaments from a real car tire

Olefin metathesis degradation is also used for the exposure of brass coated filaments which originate from real car tires. Although this degradation process does not show any difference to the degradation of the T-test block samples, the images obtained from optical light microscopy and 3D-microscopy show that the surfaces of the car tire filaments are covered to a lesser extent. Figure 60 exemplarily illustrates optical light microscopy images of the unaged reference samples from set 2.

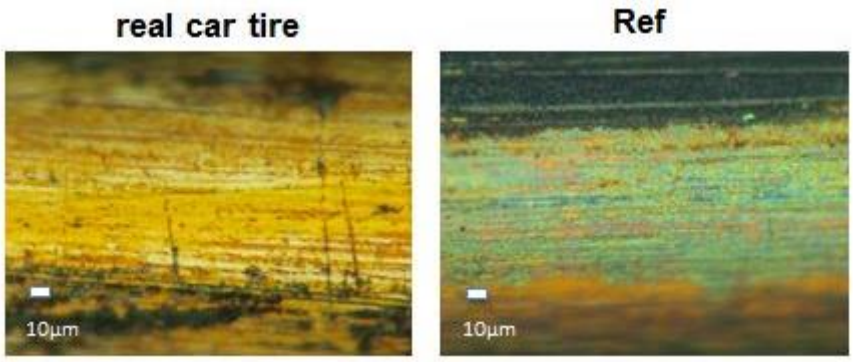

Figure 60: comparison of the exposed interfaces of a real car tire and the unaged reference samples from set 2, optical light microscopy (1000x)

This is also confirmed by the results from SEM analyses which show little amounts of sulfur (1.4%) and high levels of iron (216.2%) for the car tire filament (see Table 12). The latter originate from the core of the filament and hence suggest that the surface is comparatively uncovered from any coating and interfacial structures. SEM images do not show the presence of copper sulfide excrescences on the exposed surfaces of the car tire filaments.

Table 12: comparison of the average elemental contents of the car tire samples and the reference samples from set 2

		C[%]	Cu[%]	Fe[%]	O[%]	S[%]	Zn[%]
unaged	Ref	49.3	100.0	197.9	6.6	3.7	62.7
car tire		64.5	100.0	216.2	10.6	1.4	57.3

Due to the differences in the production procedures of real tires and the T-test block reference samples, the corresponding adhesion interfaces develop under different pressures. It is conceivable that this influences the scale of the interfacial structures.

5. Conclusion and outlook

Olefin metathesis degradation is investigated as an alternative method for the exposal of rubber metal interfaces in car tires. It is compared to the filter paper method in the first part of this work. Moreover two different sample geometries are applied. The samples used in the first part of this work are composed of brass coated steel cords which are vulcanized into the rubber. In the second part the cords are replaced by monofilaments. In order to investigate the influence of some rubber ingredients, samples of different rubber compositions are examined by means of optical light microscopy, 3D-microscopy and scanning electron microscopy. More precisely this concerns the influence of cobalt stearate on the development of the adhesion interface and its protection against aging under corrosive conditions. Furthermore the influence of the accelerator system and the amount of sulfur on the sulfidation process is investigated. TBBS or a mixture of TBBS and MBT are used as accelerator systems instead of DCBS in order to start vulcanization more rapidly and hence to reduce the time available for the sulfidation process. The rubber compound of the strip samples do not contain aging-resisters or resin systems. Thus the rubber is not protected against aging and the additional resin network is not able to improve the adhesion strength. Moreover different heating conditions during vulcanization are investigated. For that purpose samples with half the energy input are vulcanized isothermally and a series of athermally heated samples is produced. Additionally the impacts of various aging conditions are observed. The isothermally heated samples are aged for two days under oxygen at 70 °C, for fourteen days under humidity at 70 °C and for five days under steam at 105 °C. Further information about the rubber network and the adhesion strength can be obtained from physical data like pullout forces, coverage values, tensile strength, shore hardness, resilience, tear elongation and break energy density.

The results of this work prove that olefin metathesis degradation is a suitable technique to expose rubber metal interfaces in car tires without damaging them. A comparison with the filter paper method, which is the state of the art technique, shows clear advantages for the application of the metathesis degradation. On the one hand the latter provides more realistic adhesion interfaces because the rubber is in direct contact to the metal surface. On the other hand it is found that the inserted filter paper makes the adhesion interface accessible for corrosive media during aging.

The comparison of the two sample geometries show that monofilaments hold several advantages over cords: The use of monofilaments facilitates sample preparation and rubber degradation as well as the microscopic investigations. The straight form makes focusing in optical light microscopy and 3D-microscopy easier and improves the conducting level for SEM analyses. In contrast to the cords monofilaments ensure that the examined area has been in direct contact with the rubber.

Since all athermally heated samples lead to similar results it can be concluded that the maximum temperature and the heating rate have little influence on the development of the rubber metal interfaces. Actually there is not even a significant difference between the isothermally treated and athermally vulcanized samples.

The expectations concerning the adhesion impairment for the cobalt free samples, the TBBS (and MBT) accelerated samples and the low sulfur samples are not fulfilled in the unaged series. All recipes show coverage values over 90% which imply that the failure provoked in the pullout tests originates in the rubber network and not at the adhesion interface.

In contrast steam aging for five days at 105 °C causes dezincification and thus leads to partial adhesion failure at the rubber metal interface of the samples without cobalt stearate, the samples which are accelerated by a mixture of TBBS and MBT and the low sulfur samples. Moreover these conditions attack the rubber network as well. This can be seen by the drastic decrease of the tensile strength, the tear elongation and the break energy density. SEM investigations show that moss-like coverings develop on the samples' surfaces after steam aging. Furthermore EDX analyses detect significant increases of zinc, oxygen and sulfur which is another evidence for an advanced dezincification process. The average zinc level of the steam aged series accounts to 79.2% and is equivalent to the 8-fold average zinc content of the unaged samples. The sulfur content increases from an average level of 2.9% to 39.5% whereas the average oxygen content rises from 5.1% to an amount of 12.3% during steam aging.

Dezincification is caused by humidity aging for fourteen days at 70 °C as well. EDX analyses record increases of the average zinc, oxygen and sulfur levels from 55.3% to 62.6% zinc, from 2.9% to 16.9% sulfur and from 5.1% to 11.6% oxygen. Moreover humidity aging induces the development of copper sulfide nodules on the samples' surfaces.

Oxygen aging for two days at 70 °C does not affect the samples in an extent comparable to the other two aging conditions.

As cobalt protects the adhesion interface against aging and rapid dezincification, severe effects for the samples without cobalt stearate are expected after aging. These expectations are clearly fulfilled for the samples aged for five days under steam at 105 °C. Although the cobalt free samples show an excessive growth of copper sulfide after humidity aging for fourteen days at 70 °C, the corresponding coverage value of 83% does not distinctly suggest adhesion failure at the rubber metal interface here.

The replacement of DCBS by a mixture of TBBS and MBT is expected to reduce the delay of vulcanization and thus the time available for sulfidation. As a result adhesion strength is thought to diminish. However the unaged samples do not fulfill these expectations as they show coverage values of 98%. Humidity aging for fourteen days

at 70 °C does not attack the TBBS and MBT accelerated samples heavily. Dezincification is found to occur to a lesser extent than at the samples aged for five days under steam at 105 °C. The latter show highly increased sulfur and zinc values (40.9% S and 83.0% Zn) as well as a reduced coverage of 78%. According to the expectations adhesion fails partially at the rubber metal interface.

Throughout all aging stages thin adhesion interfaces are detected on the low sulfur samples. The reduced sulfur content is expected to result in a less sulfidized adhesion interface. In contrast to the expectations the unaged samples show good adhesion properties. On the other hand adhesion decreases during aging as can be concluded by the lowered coverage values which account for 75% after humidity aging and 67% after steam aging.

To sum up olefin metathesis degradation is found to be an applicable method for the exposure of real rubber metal interfaces. It enabled the investigation of the adhesion interfaces by means of SEM, optical light microscopy and 3D-microscopy with respect to their composition and optical appearance. One advantage of olefin metathesis degradation is that it provides the possibility to observe real adhesion interfaces in contrast to alternative techniques like the filter paper method or the application of squalene as model compound. Moreover the experiments of this work show, that monofilaments hold several advantages over cords in terms of sample preparation, degradation and analysis.

The comparison of the reference samples and the real car tire samples show that realistic adhesion interfaces differ from the T-test specimen samples. Thus it will be interesting to investigate adhesion interfaces from real car tires more intensively in the future. Furthermore it might be reasonable to investigate the optimum degradation time and amount of catalyst.

6. Appendix

6.1 Additional data

Figure 61 and Figure 62 show the vulcanization progresses and the shear forces for all recipes used in set 1.

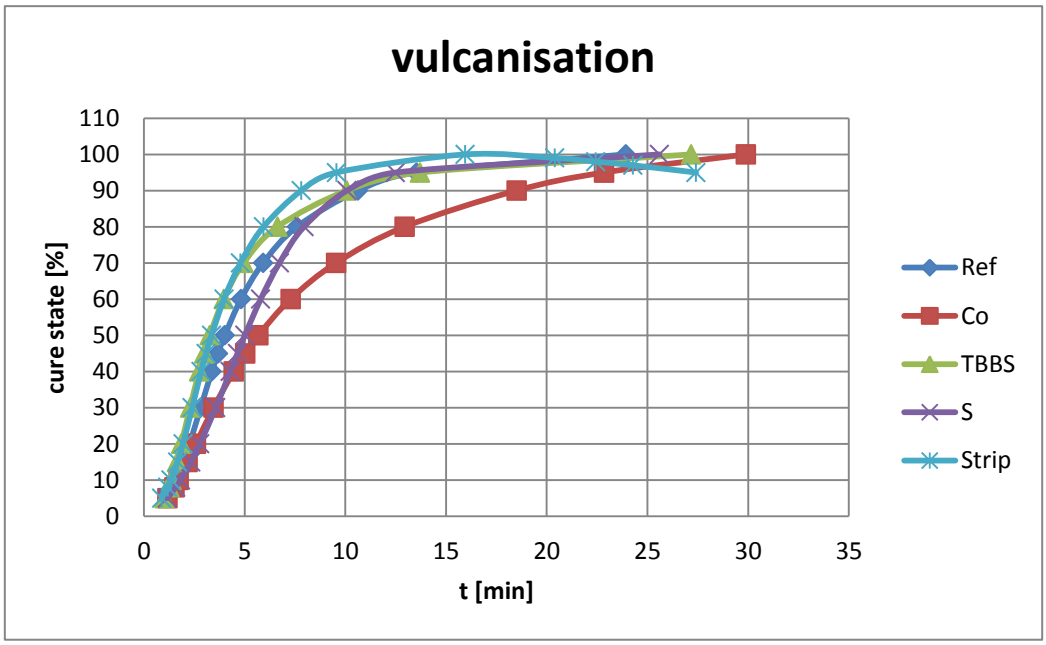

Figure 61: vulcanization progress of all recipes of set 1

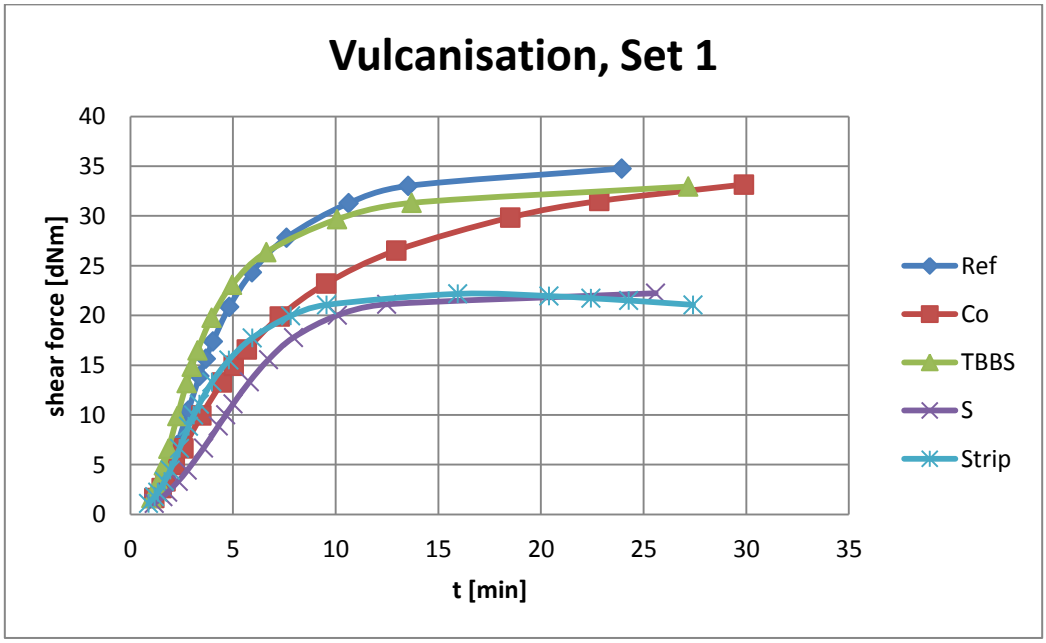

Figure 62: evolution of the shear forces of all isothermally heated recipes during vulcanization, set 1

Figure 63 and Figure 64 illustrate the pullout force and coverage data of the isothermally heated samples of set 1 which are mentioned in chapter 4.1. The pullout forces of set 1 are higher than those of set 2 because the different sample geometries. Moreover longer cord sections are vulcanized into the rubber in set 2.

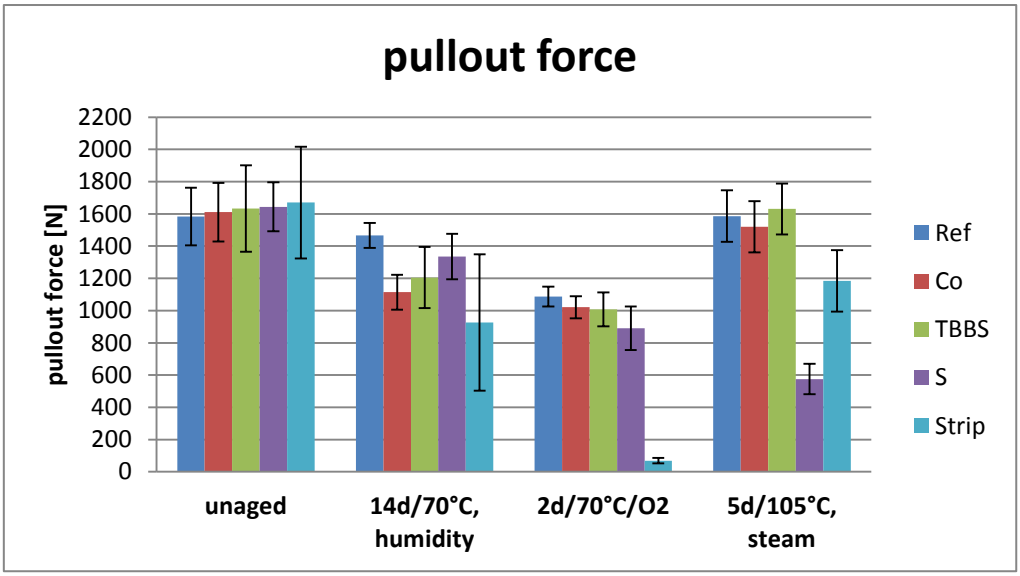

Figure 63: results for the pullout forces, isothermally heated samples, set 1

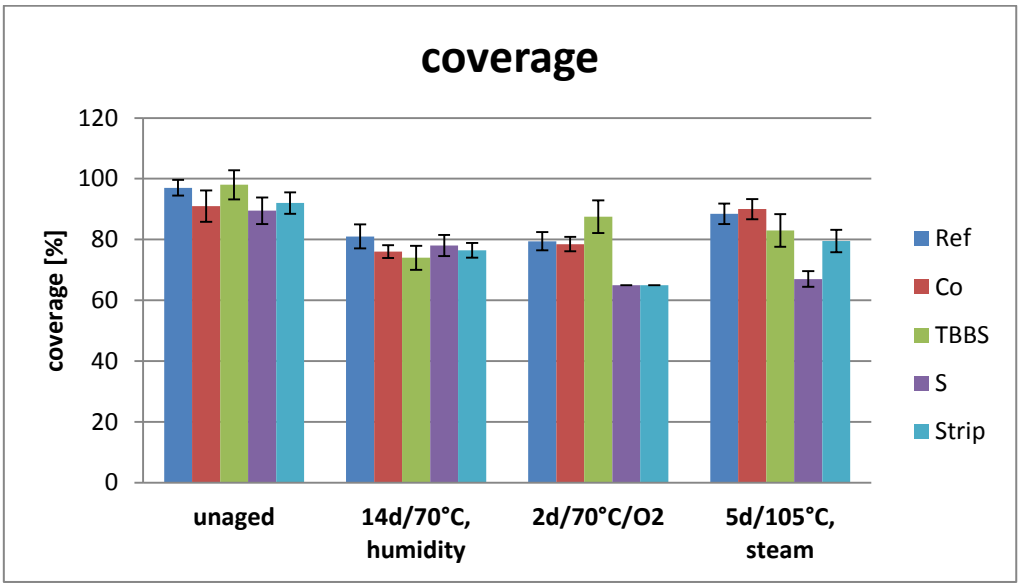

Figure 64: coverage values, isothermally heated samples, set 1

Figure 65 shows the shore hardness, the tensile strength, the tear elongation and the break energy density data of the isothermally heated samples of set 1.

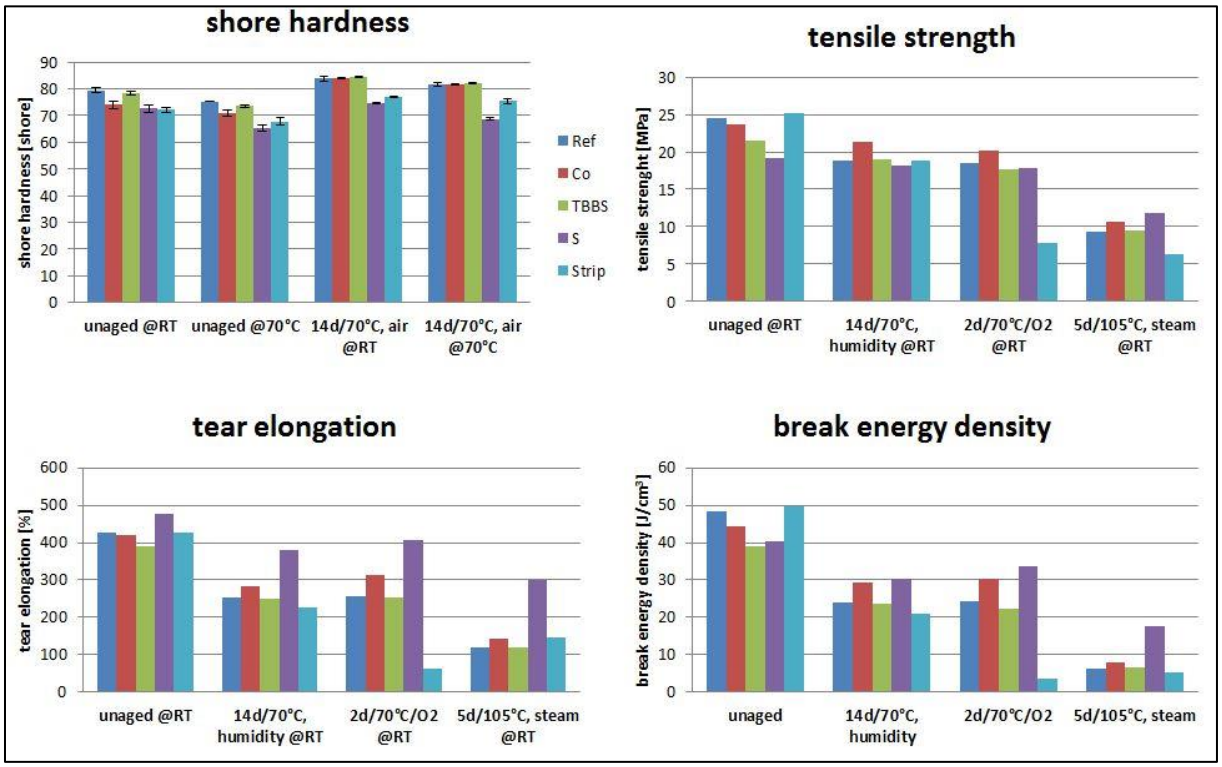

Figure 65: results for the shore hardness, tensile strength, tear elongation and break energy density, isothermally heated samples, set 1

Figure 66 illustrates the resilience data of the isothermally heated samples of set 1.

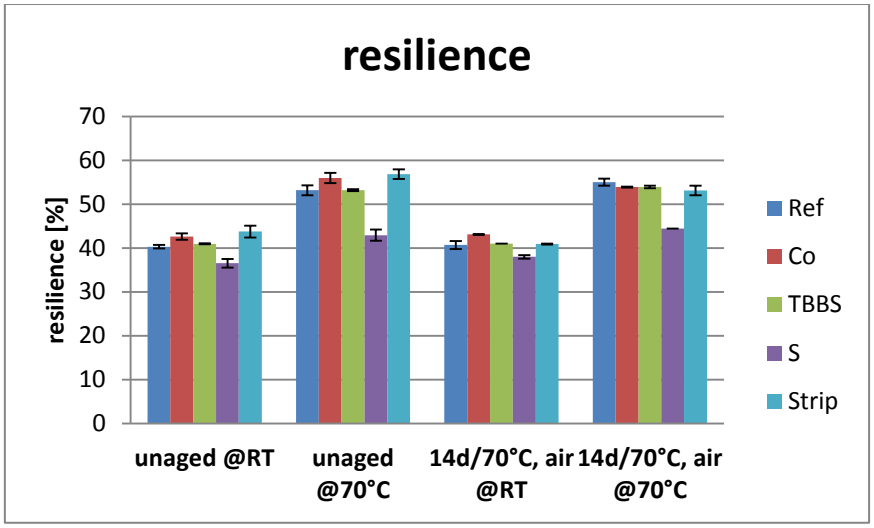

Figure 66: results for the resilience, isothermally heated samples, set 1

Table 13 lists the average elemental content of all recipes of the unaged series, the series aged for two days under oxygen at 70°of and the series aged for fourteen days under humidity at 70 °C set 1 which are exposed by filter paper method. The results for copper are normalized to 100%. The mean value is calculated from the results of all three areas investigated at a magnification of 1000 times.

Table 13: average elemental contents of all recipes of the unaged series, all samples aged for 2 days under oxygen at 70 °C and all samples aged for 14 days under humidity at 70 °C, set 1, filter paper method

		C[%]	Cu[%]	Fe[%]	O[%]	S[%]	Zn[%]
unaged	Ref	51.6	100.0	166.3	9.5	5.4	58.6
	Co	52.0	100.0	161.7	8.9	4.9	53.6
	TBBS	70.7	100.0	211.0	9.3	3.3	57.3
	S	61.8	100.0	172.5	9.4	3.8	55.6
	strip	59.9	100.0	194.5	9.9	7.4	55.4
2d, oxygen, 70°C	Ref	63.2	100.0	172.9	23.5	4.9	52.2
	Co	60.5	100.0	127.8	17.5	2.9	54.6
	TBBS	55.9	100.0	135.5	15.8	3.6	62.7
	S	66.4	100.0	161.4	14.1	3.9	55.2
	strip	69.3	100.0	152.9	17.7	5.2	59.7
14d, humidity 70°C	Ref	68.9	100.0	154.4	14.6	22.1	56.6
	Co	70.7	100.0	195.6	27.2	12.2	60.0
	TBBS	57.8	100.0	123.6	22.9	13.2	57.8
	S	54.6	100.0	141.8	20.4	6.5	59.1
	strip	73.0	100.0	180.8	26.9	21.9	54.6

Table 14 lists the average elemental content of all recipes of the unaged series, the series aged for two days under oxygen at 70 °C and the series aged for fourteen days under humidity at 70 °C set 1 which are degraded by metathesis reaction. The results for copper are normalized to 100%. The mean value is calculated from the results of all three areas investigated at a magnification of 1000 times.

Table 14: average elemental contents of all recipes of the unaged series, all samples aged for 2 days under oxygen at 70 °C and all samples aged for 14 days under humidity at 70 °C, set 1, metathesis degradation

		C[%]	Cu[%]	Fe[%]	O[%]	S[%]	Zn[%]
unaged	Ref	49.3	100.0	197.9	6.6	3.7	62.7
	Co	56.0	100.0	150.5	7.2	4.2	56.3
	TBBS	42.0	100.0	181.7	6.3	2.4	51.4
	S	30.5	100.0	178.5	5.3	3.2	58.1
	strip	59.4	100.0	178.4	7.0	7.5	59.1
2d, oxygen, 70°C	Ref	24.5	100.0	149.8	5.5	2.1	58.5
	Co	48.1	100.0	194.8	9.6	2.8	58.1
	TBBS	122.9	100.0	185.0	22.3	11.3	66.5
	S	42.5	100.0	178.0	7.6	3.4	56.5
	strip	114.3	100.0	191.7	21.0	6.6	60.0
14d, humidity, 70°C	Ref	104.9	100.0	174.9	13.1	10.3	60.0
	Co	108.0	100.0	211.7	14.0	21.4	62.9
	TBBS	102.2	100.0	177.1	16.3	19.9	63.3
	S	77.7	100.0	195.6	13.7	7.7	64.1
	strip	121.5	100.0	284.2	17.3	20.4	65.7

6.2 Abbreviations

phr	parts per hundred rubber
Å	angstrom
nm	nanometer
µm	micrometer
(k)eV	(kilo) electron-volt
°C	degree Celsius
mg	milligram
µl	microliter
min	minute(s)
d	days
N	newton
dNm	deci newton meter
(M)Pa	(mega) pacal
J/cm^3	joule per cubic centimeter
MBT	2-mercaptobenzothiazole
MBTS	2,2'-dithiobisbenzothiazole
CBS	N-cyclohexylbenzothiazole-2-sulfenamide
TBBS	N-t-butylobenzothiazole-2-sulfenamide
MBS	2-morpholinothiobenzothiazole
DCBS	N-dicyclohexylbenzothiazole-2-sulfenamide
RF	resorcinol-formaldehyde
HMMM	hexamethoxymelamine
HR-system	hexamethoxymelamin resorcinol formaldehyde- system
CM	cross metathesis
RCM	ring closing metathesis
ROCM	ring opening cross metathesis
ROMP	ring opening metathesis polymerization
ADMET	acyclic diene metathesis polymerization
RRM	ring rearrangement metathesis
NA	numeric aperture
SEM	scanning electron microscopy
BSE	back scattered electrons
WDX-spectrometer	wavelength dispersive x-ray spectrometer
EDX-spectrometer	energy dispersive x-ray spectrometer
AFM	atomic force microscopy
RT	room temperature
t	time

6.3 List of figures

6.4 List of tables

6.5 Chemicals and analytical devices

6.5.1 Chemicals

- Toluene: 99.9%, Sigma Aldrich
- 1-octene: >97%, Fluka Chemie AG
- Catalyst: synthesized at Graz University of Technology

6.5.2 Analytical devices

- Optical light microscope
  Olympus BX60
  Objektive: Olympus LMPlanFl 5x/0,13 Japan
  10x/0,25 Japan
  20x/0,40 Japan
  50x/0,50 Japan
  Kamera: Olympus E520

- 3D-microscope
  Keyence;
  digital microscope system, multi illumination light system,
  Universal zoom lense: VH Z100 UR,
  Monitor: VHX 600
  AFM Software: 5.1.6

- Scanning electron microscope
  Zeiss, EVO, MA 10,
  Brucker AXS, x-flash detector
  Software: Brucker Esprit 1.9, Quantax 2000

7. References

1. Car Tire Industry Statistics. Available at: http://business.highbeam.com/industry-reports/chemicals/synthetic-rubber-vulcanizable-elastomers.

2. Synthetic Rubber. Available at: http://business.highbeam.com/industry-reports/chemicals/synthetic-rubber-vulcanizable-elastomers.

3. Wortmann C, Dettmer F, Steiner F. Die Chemie des Reifens. *Chemie unserer Zeit*. 2013;47:300-309. doi:10.1002/ciuz.201300603.

4. Abou-Kandil AI, Awad A, Darwish N, Shehata AB, Saleh BK. Adhesion of brass plated steel cords to natural rubber: Dynamic and statistical study of adhesion failure. *Int J Adhes Adhes*. 2013;44:26-35. doi:10.1016/j.ijadhadh.2013.01.018.

5. Jeon GS. Adhesion between rubber compounds containing various adhesion promoters and brass-plated steel cords. part 1. effect of sulfur loading in rubber compounds. *J Adhes Sci Technol*. 2008;22(12):1223-1253. doi:10.1163/156856108X319917.

6. Buytaert G, Coornaert F, Dekeyser W. Characterization of the Steel Tire Cord - Rubber Interface. *Rubber Chem Technol*. 2009;82(4):430-441. doi:10.5254/1.3548256.

7. Buytaert G, Liang H, Pax G, Reis P. Steel tire cord: adhesion build-up and degradation. *Rubber Plast news*. 2010;40(9):14-16. Available at: http://cat.inist.fr/?aModele=afficheN&cpsidt=23696278. Accessed July 28, 2014.

8. Jeon GS, Kang UI, Jeong SW, CHoi SJ, Kim SH. Adhesion between rubber compounds and ternary-alloy-coated steel cords. Part II. Effect of sulfur and cobalt salt in rubber compounds.pdf. *J Adhes Sci Technol*. 2005;19(15):1325-1348. doi:10.1163/156856108X319917.

9. Hotaka T, Ishikawa Y, Mori K. CHARACTERIZATION OF ADHESION INTERLAYER BETWEEN RUBBER AND BRASS BY A NOVEL METHOD OF SAMPLE PREPARATION. *Rubber Chem Technol*. 2007;80(1):61-82. doi:http://dx.doi.org/10.5254/1.3548169.

10. Ziegler E, Kern W, Hochenauer R, Holzner A, Trimmel G. How to investigate the rubber-brass adhesive interface. In: ; 2012.

11. Whelan A, Lee KS. *Developments in Rubber Technology-1*.; 1979:105-115.

12. Coran AY. *The Science and Technology of Rubber*. 4th ed.; 2013:337-381. doi:10.1016/B978-0-12-394584-6.00007-8.

13. Van Ooij WJ. The role of XPS in the study and understanding of rubber-to-metal bonding. *Surf Sci*. 1977;68:1-9. doi:10.1016/0039-6028(77)90184-4.

14. Van Ooij WJ. Article of manifacture having a metallic surface coated with an elastomer and an intermediate cobalt-copper alloy coating to improve the adhesion of the elastomer. *United Stated Pat*. 1980:0-7.

15. Fulton WS. Steel tire cord-rubber adhesion, including the contribution of Cobalt. *Rubber Chem Technol*. 2005;78(3):426-457. doi:10.5254/1.3547891.

16. Weening WE. Theorie und Praxis bei Untersuchungen über die Gummi/Metall-Haftung*. *Kautschuk und Gummi Kunststoffe*. 1978;31(4):227-232.

17. Fulton WS. TIRE-CORD ADHESION : HOW THE SOURCE OF ZINC CAN INFLUENCE THE STRUCTURE OF THE BONDING INTERFACE. *Rubber Chem Technol*. 2006;79(5):790-805. doi:http://dx.doi.org/10.5254/1.3547967.

18. Van Ooij WJ. Mechanism and theories of rubber adhesion steel tire cords-an overview. *Rubber Chem Technol*. 1984;57(3):421-456. doi:http://dx.doi.org/10.5254/1.3536016.

19. Fulton WS, Smith GC, Titchener KJ. Interfacial microanalysis of rubber–tyre-cord adhesion and the influence of cobalt. *Appl Surf Sci*. 2004;221:69-86. doi:10.1016/S0169-4332(03)00805-5.

20. Van Ooij WJ, Harankuni PB, Buytaert G. Haftung von Reifenstahlkord an Gummi-Eine Übersicht. *GAK-Gummi Fasern Kunststoffe*. 2010;8:467-482.

21. Ziegler E, Macher J, Gruber D, et al. Investigation of the influence of stearic acid on the rubber-brass adhesion. *Rubber Chem Technol*. 2012;85(2):264-276. doi:http://dx.doi.org/10.5254/rct.12.88940.

22. Ozawa K, Kakubo T, Shimizu K, Amino N, Mase K, Komatsu T. High-resolution photoelectron spectroscopy analysis of sulfidation of brass at the rubber/brass interface. *Appl Surf Sci*. 2013;264:297-304. doi:10.1016/j.apsusc.2012.10.015.

23. Giridhar J, Van Ooij WJ. Study of Zn-Ni and Zn-Co alloy coatings electrodeposited on steel strips II: Corrosion, dezincification and sulfidation of the alloy coatings. *Surf Coatings Technol*. 1992;53:35-47. doi:10.1016/0257-8972(92)90101-F.

24. Kim JM, Van Ooij W. Study of rubber-brass adhesion mechanism by secondary ion mass spectrometry. *Rubber Chem Technol*. 2002;75(2):199-214. doi:http://dx.doi.org/10.5254/1.3544973.

25. Ashirgade A, Harakuni PB, Van Ooij WJ. Effects of Aging on the Morphology of Rubber-Brass Interfacial Layer. *Tire Sci Technol*. 2011;39(1):20-43. doi:10.2346/1.3555084.

26. Hammer GE. A new look at the steel cord–rubber adhesive interphase by chemical depth profiling. *J Vac Sci Technol A*. 2001;19(6):2846-2850. doi:10.1116/1.1410945.

27. Van Ooij WJ, Giridhar J, Ahn JH. Review of recent advances in bonding rubber to steel tire cords. *Kautschuk und Gummi Kunststoffe*. 1991;44(4):348-359.

28. Kleinhesselink A, Van Ooij WJ. Application of XPS to the study of polymer-metal interface phenomena. *Appl Surf Sci*. 1980;4(3-4):324-339. doi:10.1016/0378-5963(80)90082-3.

29. Van Ooij W, Biemond MEF. A novel class of rubber to steel tire cord adhesion promoters. *Rubber Chem Technol*. 1984;57(4):686-702. doi:http://dx.doi.org/10.5254/1.3536026.

30. Patil PY, Van Ooij WJ. Mechanism of adhesion degradation of rubber to brass-plated steel cords. *J Adhes Sci Technol*. 2004;18(12):1367-1394. doi:http://dx.doi.org/10.5254/1.3536016.

31. Holtkarnp D, Elschner A, Müller G, Pieroth M. Novel Model System to Study the Influence of Rubber Compound Formulation on the Structure and Composition of the Rubber-Brass Interphase. *Surf interface Anal*. 1995;23(3):155-162. doi:10.1002/sia.740230306.

32. Kim JM, Van Ooij W. Study of the effects of compound ingredients on the adhesion layer between squalene model compound and brass by GPC and TOF-SIMS. *J Adhes Sci Technol*. 2003;17(2):165-178. doi:10.1163/156856103762301989.

33. Van Ooij WJ. *Handbook of Rubber Bonding*. (Growther BG, ed.). Rapra Technology Limited; 2001:163-195.

34. Haemers G, Mollet J. The role of the brass surface composition with regard to steel cord rubber adhesion. *J Elastomers Plast*. 1978;10(3):241-261. doi:10.1177/009524437801000304.

35. Waddell WH, Evans LR, Goralski EG, Snodgrass LJ. Mechanism by which precipitated silica improves brass-coated wire-to-natural rubber adhesion. *Rubber Chem Technol*. 1996;69(1):48-58. doi:http://dx.doi.org/10.5254/1.3538356.

36. Jeon GS, Han MH, Seo G. Enhancing adhesion properties between rubber compound and brass-plated steel cord by incorporating silica into rubber. *J Adhes Sci Technol*. 1999;13(2):153-168. doi:10.1163/156856199X00361.

37. Chandra AK, Biswas A, Mukhopadhyay R, Bhowmick AK. Effect of anion in cobalt promoters on the adhesion between steel cord and rubber compound. *J Adhes Sci Technol*. 1994;44(3):177-196. doi:10.1080/00218469408027076.

38. Patil PY, Van Ooij WJ. Mechanism of improved aged rubber-to-brass adhesion using one component resins. *Rubber Chem Technol*. 2005;78(1):155-173. doi:http://dx.doi.org/10.5254/1.3547868.

39. Jeon GS. Enhancing the adhesion retention by controlling the structure of the adhesion interphase between rubber compound and metal. Part I. Effect of cobalt salt. *J Adhes Sci Technol*. 2009;23(6):913-930. doi:10.1163/156856109X411256.

40. Ball JJ, Gibbs HW, Tate PER. A study of brass/squalene interfacial compositions using surface analytical technique. *J Adhes*. 1990;32(1):29-44. doi:10.1080/00218469008030178.

41. Ishikawa Y, Hotaka T. Haftung von Gummi auf Stahlcord-Wirkung von Mischungsbestandteilen. *GAK-Gummi Fasern Kunststoffe*. 2004;57:642-652.

42. Pieroth M, Holtkamp D, Elschner A. The influence of boric acid ester on the structure and composition of the rubber/brass interface of Co-containing bonding compounds. *Kautschuk und Gummi Kunststoffe*. 1993;46(2):112-115.

43. Jeon GS, Han MH, Seo G. The adhesion properties of stearic acid-loaded rubber compounds to brass-plated steel cords. *Korean J Chem Eng*. 1999;16(4):434-440.

44. Jeon GS. Enhancing the adhesion retention by controlling the structure of adhesion interface between rubber compound and metal. Part II: Effect of zinc borate. *J Adhes Sci Technol*. 2010;24(4):709-729.

45. Patil PY, Van Ooij WJ. Mechanistic study of the effect of adhesion-promoter resins on the crystal structure of the copper sulfide adhesion layer at the rubber-brass interface. *Rubber Chem Technol*. 2006;79(1):82-93. doi:http://dx.doi.org/10.5254/1.3547931.

46. Hotaka T, Ishikawa Y, Mori K. Effect of compound ingredients on adhesion between rubber and brass-plated steel cord. *Rubber Chem Technol*. 2005;78(2):175-187. doi:http://dx.doi.org/10.5254/1.3547876.

47. Hamed GR, Huang J. Combining cobalt and resorcinolic bonding agents in brass-rubber adhesion. *Rubber Chem Technol*. 1991;64(2):285-295. doi:http://dx.doi.org/10.5254/1.3538559.

48. Jayaseelan SK, Van Ooij WJ. Gummi-Metall-Bindung durch Silane. *GAK-Gummi Fasern Kunststoffe*. 2003;56:497-509.

49. Delattre JL, D'Agostino R, Fracassi F. Plasma-polymerized thiophene films for enhanced rubber–steel bonding. *Appl Surf Sci*. 2006;252:3912-3919. doi:10.1016/j.apsusc.2005.05.069.

50. Kretzschmar T, Hofer F, Hummel K, Sommer F. Rubber Metal Bonding: Investigation of rupture behaviour of the bonding layer by means of transmission electron microscopy and bonding strength measurments. *Kautschuk und Gummi Kunststoffe*. 1993;46(9):710-717.

51. Giridhar J, Van Ooij WJ. Study of Zn-Ni and Zn-Co alloy coatings electrodeposited on steel strips I: Alloy electrodeposition and adhesion of coatings to natural rubber compounds. *Surf Coatings Technol*. 1992;52(1):17-30. doi:10.1016/0257-8972(92)90367-J.

52. Giridhar J, Van Ooij WJ. Adhesion and corrosion properties of a new NiZn/ZnCo-coated steel tire cord. *Surf Coatings Technol*. 1992;53(3):243-255. doi:10.1016/0257-8972(92)90383-L.

53. Kim JM. Investigation of the adhesion layer formed on brass using field emission-scanning electron microscopy. *Rubber Chem Technol*. 2005;78(5):844-854. doi:http://dx.doi.org/10.5254/1.3547917.

54. Slugovc C. The Ring Opening Metathesis Polymerisation Toolbox. *Macromol Rapid Commun*. 2004;25(14):1283-1297. doi:10.1002/marc.200400150.

55. Grubbs RH. Olefin metathesis. *Tetrahedron*. 2004;60(34):7117-7140. doi:10.1016/j.tet.2004.05.124.

56. Sanford MS, Love J a, Grubbs RH. Mechanism and activity of ruthenium olefin metathesis catalysts. *J Am Chem Soc*. 2001;123(27):6543-54. Available at: http://www.ncbi.nlm.nih.gov/pubmed/11439041.

57. Olefinmetathese. Available at: http://www.organische-chemie.ch/OC/Namen/Olefinmetathese.htm.

58. Fainleib A, Pires R V., Lucas EF, Soares BG. Degradation of non-vulcanized natural rubber renewable resource for fine chemicals used in polymer synthesis. *Polímeros Ciência e Tecnol*. 2013:441-450. doi:10.4322/polimeros.2013.070.

59. Obrecht W, Müller JM, Nuyken O. Verfahren zum Metathese-Abbau von Nitrilkautschuk. 2009:1-50.

60. Grubbs RH. Olefin-metathesis catalysts for the preparation of molecules and materials (Nobel Lecture). *Angew Chem Int Ed Engl*. 2006;45(23):3760-5. doi:10.1002/anie.200600680.

61. Scholl M, Ding S, Lee CW, Grubbs RH. Synthesis and activity of a new generation of ruthenium-based olefin metathesis catalysts coordinated with 1,3-dimesityl-4,5-dihydroimidazol-2-ylidene ligands. *Org Lett*. 1999;1(6):953-6. doi:10.1021/ol990909q.

62. Ouardad S, Peruch F. Metathetic degradation of trans-1,4-polyisoprene with ruthenium catalysts. *Polym Degrad Stab*. 2014;99(2014):249-253. doi:10.1016/j.polymdegradstab.2013.10.022.

63. Solanky SS, Campistron I, Laguerre A, Pilard J-F. Metathetic Selective Degradation of Polyisoprene: Low-Molecular-Weight Telechelic Oligomer Obtained from Both Synthetic and Natural Rubber. *Macromol Chem Phys*. 2005;206(10):1057-1063. doi:10.1002/macp.200400416.

64. Craig SW, Manzer JA, Coughlin EB. Highly Efficient Acyclic Diene Metathesis Depolymerization Using a Ruthenium Catalyst Containing a N-heterocylcic Carbene Ligand. *Macromolecules*. 2001;34:7929-7931.

65. Sedransk KL, Kaminski CF, Hutchings LR, Moggridge GD. The metathetic degradation of polyisoprene and polybutadiene in block copolymers using Grubbs second generation catalyst. *Polym Degrad Stab*. 2011;96:1074-1080. doi:10.1016/j.polymdegradstab.2011.03.007.

66. Tlenkopatchev MA, Barcenas A, Fomine S. Computational Study of Metathesis Degradation of Rubber , 3 a Distribution of Cyclic and Linear Oligomers via Intermolecular Degradation of cis - Poly (butadiene). *Macromol Theory Simulations*. 2001;10(7):729-735.

67. Lorber F, Hummel K. Ein kinetischer Effekt bei der Metathese-Reaktion von ungesättigten Polymeren mit niedermolekularen Olefinen. *Die Makromol Chemie*. 1973;171(1973):257-260.

68. Tlenkopatchev M a., Barcenas A, Fomine S. Computional Study of Metathesis Degradation of Rubber, 2. Distribution of Cyclic Oligomers via Intramolecular Metathesis Degradation of Natural Rubber. *Macromol Theory Simulations*. 2001;10(5):441-446. doi:10.1002/1521-3919(20010601)10:5<441::AID-MATS441>3.0.CO;2-#.

69. Gutiérrez S, Tlenkopatchev M a. Metathesis of renewable products: degradation of natural rubber via cross-metathesis with β-pinene using Ru-alkylidene catalysts. *Polym Bull*. 2010;66(8):1029-1038. doi:10.1007/s00289-010-0330-x.

70. Gutiérrez S, Tlenkopatchev MA. DEGRADATION OF NATURAL RUBBER VIA CROSS-METATHESIS WITH FUNCTIONALIZED OLEFINS USING RUTHENIUM ALKYLIDEN CATALYSTS. *Supl Rev Latinoam Metlurgia y Mater*. 2009;1(4):1463-1467.

71. Zümreoglu-Karan B, Bozkurt C, Imamoglu Y. Degradation of Sulfur Crosslinked cis 1,4-polybutadiene by metathesis catalyst. *Polym J*. 1992;24(1):25-29.

72. Wolf S, Plenio H. On the ethenolysis of natural rubber and squalene. *Green Chem*. 2011;13(8):2008. doi:10.1039/c1gc15265c.

73. Hummel K, Stelzer F, Hobisch G, Hartmann B. Determination of Ethylene-Propylene Rubber in Crosslinked Blends with 1 , 4-Polybutadiene. *Die Angew Makromol Chemie*. 1987;155:143-149.

74. Sadaka F, Campistron I, Laguerre A, Pilard J-F. Telechelic oligomers obtained by metathetic degradation of both polyisoprene and styrene–butadiene rubbers. Applications for recycling waste tyre rubber. *Polym Degrad Stab*. 2013;98:736-742. doi:10.1016/j.polymdegradstab.2012.12.018.

75. Reyx D, Campistron I. Controlled Degradation in Tailor-made Macromolecules elaboration. Controlled Chain-Cleavages of Polydienes by Oxidation and by Metathesis. *Die Angew Makromol Chemie*. 1997;247:197-211.

76. Hummel K, Kiattanavith N, Bernard E. Determination of carbon black fillers in vulcanizates of natural rubber by metathesis degradation. *Angew Makromol Chemie*. 1993;207:137-143.

77. Stelzer F, Hobisch G, Pongratz T, Hummel K. Metathesis degratation of acrylonitrile/butadiene copolymers. *J Mol Catal*. 1988;46:433-444.

78. Murphy DB, Davidson MW. *Fundamentals of Light Microscopy and Electronic Imaging*. 2nd ed.; 2013.

79. Craig Freudenrich PD. How Light Microscopes Work. Available at: http://science.howstuffworks.com/light-microscope.htm.

80. Watt IM. *The Principles and Practice of Electron Microscopy*. 2nd ed.; 1997:1-7.

81. Vernon-Parry KD. Scanning electron microscopy: an introduction. *III-Vs Rev*. 2000;13(4):40-44. doi:10.1016/S0961-1290(00)80006-X.

82. Scanning Electron Microscopy. Available at: http://www.nanoscience.com/products/sem/technology-overview/.

83. Omoto CK, Folwell J. Using Darkfield Microscopy To Enhance Contrast: An Easy and Inexpensive Method. Available at: http://public.wsu.edu/~omoto/papers/darkfield.html.

84. Infinite Focus Microscope (IFM). Available at: http://www.shu.ac.uk/research/meri/infinite-focus-microscope-ifm.

85. InfiniteFocus G4. Available at: http://www.optimaxonline.com/non-contact-metrology-3d-surface-characterisation/37/IFM-G4-cut-out-web.

86. No Title. Available at: http://de1.keyence.eu/products/microscope/microscope/vk9700/vk9700_features_9.php.

87. Lehrle RS, Niederost KJ. Steel tyre surface analysis in the study of brass-rubber adhesion. *Prog Rubber Plast Technol*. 1992;8(3):221-239.

88. Hamed GR, Donatelli T. Effect of accelerator type on brass-rubber adhesion. *Rubber Chem Technol*. 1983;56(2):450-464. doi:http://dx.doi.org/10.5254/1.3538138.

89. Butler JH, Joy DC, Bradley GF, Krause SJ. Low-voltage scanning electron microscopy of polymers. *Polymer (Guildf)*. 1995;36(9):1781-1790. doi:10.1016/0032-3861(95)90924-Q.

90. No Title. Available at: http://www.ammrf.org.au/myscope/images/sem/sem-ve-lm.png.

91. Physical Methods in Chemistry and Nano Science. Available at: http://cnx.org/contents/ba27839d-5042-4a40-afcf-c0e6e39fb454@20.16:110.

92. Teaching O for learning and. My scope-training for advanced reserch. 2013. Available at: http://www.ammrf.org.au/myscope/analysis/eds/xraydetection/.

93. Hafner B. Energy dispersive spectroscopy on the SEM: A primer. Available at: http://www.charfac.umn.edu/instruments/eds_on_sem_primer.pdf.

94. Hamed GR, Paul R. Effect of various bonding agents on the sulfidation of brass-plated steel cords immersed in squalene mixtures. *Rubber Chem Technol*. 1997;70(4):541-548. doi:http://dx.doi.org/10.5254/1.3538441.